National Library of Canada
Canadian Theses Service
Ottawa, Canada
K1A 0N4

Bibliothèque nationale du Canada
Services des thèses canadiennes

CANADIAN THESES

THÈSES CANADIENNES

NOTICE

The quality of this microfiche is heavily dependent upon the quality of the original thesis submitted for microfilming. Every effort has been made to ensure the highest quality of reproduction possible.

If pages are missing, contact the university which granted the degree.

Some pages may have indistinct print especially if the original pages were typed with a poor typewriter ribbon or if the university sent us an inferior photocopy.

Previously copyrighted materials (journal articles, published tests, etc.) are not filmed.

Reproduction in full or in part of this film is governed by the Canadian Copyright Act, R.S.C. 1970, c. C-30.

AVIS

La qualité de cette microfiche dépend grandement de la qualité de la thèse soumise au microfilmage. Nous avons tout fait pour assurer une qualité supérieure de reproduction.

S'il manque des pages, veuillez communiquer avec l'université qui a conféré le grade.

La qualité d'impression de certaines pages peut laisser à désirer, surtout si les pages originales ont été dactylographiées à l'aide d'un ruban usé ou si l'université nous a fait parvenir une photocopie de qualité inférieure.

Les documents qui font déjà l'objet d'un droit d'auteur (articles de revue, examens publiés, etc.) ne sont pas microfilmés.

La reproduction, même partielle, de ce microfilm est soumise à la Loi canadienne sur le droit d'auteur, SRC 1970, c. C-30.

THIS DISSERTATION HAS BEEN MICROFILMED EXACTLY AS RECEIVED

LA THÈSE A ÉTÉ MICROFILMÉE TELLE QUE NOUS L'AVONS REÇUE

NL-339 (r.86/06)

Canada

THE UNIVERSITY OF ALBERTA

DIAGENESIS OF THE VIKING FORMATION, SOUTH-CENTRAL ALBERTA

by

M.E.DEAN

A THESIS

SUBMITTED TO THE FACULTY OF GRADUATE STUDIES AND RESEARCH

IN PARTIAL FULFILMENT OF THE REQUIREMENTS FOR THE DEGREE

OF MASTER OF SCIENCE

DEPARTMENT OF GEOLOGY

EDMONTON, ALBERTA

SPRING, 1986

Permission has been granted to the National Library of Canada to microfilm this thesis and to lend or sell copies of the film.

The author (copyright owner) has reserved other publication rights, and neither the thesis nor extensive extracts from it may be printed or otherwise reproduced without his/her written permission.

L'autorisation a été accordée à la Bibliothèque nationale du Canada de microfilmer cette thèse et de prêter ou de vendre des exemplaires du film.

L'auteur (titulaire du droit d'auteur) se réserve les autres droits de publication; ni la thèse ni de longs extraits de celle-ci ne doivent être imprimés ou autrement reproduits sans son autorisation écrite.

ISBN 0-315-30141-4

THE UNIVERSITY OF ALBERTA

RELEASE FORM

NAME OF AUTHOR M.E.DEAN

TITLE OF THESIS DIAGENESIS OF THE VIKING FORMATION, SOUTH-CENTRAL ALBERTA

DEGREE FOR WHICH THESIS WAS PRESENTED MASTER OF SCIENCE

YEAR THIS DEGREE GRANTED SPRING, 1986.

Permission is hereby granted to THE UNIVERSITY OF ALBERTA LIBRARY to reproduce single copies of this thesis and to lend or sell such copies for private, scholarly or scientific research purposes only.

The author reserves other publication rights, and neither the thesis nor extensive extracts from it may be printed or otherwise reproduced without the author's written permission.

(SIGNED) Michael Dean

PERMANENT ADDRESS:

#2104E 920- 9th Ave

S.W. Calgary

T2P 2T9

DATED Nov 4 1985

THE UNIVERSITY OF ALBERTA

FACULTY OF GRADUATE STUDIES AND RESEARCH

The undersigned certify that they have read, and recommend to the Faculty of Graduate Studies and Research, for acceptance, a thesis entitled DIAGENESIS OF THE VIKING FORMATION, SOUTH-CENTRAL ALBERTA submitted by M.E.DEAN in partial fulfilment of the requirements for the degree of MASTER OF SCIENCE.

Fred J. Longstaffe

Supervisor

Frances J. Hein

Supervisor

J. Hubert Kuo

Fay J. Dudas

Date. NOV. 4. 1985

ABSTRACT

In south-central Alberta, the Viking Formation consists of a lower coarsening upward sequence of clastic rocks (Viking "B" deposits) and overlying sheet-like deposits (Viking "A" deposits). Sedimentological, mineralogical and geochemical studies have helped to reveal the diagenetic history of these clastic rocks during both burial and uplift stages of the Alberta basin.

The main rock types present are conglomerate, coarse and fine-grained sandstone and shale. The Viking "B" deposits consists of a lower coarsening upward unit of shale, silt and conglomerate (15-20m) and an upper coarsening upward unit of shale, fine-grained sandstone and conglomerate (20-25m). The Viking "A" rocks consist of one to three, sheet-like deposits of coarse-grained sandstone and conglomerate (0.5-2m) that lie above the Viking "B" within the Lloydminster shales.

The mineralogy of the shales consists mostly of illite (60-85%) and lesser amounts of illite/smectite (5-25%), kaolin group minerals (trace-20%), chlorite (trace-10%) and smectite (not detected - 5%). Detrital minerals in the conglomerates and sandstones consist of quartz (5-60%), chert (5-80%), rock fragments (not detected - 24%) and feldspar (not detected - 30%). Viking "A" rocks usually contain higher percentages of feldspar (2-30%) than Viking "B" rocks (not detected - 5%).

Diagenetic minerals in the sandstones and conglomerates consist of glauconite, pyrite, chamosite, siderite, quartz, albite, Fe-calcite, ankerite, dickite, illite, illite/smectite, and smectite. Siderite is a common cement, especially in the fine-grained sandstones (t-63%). Quartz cementation is more extensive in the fine and coarse-grained sandstones (3-25%) than in the conglomerates (2-14%). Albite, Fe-calcite, and ankerite are minor components but are usually more abundant in Viking "A" rocks and may have formed during albitization of feldspar. Dickite is the most abundant clay mineral, especially in the coarse-grained rocks (up to 10%). The composition of illite/smectite in the sandstones was probably controlled by fluid composition, whereas the composition of illite/smectite in the shales was probably controlled by increasing depth and temperature during burial.

The combination of petrographic and stable isotope data indicate that siderite ($\delta'^{8}O$ = +18.1 to +23.9 SMOW, $\delta'^{3}C$ = -1.5 to -6.33 PDB) formed during shallow burial from ^{13}C - rich CO_2, probably derived from bacterial fermentation, and from ^{18}O - rich connate water. Quartz ($\delta'^{8}O$ = +20.2), Fe-calcite ($\delta'^{8}O$ = +13.9 to +14.6, $\delta'^{3}C$ = -7.2 to -8.4), ankerite ($\delta'^{8}O$ = +16.5 to +16.6, $\delta'^{3}C$ = -6.3 to -12.4) and dickite ($\delta'^{8}O$ = +12.4 to +12.6) crystallized from ^{18}O - poor water that may represent an influx of meteoric water during uplift. Carbon for Fe-calcite and ankerite was probably derived from the CO_2 released from the thermal destruction

of organic matter.

Diagenesis of the Viking Formation reflects a large meteoric water influence associated with second phase of the Laramide orogeny (uplift stage). Glauconite, early pyrite, chamosite + minor quartz, and siderite are the only phases that record changing fluid chemistry during burial of the Viking. These cements probably formed during shallow burial and during the bacterial breakdown of organic matter. The crystallization of quartz, Fe-calcite, albite, ankerite, late pyrite, dickite, illite/smectite, and smectite reflects changes in fluid chemistry associated with an influx of meteoric waters and fluids released during the thermal maturation of organic matter.

Table of Contents

Chapter — Page

I. INTRODUCTION 1

A. Purpose of Study 1

B. Location and Stratigraphy 4

C. Geologic History 7

Tectonic Setting 7

Late Albian Transgressions 8

Laramide Orogeny 8

D. Previous Work 12

E. Analytical Methods 15

II. REGIONAL VARIATIONS IN LITHOLOGIES 27

A. Viking "B" Deposits 27

Lower Coarsening-Upward Unit 27

Lower Conglomerate 29

Upper Coarsening-Upward Unit 29

Upper Conglomerate 30

B. Viking "A" Deposits 34

III. RESULTS OF MINERALOGY & ANALYTICAL GEOCHEMISTRY ... 36

A. Mineralogy of Shales 36

Nature of Illite/Smectite 36

B. Detrital Mineralogy of Sandstones and Conglomerates 41

Conglomerates 41

Coarse-Grained Sandstones 42

Fine-Grained Sandstones 43

Classification 43

C. Authigenic Mineralogy of Sandstones and Conglomerates 67
Glauconite 67
Pyrite 67
Chlorite 68
Siderite 70
Quartz 71
Feldspar 72
Fe-Calcite 72
Ankerite 72
Kaolin Group Minerals 73
Illite 75
Illite/Smectite 77
Smectite 82
Paragenetic Sequence 103
D. Stable Isotopes 106
Carbonates Minerals 106
Silicates Minerals 109
Oxygen Isotope Geothermometry 111
E. Microprobe Analysis 114
IV. DIAGENESIS 116
A. Interpretation of Paragenetic Sequence 116
Early Iron-Rich Cements 117
Quartz Cementation 123
Albitization 126
Ankeritization 129
Late Clay Minerals 132

B. Isotopic Constraints on Diagenesis 135
C. Diagenetic Model - Summary 145
CONCLUSIONS 151
BIBLIOGRAPHY 157
APPENDIX I 183

LIST OF TABLES

Table 3.1 X-Ray Diffraction Analysis of Shales..... 37

Table 3.2 Petrography of Sandstones and Conglomerates.... 46

Table 3.3 X-Ray Diffration Analysis of Sandstones and Conglomerates..... 51

Table 3.4 Nature of Illite/Smectite in Sandstones..... 81

Table 3.5 Isotope Results for Carbonates..... 107

Table 3.6 Isotope Results for Silicates..... 110

Table 3.7 Microprobe Results..... 115

LIST OF FIGURES

Figure 1.1 Location Map.....5
Figure 1.2 Stratigraphic Correlation of The Viking..... 6
Figure 1.3 Albian Seaways.....9
Figure 1.4 Paleohydrology..... 11
Figure 1.5 Grain Size Scale..... 16
Figure 1.6 Lithologic Symbols..... 17
Figure 1.7 Geophysical to Litholog Correlation..... 19
Figure 2.1 Cross-Section - Caroline to Gilby..... 28
Figure 2.2 Fence Diagram - Ferrier..... 31
Figure 2.3 Fence Diagram - Willesden Green..... 32
Figure 2.4 Fence Diagram - Gilby..... 33
Figure 2.5 Fence Diagram - Caroline..... 35
Figure 3.1 Nature of Illite/Smectite in Shales..... 38
Figure 3.2 Classification of Bulk Mineralogy..... 44
Figure 3.3 X-Ray Diffraction Analysis of Chlorite..... 69
Figure 3.4 Degree of Ankeritization of Detrital Dolomite. 74
Figure 3.5 X-Ray Diffraction Analysis of Kaolin Group Minerals..... 76
Figure 3.6 Clay Minerals in Coarse-Grained Rocks..... 78
Figure 3.7 Nature of Illite/Smectite in Fine-Grained Sandstones..... 79
Figure 3.8 Paragenetic Sequence..... 104
Figure 3.9 Summary of Oxygen-Isotopes..... 112
Figure 4.1 Summary of Carbon-Isotopes..... 122
Figure 4.2 Chemical Composition of Ankerite..... 131
Figure 4.3 Location of samples for Stable Isotopes..... 139

Figure 4.4 Fluid Evolution Model..... 141
Figure 4.5 Diagenetic Model..... 146

LIST OF PLATES

Plate 3.1 Thin Section Photomicrographs..... 63

Plate 3.2 Thin Section Photomicrographs..... 65

Plate 3.3 Thin Section Photomicrographs..... 83

Plate 3.4 SEM Photomicrographs..... 85

Plate 3.5 SEM Photomicrographs..... 87

Plate 3.6 SEM Photomicrographs..... 89

Plate 3.7 Thin Section Photomicrographs..... 91

Plate 3.8 SEM Photomicrographs..... 93

Plate 3.9 Thin Section Photomicrographs..... 95

Plate 3.10 Thin Section Photomicrographs..... 97

Figure 3.11 SEM Photomicrographs..... 99

Figure 3.12 SEM Photomicrographs..... 101

LIST OF ABBREVIATIONS

The following abbreviations are used in the Tables and Figures:

ROCK TYPES

Congl. = Conglomerate

C.Sst. = Coarse-Grained Sandstone

M.Sst. = Medium-Grained Sandstone

F.Sst. = Fine-Grained Sandstone

BULK MINERALOGY FROM THIN SECTION

Ch= Chert

Q = Quartz

F = Feldspar

RF= Rock Fragments

Dol= Dolomite

Cal= Calcite

Ank= Ankerite

Sid = Siderite

C = Clay Minerals

MINERALOGY FROM X-RAY DIFFRACTION, THIN SECTION, AND SCANNING ELECTRON MICROSCOPY

1 μm = Micrometer (1 X 10^{-4} meters)

1 Å = Angstrom (1 X 10^{-10} meters)

Q = Quartz

F = Feldspar

C = Clay Minerals

IS= Illite/Smectite

SM= Smectite

Chl= Chlorite

I = Illite

K = Kaolinite

AF= Authigenic Feldspar

AQ= Authigenic Quartz

2 ø =Secondary Porosity

Chl=Chlorite

Ank=Ankerite

Dol=Dolomite

Sid= Siderite

Py= Pyrite

Gl=Glauconite

MINERAL ABUNDANCES

nd= Not Detected

t = Trace (<2%)

mt= Minor or Trace (2-5%)

m = Minor (5-10%)

mM= Moderate (10-35%)

M = Major (>35%)

I. INTRODUCTION

A. Purpose of Study

The purpose of this study is to determine the diagenetic history of the Viking Formation in south-central Alberta. Over the last ten years, studies of clastic diagenesis have evolved from a purely descriptive science into a much more applied science. This is because diagenetic changes can severely alter the porosity and permeability of sandstone reservoirs. By understanding diagenetic processes it is possible to develop exploration models that may better predict reservoir quality.

Much of the understanding of clastic diagenesis has come from studies of sandstone reservoirs in the United States, particularly in the Gulf Coast and the northwestern States. The Gulf Coast area contains a thick sequence of Tertiary clastic rocks and mineralogical changes within a formation can be observed with depth (e.g., Boles and Franks, 1979; Milliken et al., 1981; Land, 1984). Studies in the Gulf Coast have provided useful information concerning diagenetic processes that occur in an actively subsiding sedimentary basin. Some of these processes include the possible influence that shale diagenesis has on sandstone cementation (e.g., Boles and Franks, 1979), and the influence that organic matter maturation in shales has on sandstone cementation (e.g., Franks and Forester, 1984). Studies of Cretaceous clastic rocks in the northwestern

United States have provided useful information concerning the formation of early diagenetic cements through biogenic and bacterial action (e.g., Gautier, 1982, 1983).

The interpretation of the diagenesis of sandstones within the Alberta basin is more complicated than in the Gulf Coast because of uplift and erosion. The second phase of the Laramide orogeny (early Eocene) resulted in overthrusting, uplift and erosion of Tertiary sediments (Taylor et al., 1964; Hitchon, 1984). The beginning of overthrusting would have also allowed meteoric water to penetrate into the basin and mix with original connate water (Hitchon and Friedman, 1969; Hitchon, 1984). Thus, the evolution of fluids in the Viking Formation probably includes a significant meteoric water influence, simple thermal or compactional models, such as those proposed for the Gulf Coast (e.g., Galloway, 1984) may not pertain. Isotopic studies of clastic rocks lying stratigraphically above the Viking (e.g., Milk River and Belly River Formations) indicate that diagenesis has been significantly affected by meteoric waters (e.g., Longstaffe, 1983, 1984, in press; Ayalon and Longstaffe, 1985).

In order to interpret the diagenesis of the Viking Formation the effects of uplift and meteoric water invasion must be determined. During burial of the Viking diagenetic phases probably crystallized but may have been dissolved during an influx of meteoric water. Many diagenetic phases present in the Viking sandstones probably crystallized after

the influx of meteoric water. In order to determine when diagenetic phases formed detailed petrographic studies must be performed. This will help to establish how cementation varies between different lithologies and help to establish the paragenetic sequence of mineral emplacement. Studying the stable isotope geochemistry of certain authigenic minerals will help to determine the types of fluids and temperatures present during their crystallization. By combining petrographic and stable isotope data it may be possible to determine the effects that burial, uplift and meteoric water mixing had on diagenesis in the Viking.

The specific objectives of this study are as follows: (1) to describe the types of lithologies present and their distribution; (2) to describe the detrital and authigenic mineralogy of the different lithologies in order to determine any initial controls on diagenesis and to establish the paragenetic sequence of mineral emplacement; (3) to relate the paragenetic sequence to processes that have been established from other studies of clastic diagenesis, such as in the Gulf Coast and northwestern United States; (4) to study the stable isotope geochemistry of certain authigenic minerals in order to determine the types of fluids that were present during various stages of diagenesis; and (5) to develop a model that accounts for the diagenesis of the Viking Formation during both burial and uplift.

B. Location and Stratigraphy

In south-central Alberta, the Viking Formation consists of a northeastward thinning clastic wedge deposited on a shallow marine shelf during lower Cretaceous time. Proven reserves of 98 mbbl oil and 31 tcf of raw gas are contained within the Viking and are concentrated in a number of isolated fields (Figure 1.1). All the fields occur in the subsurface at burial depths that range between 1200 and 3000 meters. Most of the production comes from coarse-grained sandstones and conglomerates with minor production from fine-grained sandstones.

The Viking Formation in central Alberta (Figure 1.2) consists of marine clastic rocks underlain by marine shales of the Joli Fou Formation and overlain by the marine Lloydminster Shales. Formations that are stratigraphically equivalent to the Viking include the Bow Island (southern Alberta), Peace River (northwestern Alberta) and Pelican (northeastern Alberta)(Figure 1.2). The Viking Formation has also been correlated to the Muddy and New Castle sandstones (Ashville Formation) in northwestern United States (Magdich 1955; Stelck, 1958, 1975; Glaister 1959; Rubkin, 1964; Berg and David, 1968).

Bentonites within the Viking Formation have been radiometrically dated at 100 ± 2 Ma (Tizzard, 1974); these data agree with biostratigraphic evidence placing this formation in the mid-upper Albian stage (Stelck, 1958, 1975) (Figure 1.2).

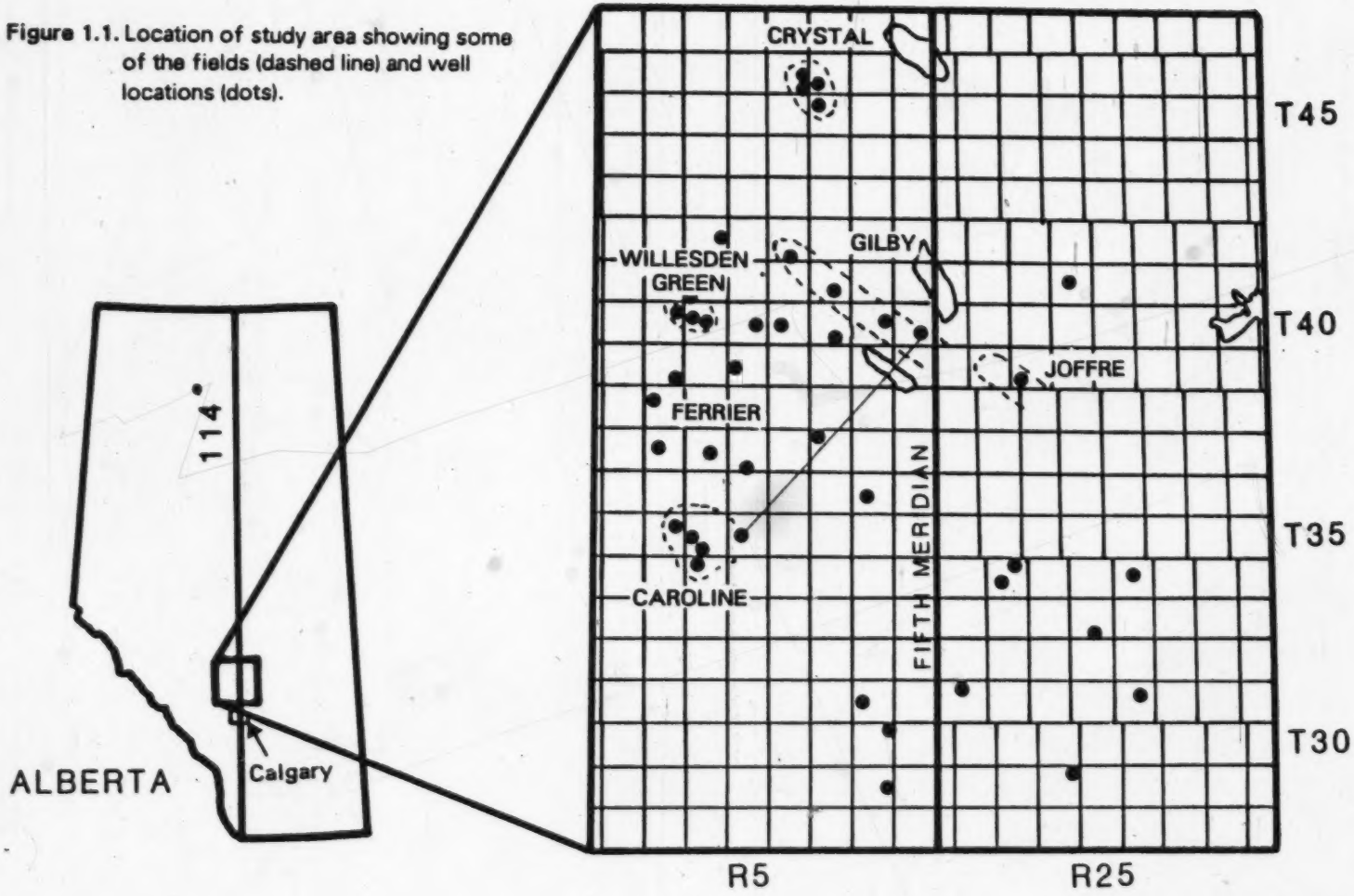

Figure 1.1. Location of study area showing some of the fields (dashed line) and well locations (dots).

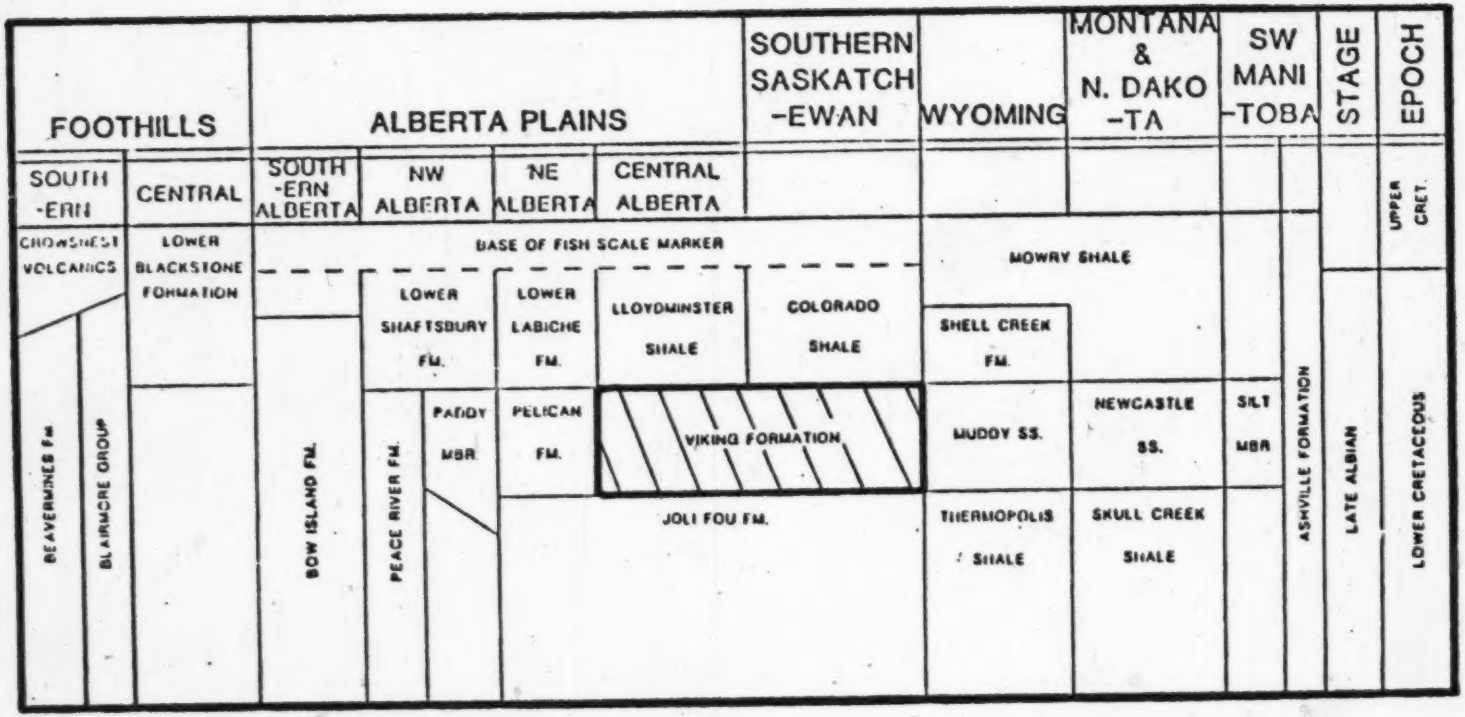

Figure 1.2. Stratigraphic correlation of the Viking Formation in Alberta, Saskatchewan and northwestern United States (modified after Amajor, 1980).

C. Geologic History

Tectonic Setting

The Viking Formation was deposited in a subsiding basin east of the Alberta fold-and-thrust belt that resulted from the subduction of the Pacific plate beneath the western edge of the North American plate (Price, 1973; Dickinson and Synder, 1978; Beaumont, 1981; Jordon, 1981). The first phase of subduction (late Jurassic to early late Cretaceous) is commonly referred to as the Columbian orogeny and reflects an eastward migration of the fold-and-thrust belt (Amajor, 1980). Deformation during the early Jurassic (Nevadan orogeny) was restricted to the Omineca Geanticline (western British Columbia). By Aptian/Albian time, the collision of the island arc complex with the continent resulted in extensive plutonism and volcanism in the Cordilleran geosyncline.

These early phases of mountain building uplifted the previously formed miogeoclinal wedge and created a source for most of the Jurassic and Cretaceous sediments (Beaumont, 1981). The combination of thrust loading and sediment loading after erosion probably enhanced basin subsidence and the development of a foredeep in Western Alberta (Rice, 1980; Jordan, 1981).

Late Albian Transgressions

Minor variations in subsidence rates resulted in two major transgressions during the late Albian. The Joli Fou Formation (Figure 1.2) represents a period of maximum transgression of the Boreal and Gulfian seas during the early late Albian (Williams and Stelck, 1975; Weimer, 1983) (Figure 1.3A). A regressive phase in the late late Albian marks the beginning of Viking deposition as sediments eroded off the rising Cordilleran prograded onto the shallow, epicontinental shelf of the Mowry sea (Figure 1.3B). The second major transgression occurred in the late early Turonian and deposited the Colorado and Lloydminster shales (Figure 1.3C).

Laramide Orogeny

The early phase of the Laramide orogeny began in the late Cretaceous and was characterized by extensive thrusting and uplift along the eastern Cordilleran (Taylor et al., 1964; Dickinson and Snyder, 1978). Thrusting and erosion continued into the early Tertiary and resulted in the deposition of a thick sequence of Paleocene clastic rocks and caused maximum downwarping of the basin (Beaumont, 1984). Maximum burial depths were attained in the late Paleocene to early Eocene (50 Ma) and correspond to the end of this initial orogenic pulse (Taylor et al. 1964; Hitchon, 1984).

A. EARLY LATE ALBIAN

Deposition of the Joli Fou Formation.

B. LATE LATE ALBIAN

Deposition of the Viking Formation.

C. LATE EARLY TURONIAN

Deposition of the Lloydminster Shale.

Figure 1.3. Position of the Cretaceous seaways during the late Albian and early Turonian (modified after Williams and Stelck, 1975).

The second phase of the Laramide orogeny occurred in the early Eocene and caused extensive uplift and erosion of Paleocene and upper Cretaceous rocks. Erosion has removed all but a small portion of the Paleocene clastic rocks that are still present adjacent to the foothills (i.e., Paskapoo and Porcupine Hills Formations)(Taylor et al., 1964; Wheeler et al., 1974; Beaumont, 1981).

Isotopic studies of formation waters from the western Canada sedimentary basin indicate that original connate waters have probably been modified by mixing with meteoric waters (Clayton et al., 1966; Hitchon and Friedman, 1969; Kharaka et al., 1973; Longstaffe, 1983, 1984, in press). The beginning of overthrusting associated with the second Laramide orogenic pulse (early Eocene) created a large hydraulic head in the eastern foothills and allowed meteoric waters to penetrate deep within the basin and discharge eastward (Hitchon and Friedman, 1969; Hitchon, 1984)(Figure 1.4). Toth (1980) indicated that the present hydraulic head in the Rocky Mountains allows groundwater to circulate to depths in excess of 3000 meters. The influx of meteoric water has continued throughout the Tertiary to the present and has resulted in the movement of large amounts of dissolved material through the subsurface (Toth, 1980; Hitchon, 1984).

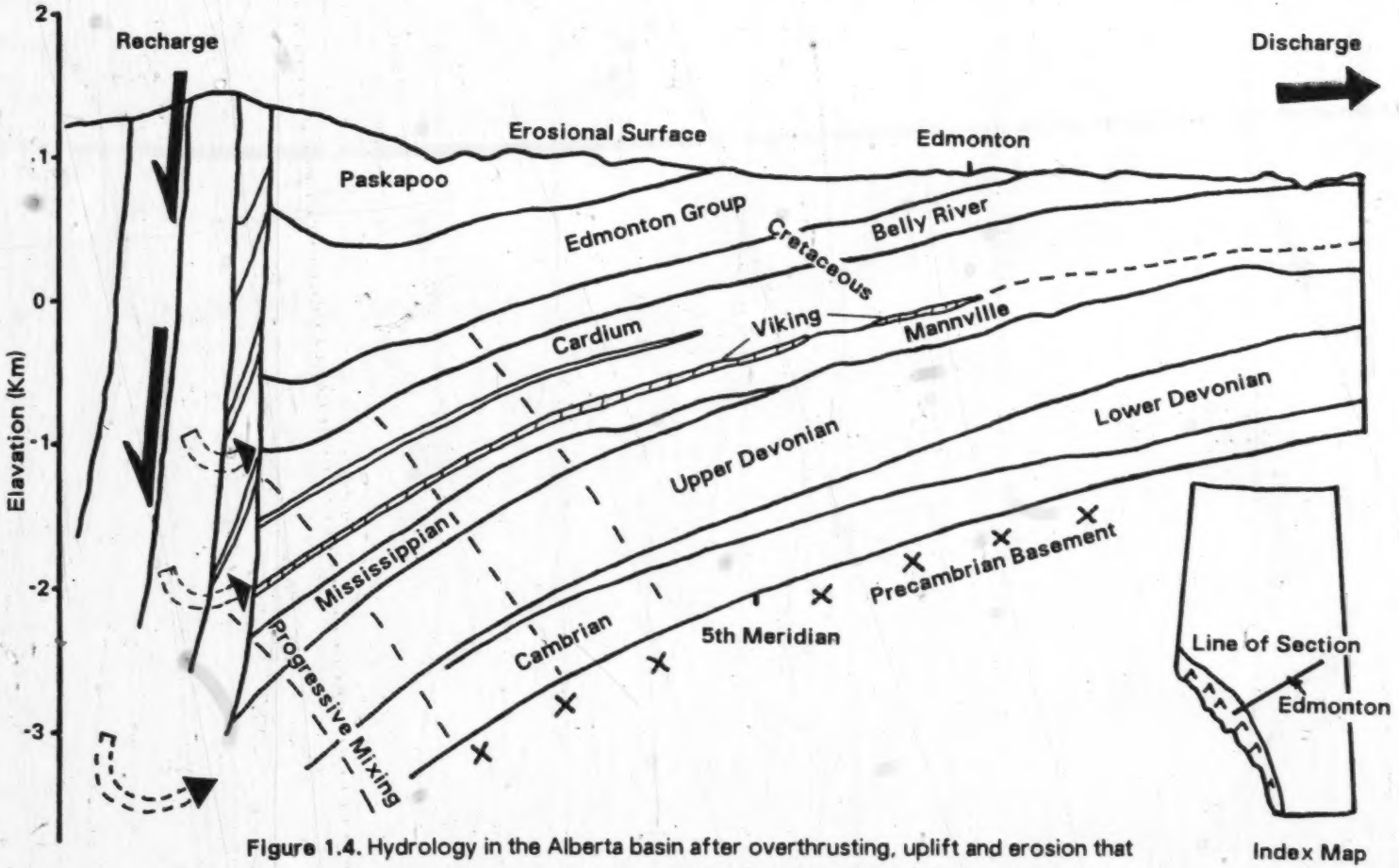

Figure 1.4. Hydrology in the Alberta basin after overthrusting, uplift and erosion that occurred during the second phase of the Laramide orogeny (modified after Hitchon and Friedman, 1969; Jackson, 1975).

D. Previous Work

The Viking was first described by Slipper (1918) and since then numerous studies have been carried out mainly on lithostratigraphy and depositional environments (e.g., Hume, 1933; Nauss, 1945; Bullock, 1950; Gammell, 1955; DeWeil, 1956; Glaister, 1958, 1959; Roessingh, 1959). Recent interest in the Viking has also been placed upon depositional processes (e.g., Amajor, 1978, 1980, 1984; Thomas, 1977; Beaumont, 1984; Hein et al., in press; Leckie, in press).

Hein et al. (in press) studied regional patterns of sedimentology of the Viking Formation at Caroline, Harmattan East and Garrington of western south-central Alberta. The Viking was characterized as a coarsening-upward sequence consisting of 20-25 m of interbedded and loaded fine-grained sandstone and shale, 6-12 m of fine-grained sandstone containing low angle, cross-stratification, and up to 4 m of chert-pebble conglomerate and pebbly sandstone. Three main periods of deposition were recognized, the first consisting of progradation of a shoreline-attached, clastic wedge during a regression that resulted in the deposition of the fine-grained sandstones and shales. The second phase was characterized by the cut-and-filling of conglomeratic channels. The third phase consisted of marine reworking of material on the shelf into sheet-like deposits of sandstone and conglomerate.

Leckie (in press) studied the Viking at Caroline and reported similar features as above. These included a lower regressive sequence of fine-grained sandstones, shales and siltstones and an upper transgressive complex of medium to coarse-grained sandstones and conglomerates.

Studies concerning the mineralogy and diagenesis of the Viking are less common. The Viking was described by Gammell (1955) as a succession of silty and sandy bentonites and sandstones. The sandstones were described as subgraywackes consisting of white quartz and rounded black chert grains cemented mostly by silica. Glauconite, white chert, kaolin group minerals and ironstone concretions were also observed in varying amounts.

Glaister (1959) described the Viking in central Alberta as a succession of "salt-and-pepper" protoquartzites or agrillaceous protoquartzites interbedded with gray to dark grey siltstones and shales. The sandstones were described as consisting mostly of clear quartz and black to dark gray, subangular to subrounded chert grains; glauconite and mica were common accessory minerals. Silica was identified as the dominant cement. Grain size and the amount of argillaceous matrix were shown to increase southwestward, towards the source.

Thomas and Oliver (1979) conducted a regional study of the Viking and Cardium Formations of central Alberta. They indicated that the Viking shows a normal decrease in porosity with depth from 640m to 2640m which was attributed

to mechanical compaction, chemical compaction (pressure solution) and quartz overgrowth development. It was shown that at shallow depths mechanical compaction was more evident in the coarse-grained rocks than in the fine-grained rocks. The higher resistance to mechanical compaction in the fine-grained rocks was attributed to a greater number of grain contacts per unit volume. However, it was also indicated that at greater depths a higher number of grain contacts may have enhanced pressure solution and may be the reason that the fine-grained rocks are more extensively cemented by quartz than the coarse-grained rocks. Authigenic clays, including kaolin group minerals, illite, chlorite and smectite were also detected but their occurrences did not show any relationship to depth-porosity changes. It was indicated that early clay coats may have inhibited quartz cementation.

Foscolos et al. (1982) studied the Viking in east-central Alberta (Provost) where burial depths are approximately 1000 m. In this area two sandstones were identified, a shallow buried lithic arkose containing minor glauconite and a deeper buried sublitharenite with abundant glauconite and clay minerals. In the shallow sandstone, kaolin group minerals were the dominant authigenic phase and were reported to have formed through the replacement of feldspar. In the deeper sandstone, calcite was more abundant and where the calcite was absent, quartz cementation was extensive; calcite was interpreted to be an early phase that

may have inhibited quartz cementation. In the lower sandstone shrinkage porosity was detected and attributed to the alteration of glauconite. Smectite and mixed-layered clays were detected in both types of sandstone.

Tooth et al. (1984) studied the Viking at Dodsland, Saskatchewan where burial depths are near 700 m. The sandstones in this area were described as consisting mostly of quartz and lesser amounts of chert, clay minerals, feldspar, glauconite and mica. The dominant cements were determined to be quartz, feldspar and clays but minor pyrite, siderite and dolomite were also detected. The dominant clays were reported to be illite, smectite and mixed layered illite/smectite; minor kaolinite and chlorite were also reported.

E. Analytical Methods

Core Description

Regional variations in lithologies were documented by describing 27 cores in detail (for core descriptions see Appendix-I). Grain size (phi scale) was measured using a binocular microscope and grain size charts (Figure 1.5). The cores were described with careful notation of grain size, sedimentary and biogenic structures, nature of all lithologic contacts, and mineralogy. Cross sections and fence diagrams were constructed to reveal regional variations in lithologies. Sections were drawn using standard lithologic symbols (Figure 1.6). Problems in

Millimeters	Phi (ϕ)	Wentworth Size Class	
4096	-12		
1024	-10	Boulder (-8 to -12ϕ)	GRAVEL
256	- 8		
		Cobble (-6 to -8ϕ)	
64	- 6		
16	- 4	Pebble (-2 to -6ϕ)	
4	- 2		
3.36	- 1.75		
2.83	- 1.5	Granule	
2.38	- 1.25		
2.00	- 1.0		
1.68	- 0.75		
1.41	- 0.5	Very coarse sand	
1.19	- 0.25		
1.00	0.0		
0.84	0.25		
0.71	0.5	Coarse sand	
0.59	0.75		
1/2 — 0.50	1.0		SAND
0.42	1.25		
0.35	1.5	Medium sand	
0.30	1.75		
1/4 — 0.25	2.0		
0.210	2.25		
0.177	2.5	Fine sand	
0.149	2.75		
1/8 — 0.125	3.0		
0.105	3.25		
0.088	3.5	Very fine sand	
0.074	3.75		
1/16 — 0.0625	4.0		
0.053	4.25		
0.044	4.5	Coarse silt	
0.037	4.75		
1/32 — 0.031	5.0		
1/64 0.0156	6.0	Medium silt	MUD
1/128 0.0078	7.0	Fine silt	
1/256 — 0.0039	8.0	Very fine silt	
0.0020	9.0		
0.00098	10.0	Clay	
0.00049	11.0		
0.00024	12.0		
0.00012	13.0		
0.00006	14.0		

Figure 1.5. Grain Size Scale (after Folk, 1968).

Figure 1.6. Lithologic symbols and sedimentary structures.

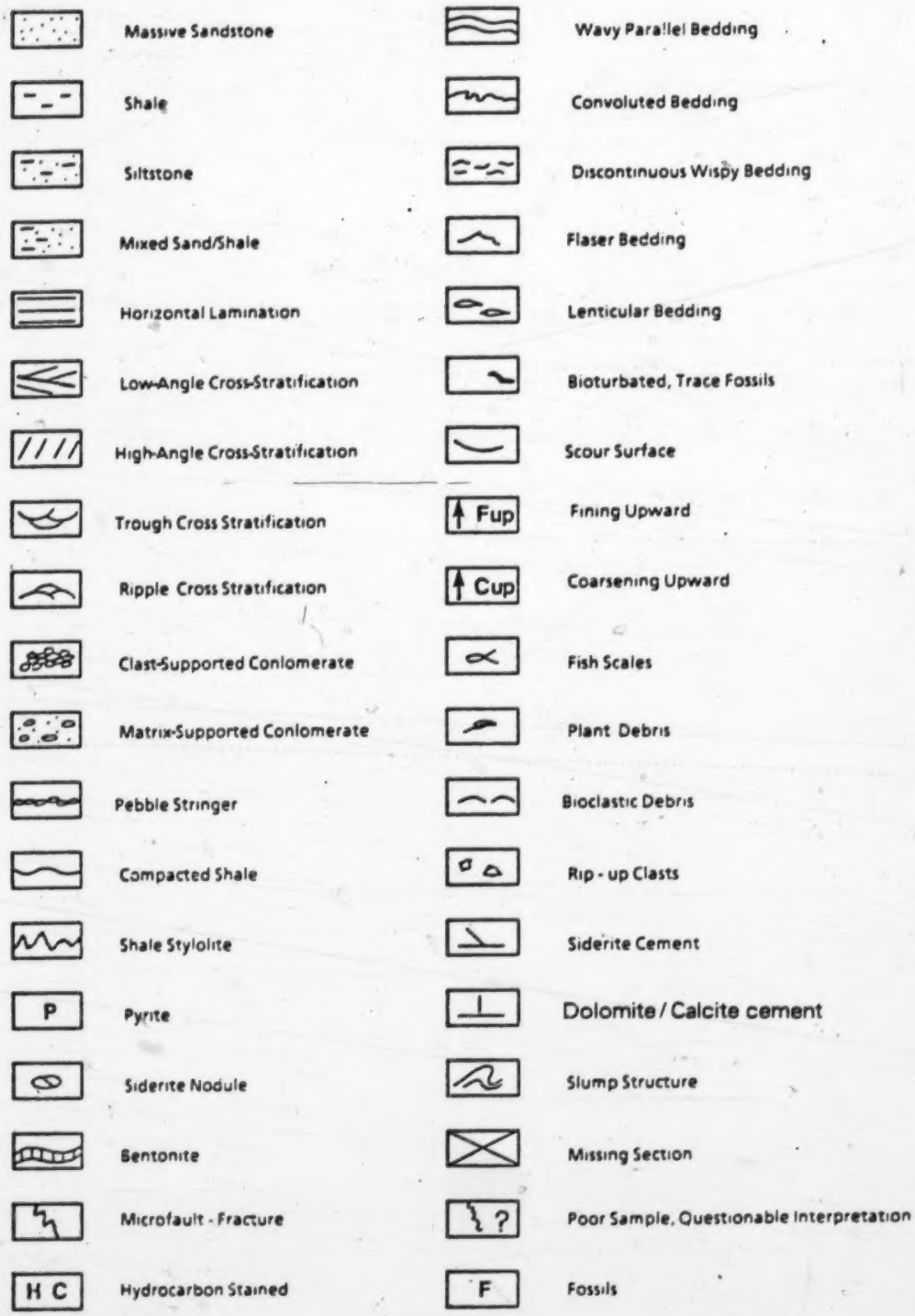

logging of core occurred where portions were missing, removed, broken or scored by the core barrel.

Correlation of Geophysical Logs

Geophysical logs (gamma-ray, spontaneous potential, and shallow resistivity) were used to supplement lithologic logs for the purpose of constructing sections (Figure 1.7). The Base of Fish Scales Marker has been used as a regional datum in all sections and is considered a good time stratigraphic marker (Amajor, 1978, 1980). Where coring has not penetrated complete Viking sections geophysical logs are used to determine thicknesses of lithologic units (Figure 1.7).

Core Sampling

Samples for mineralogical analysis were obtained by cutting one cm^3 of the core at various intervals. More than 300 samples were selected from all lithologies, including conglomerates, coarse and fine-grained sandstones, and shales.

Hydrometer Analysis

The percentage of fine-grained material in each sample was determined by hydrometer analysis. Prior to analysis, each sample was disaggregated, care being taken to preserve the original grain-size distribution. Grains larger than 2 mm were removed by sieving. A minimum of 20 grams of material from each sample was soaked in 125 ml of a 4 % sodium hexametaphosphate solution for 8 hours to further disperse the particles. Ultrasonic disaggregation was used as a final step to ensure thorough dispersion of clay-sized

Figure 1.7. Correlation of lithologs to resistivity logs.

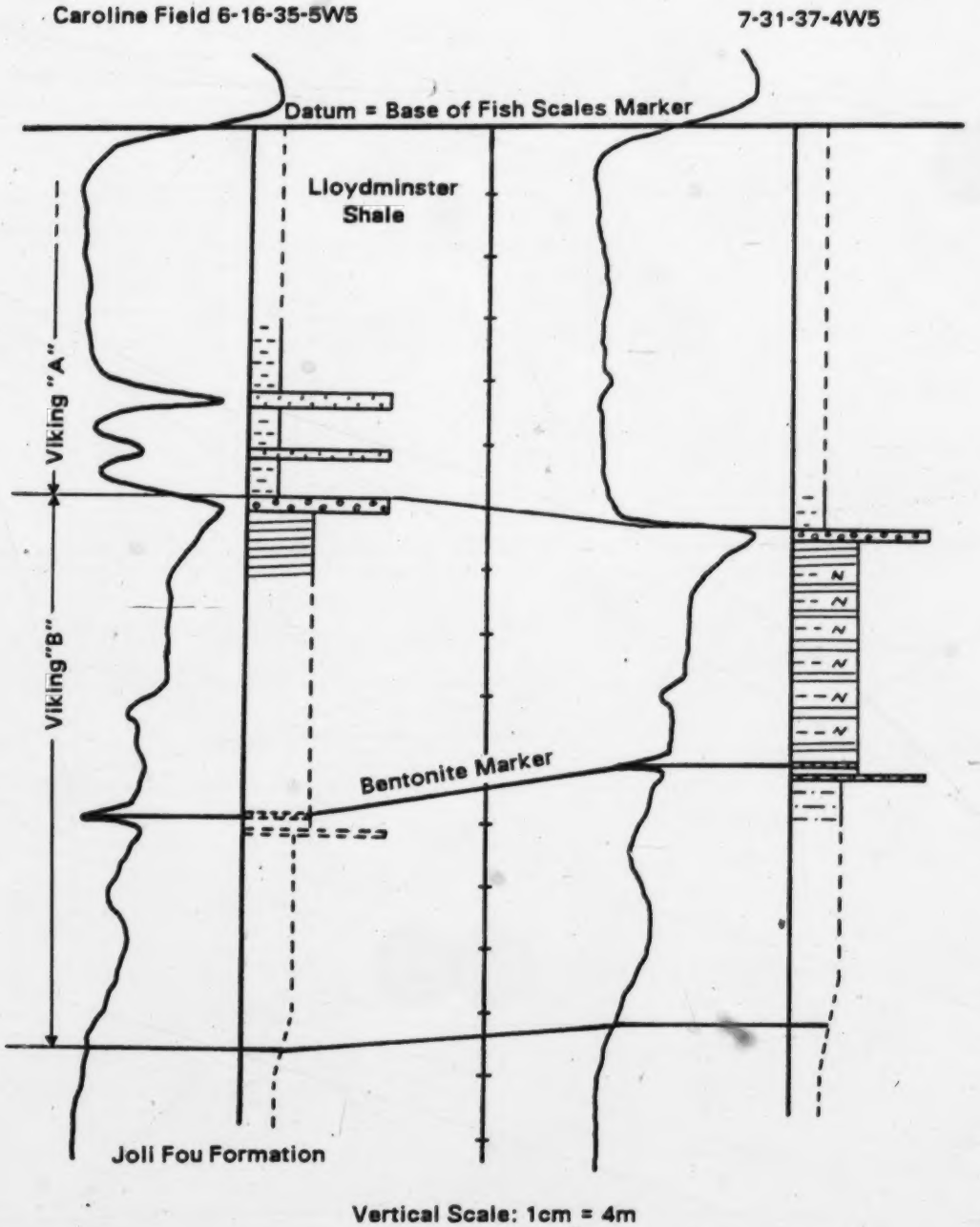

particles.

X-ray Diffraction Analysis

Following hydrometer analysis, the solutions were redispersed and the requisite mineral size-fractions (<0.2, <2.0, 2-5 and 5-20μm) separated at the appropriate time, according to Stoke's Law. To ensure complete separation, the dispersion and settling process was repeated three times for each size-fraction. Approximately 200 ml of sodium hypochlorite was added to flocculate the mineral matter in each size-fraction and to dissolve any organic matter present. The solutions were then heated for two days at 60°C to destroy any residual organic matter. The solutions were thoroughly washed with distilled water using a high speed centrifuge. The <2μm size-fraction was then divided into two portions, one saturated with Ca^{2+} and the other with K^{+}. All the size-fractions were freeze-dried and deposited by suction upon a ceramic disc.

X-ray diffractograms for the discs were obtained using the following conditions (Ignasiak et al., 1983):

1. Co K-alpha radiation, with graphite monochromator;
2. 1 degree divergent slit; time constant = 2;
3. 1 degree two theta/minute at 600 mm/h;
4. 50 KV, 20mA;

The following X-ray charts were obtained for the <2 μm size-fraction:

1. Ca-disc at 54% relative humidity, 2-40 degrees two-theta;
2. Ca-glycolated, 2-62 degrees two-theta;

3. K-disc at 0% relative humidity, 2-40 degrees two-theta;
4. K-disc at 54% relative humidity, 2-22 degrees two-theta;
5. K-disc at 300°C, 2-28 degrees two-theta;
6. K-disc at 550°C, 2-28 degrees two-theta.

For the 2-5μm and the 5-20μm size-fractions, X-ray data was obtained for the unsaturated discs at 54% relative humidity. For the <0.2μm size-fraction X-ray data was obtained for the unsaturated discs at 54% relative humidity, glycolated and at 550°C. For all samples the appropriate conditions were maintained prior to, and throughout, the X-ray analysis. This combination of procedures permits unambiguous identification of the various clay mineral families.

The relative percentage of clay minerals in each size-fraction was determined using diffraction peak-heights (Scafe, personal communication). For the <0.2μm and <2μm material, the heights of (001) X-ray diffraction peaks were measured for smectite, illite and kaolin group minerals using diffractograms for the Ca-saturated, ethlyene-glycol treated samples. The (002) or (003) X-ray diffraction peaks (d = 13 Å) were used for mixed-layer clays present in the samples. For chlorite, the height of the (001) X-ray diffraction was determined from the K-saturated, heat-treated (550°C) XRD pattern. For the 2-5μm and the 5-20 μm size-fractions, all measurements were made using the XRD patterns obtained at 54% relative humidity. To account for the variation in crystallinity of each clay mineral family, form factors were assigned in the following manner:

1. Illite (10 Å) = 1.000;
2. Mixed-layer clay (13 Å) = height of 13 Å peak/2 x height of 10 Å peak;
3. Smectite (17 Å) = height of 17 Å peak/4 x height of 10 Å peak;
4. Chlorite (14 Å) = height of 14 Å peak/3 x height of 10 Å peak;
5. Kaolin group minerals (7 Å) = height of 7 Å peak/2.5 x height of 10 Å peak.

These form factors were summed and the relative percentages calculated for all the phases. For samples containing both chlorite and kaolin group minerals, the kaolinite group mineral (001) and the chlorite (002) basal diffractions overlap. Hence, the amount of kaolin group minerals may be overestimated. To correct for this discrepancy, percentage of chlorite (14 Å) is subtracted from the percentage of kaolin group minerals (7 Å); all results are renormalized to 100% and rounded to the nearest 5%.

Powdered, bulk rock samples were also analyzed by X-ray diffraction. Crushed samples were placed in an aluminum holder and analyzed from 2-62 degrees two theta at room humidity.

Values for relative abundances of quartz, feldspar and clay minerals were determined graphically using standard mixtures of well crystallized kaolinite (KGa1) and quartz for calibration. Relative abundances are reported as

follows:

1. >35% of phase present in sample = major (M);
2. 10-35% of phase present in sample = moderate (mM);
3. 5-10% of phase present in sample = minor (m);
4. 2-5% of phase present in sample = minor to trace (mt);
5. <2% of phase present in sample = trace (t).

Scanning Electron Microscopy

A small chip from the center of each sample was mounted on SEM stubs using conductive silver paint. The stubs were sputter-coated with 20 nm of gold to ensure proper grounding during the analysis. The instrument used for the microscopy was the Cambridge Stereoscan S250. Its accelerating voltage was fixed at 25 KV.

The ratio of crystal widths to pore-throat diameters was determined using SEM. Pore-throat sizes determined in this manner are only an approximation; other techniques, such as acetate peels and mercury injection can be used to quantify these estimates.

A Kevex system 7000 (energy dispersive X-ray analysis, EDAX), coupled to the SEM, was used to obtain chemical data for mineral phases. Analysis were obtained using a beam diameter of 1μm (spot analysis). Accelerating voltages were kept at 20 KEV for all analysis and samples were oriented to minimize beam scatter. Count rates were maintained between 500 and 900 counts per second and the duration of the analysis varied between 30 and 50 seconds. When chemical comparisons are made it should be noted that elements with

low atomic numbers (e.g., Na and Mg) are suppressed while elements with high atomic numbers (e.g., Fe) are enhanced. For these reasons chemical analysis obtained in this manner are qualitative only.

Thin Section Analysis

Thin section analysis was performed to determine the nature and abundance of detrital and authigenic phases. Before preparation samples were impregnated with blue epoxy to emphasize porosity and preserve pore-filling material. Thin sections were stained with potassium ferrocyanide and alizarin red for identification of carbonates. Mineral abundances were obtained by point counts (500 counts per thin section). Classification of rocks was based on the types of framework grains present or originally present, prior to diagenesis.

Polished thin sections were made for selected samples for microprobe analysis. No stains or epoxys were introduced during sample preparation.

Microprobe Analysis

Polished thin sections were analyzed using a microprobe to obtain semi-quantitative chemical compositions of some authigenic phases. The instrument used was an Applied Research Laboratories (ARL-SEMQ) fitted with a 4-wavelength spectrometer and an energy dispersive spectrometer. All analysis were done using a beam diameter of 1μm (spot analysis); the results were accurate to ± 2%.

Stable Isotopes

Kaolin group minerals, quartz, Fe-calcite, ankerite, dolomite and siderite were studied because they are indicative of major diagenetic events and they occur in sufficient abundance for accurate oxygen- and carbon-isotope analysis.

Oxygen-isotope analysis of kaolin group minerals and quartz were performed using the BrF_5 method of Clayton and Mayeda (1963). Petrographic analysis was used to determine whether samples contained authigenic or detrital quartz and kaolin group minerals. The 5-20μm size-fraction was selected for these samples for isotopic analysis because quartz and kaolin group minerals were usually the dominant phases (determined by X-ray diffraction). This material was treated with a boiling 6N HCl solution to remove any traces of chlorite or carbonates. The 5-20μm material was then split into two 100mg portions; the first was retained for isotopic analysis. The second portion was reacted with 10ml of H_2SiF_6 for three days and then washed with 0.1N HF and distilled water. This treatment was followed by a 5ml saturated H_3BO_3 solution for 12 hours. These procedures removed kaolin group minerals, leaving only quartz for isotopic analysis. The isotopic compositions of the quartz is not affected by these treatments (Syers et al., 1968). The isotopic composition of the kaolin group minerals were determined by extrapolation using the quartz isotopic composition and the isotopic composition of the mixture of quartz and kaolin group minerals. The relative abundance of quartz and kaolin group

minerals in each sample was determined by X-ray diffraction.

Prior to isotopic analysis, all samples were dried at +105°C for two hours and maintained at zero humidity for 24 hours before treatment with BrF_5. Replicate analyses of the silicate minerals were better than ± 0.2 permill.

Carbonate minerals were prepared for isotopic analysis by reacting organic-free, powdered rock samples (<44μm) in phosphoric acid using the procedure described by Walthers et al. (1972), modified after McCrea (1950) and Epstein et al. (1964). Petrographic and XRD studies were used to select samples containing >90% of only one carbonate phase. Mixtures of dolomite and ankerite, in varying percentages, were also analyzed. Replicate analyses of carbonate minerals were better than ± 0.2 permill.

The isotope data are presented in the usual δ notation with respect to Standard Mean Ocean Water (SMOW) for oxygen (Craig, 1961) and the *Belemnitella americana* from the Peedee Formation (PDB) for carbon (Craig, 1957). The partitioning of ^{18}O between two phases, A and B, is given by

$$\Delta A\text{-}B = 10^3 \ln\alpha A\text{-}B \simeq (\alpha-1)10^3 \simeq \delta A - \delta B$$

where α is the oxygen-isotope fractionation factor between A and B.

II. REGIONAL VARIATIONS IN LITHOLOGIES

The Viking Formation consists of two main depositional units that are discernable on geophysical logs and in core: (1) Viking "B" deposits and (2) Viking "A" deposits (Figures 1.7 & 2.1). These units reflect alternating periods of progradation and represent a southward stacking of marine sand bodies in response to rising sea levels. A similar feature of the Viking in southern Saskatchewan and south-central Alberta was reported by Amajor (1980). A detailed description of the sedimentary facies comprising these units is given by Hein et al. (in press).

A. Viking "B" Deposits

Lower Coarsening-Upward Unit

The lower part of the Viking "B" records a coarsening-upward sequence of silt and shale (Figure 2.1). The base of the wedge grades upward from the Joli Fou Shale into silty shales of the Viking Formation and reflects the first influx of coarse clastic sediments onto the shelf. The lower coarsening-upward unit is usually 15 to 20 meters thick (thickness were determined using geophysical logs, Figure 1.7) and is continuous over most of the area (Figure 2.1).

Figure 2.1. Cross Section of the Viking Formation from Caroline to Gilby (see Figure 1.1 for line of section).

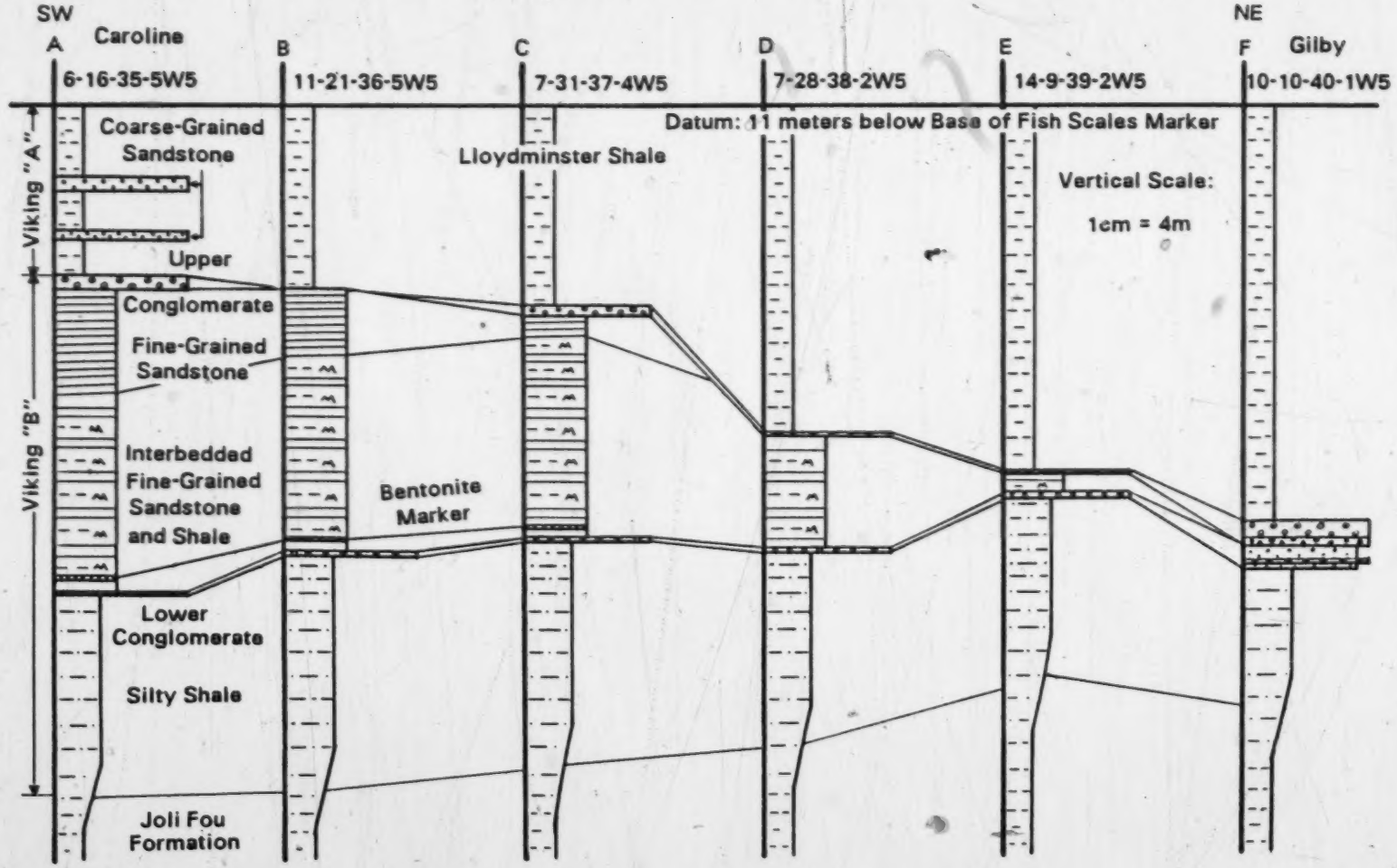

Lower Conglomerate

The silty shale is commonly capped by a thin conglomerate 0.2 to 2 meters thick (Figure 2.1). Towards the south the conglomerate is usually poorly defined and occurs as a thin pebble stringer within the shale. The lower conglomerate reaches thicknesses of up to 2 meters in the north (e.g., Gilby field, Figure 2.1) and has an erosional contact with the underlying silty shale. The southward and northeastward thinning of the lower conglomerate suggests that the source was mainly from the west.

The appearance of the lower conglomerate probably reflects a minor tectonic event that disrupted the overall progradation. A thin bentonite usually occurs along with this conglomerate (Figure 2.1) suggesting increased volcanic activity. The bentonite was useful in correlating the lower conglomerate southward where cores of complete Viking sections are usually not recovered (e.g., Figure 1.7).

Upper Coarsening-Upward Unit

After emplacement of the lower conglomerate, progradation continued from the southwest depositing a coarsening-upward sequence of fine-grained clastic rocks. This unit is thick in the southwest (e.g., Caroline field, Figure 2.1), varying between 20 and 25 meters. Shale content decreases up section and the top 8 to 10 meters usually consists of parallel to low-angle, cross-stratified fine-grained sandstones. The fine-grained sandstone unit

decreases in thickness and its shale content increases towerds the northeast (Figure 2.1). A fence diagram of the Ferrier field (Figure 2.2) indicates that the fine-grained sandstone unit also pinches out towards the northwest, as well as the northeast, suggesting a southwesterly source.

Upper Conglomerate

The top of the Viking "B" is capped by another conglomerate (Figure 2.1). This conglomerate is the dominant reservoir in the Caroline, Ferrier, Willesden Green and Gilby fields and varies from <1 to 8 meters in thickness. The conglomerate has an erosional base with the underlying fine-grained sandstones and this contact may reflect renewed tectonic activity and/or maximum regression of the Mowry sea (Figure 1.3B). The variable thickness of the upper conglomerate suggests marine reworking may have occurred during the following transgression. Extensive reworking of the Viking "B" conglomerates into ridge-and-swale topographies at Garrington was reported by Robb (1985).

Up to 8 meters of conglomerates and coarse-grained sandstones occur at Willesden Green (well # 5-6-41-6W5, Figure 2.3) and up to 4 meters occur at Gilby (well # 10-10-40-1W5, Figure 2.1 and 2.4). These thicker accumulations occur in stratigraphic lows and may represent channel deposition. Within the channels individual coarsening-upward beds are peserved indicating that winnowing of fines did not occur after deposition. A similar

Figure 2.2. Fence diagram east of the Ferrier field.

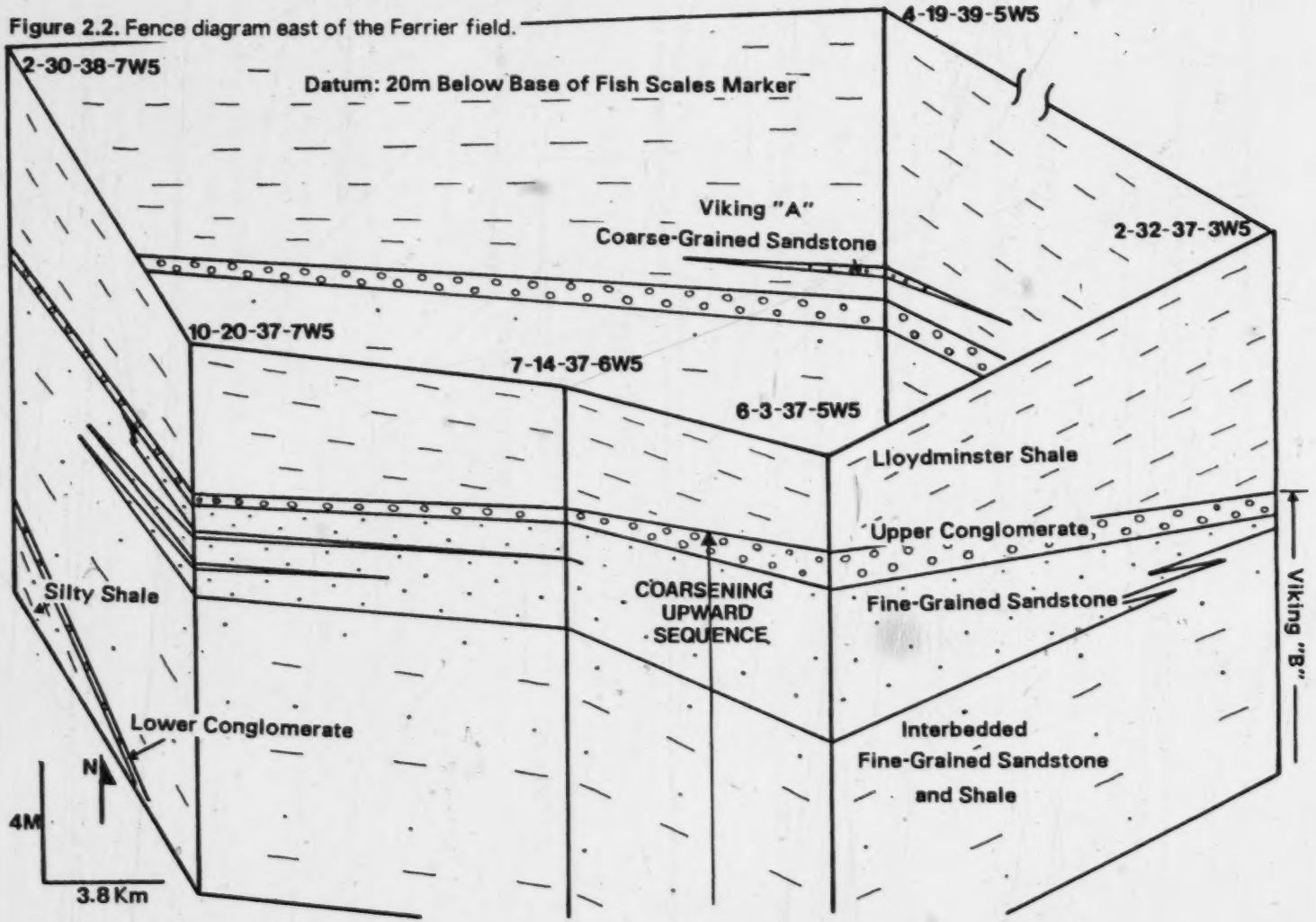

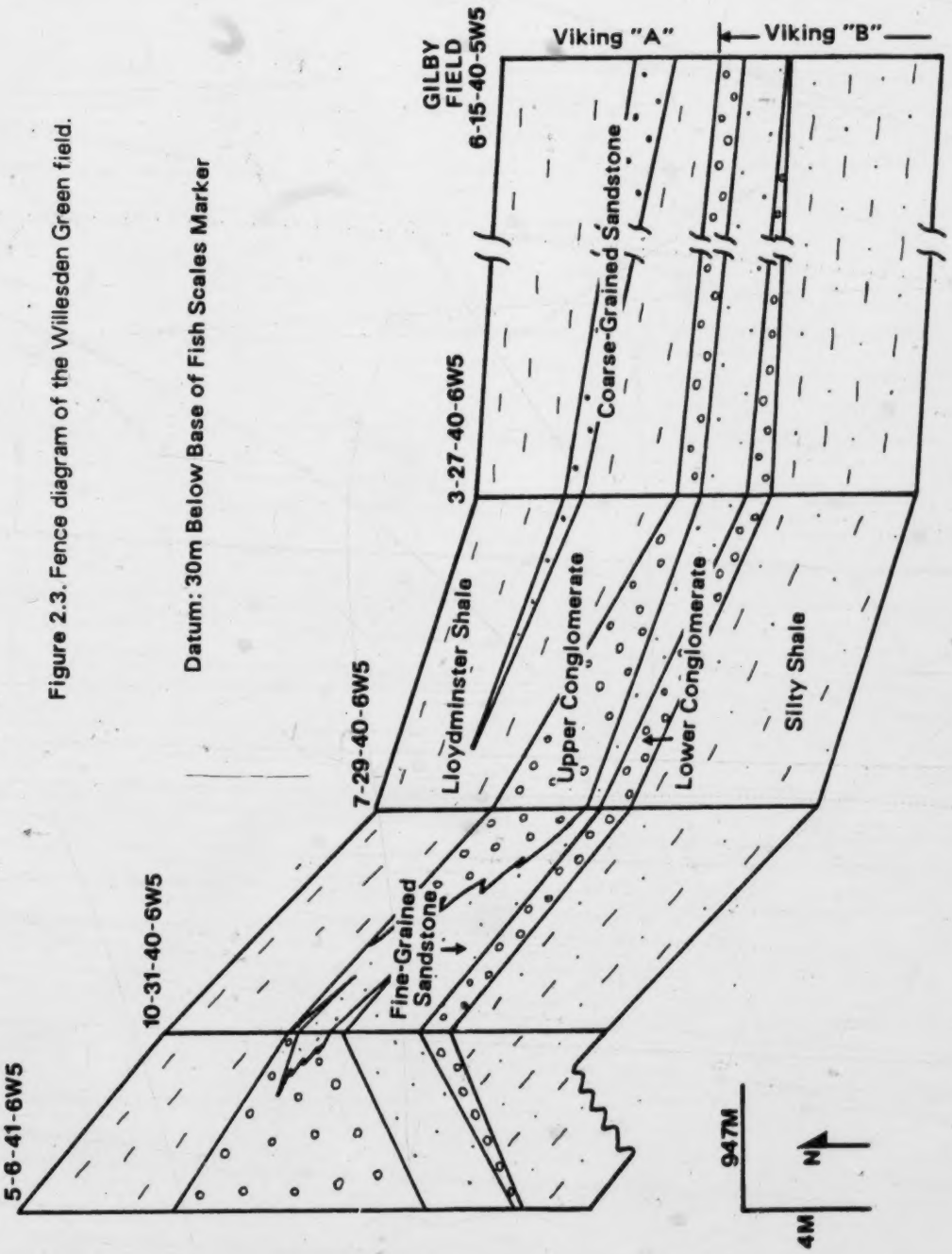

Figure 2.3. Fence diagram of the Willesden Green field.

Datum: 30m Below Base of Fish Scales Marker

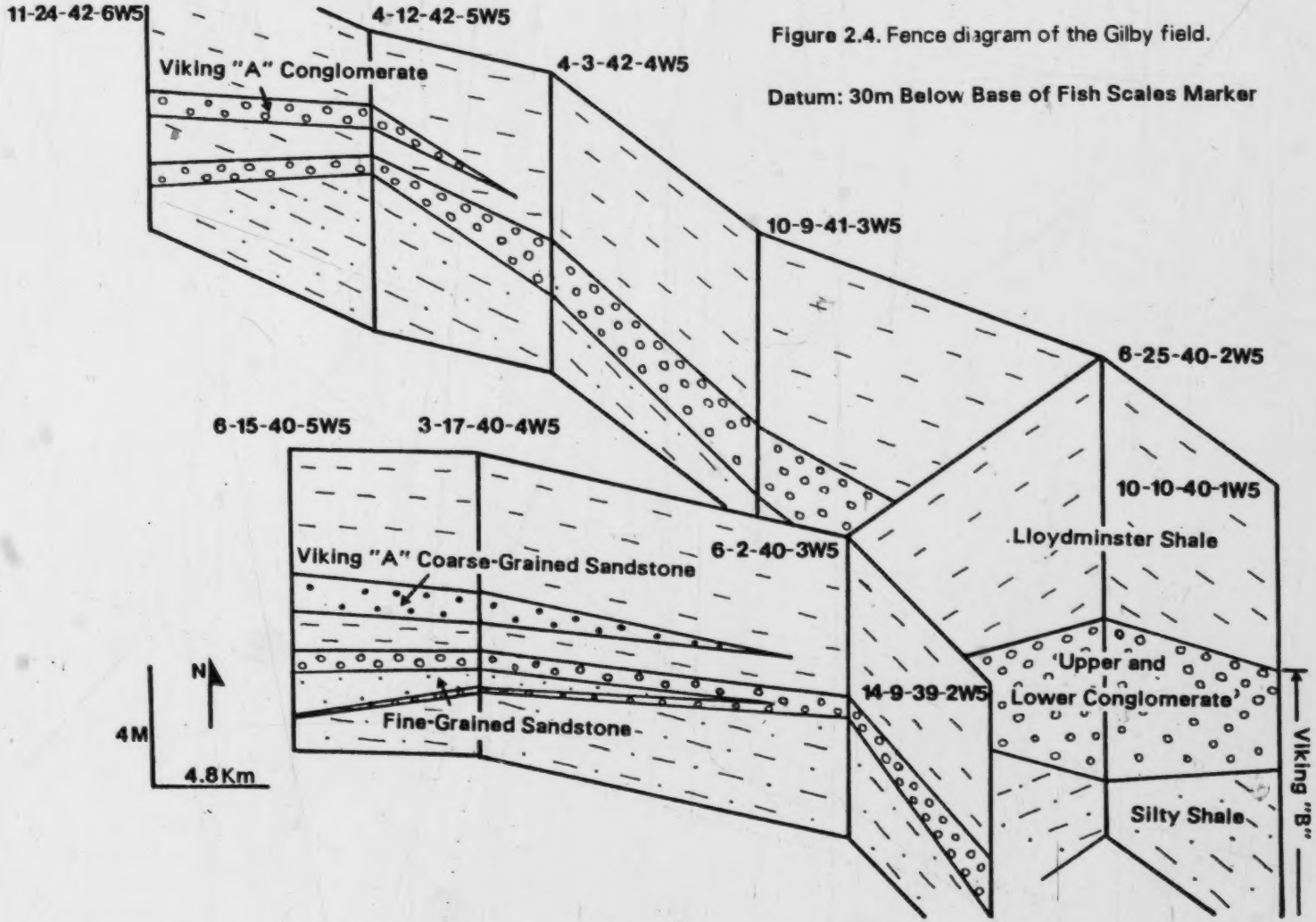

Figure 2.4. Fence diagram of the Gilby field.

Datum: 30m Below Base of Fish Scales Marker

control on the deposition of gravel was suggested by Grant (1985) for the Viking Formation at Harmattan East.

B. Viking "A" Deposits

Viking "A" deposits reflect minor progradational/regressive events during a major transgression that deposited the Lloydminster Shale (Figure 1.3C). The Viking "A" at Caroline (Figure 2.1 and 2.5) consists of two to three pulses of coarse-grained sandstone that are 0.5 to 2m thick and have sheet-like morphologies. These deposits pinch out towards the northeast (Figure 2.1), suggesting a southwesterly source. Viking "A" deposits are also seen in the northwestern part of the Gilby and Willesden Green fields (Figure 2.3 and 2.4) and consist of 1 or 2 pulses of conglomerate or coarse-grained sandstone 0.5 to 1m thick. These deposits pinch out towards the east suggesting a westerly source (Figure 2.4). A change in source for the Viking "A" is also reflected in their detrital mineralogy, as discussed later.

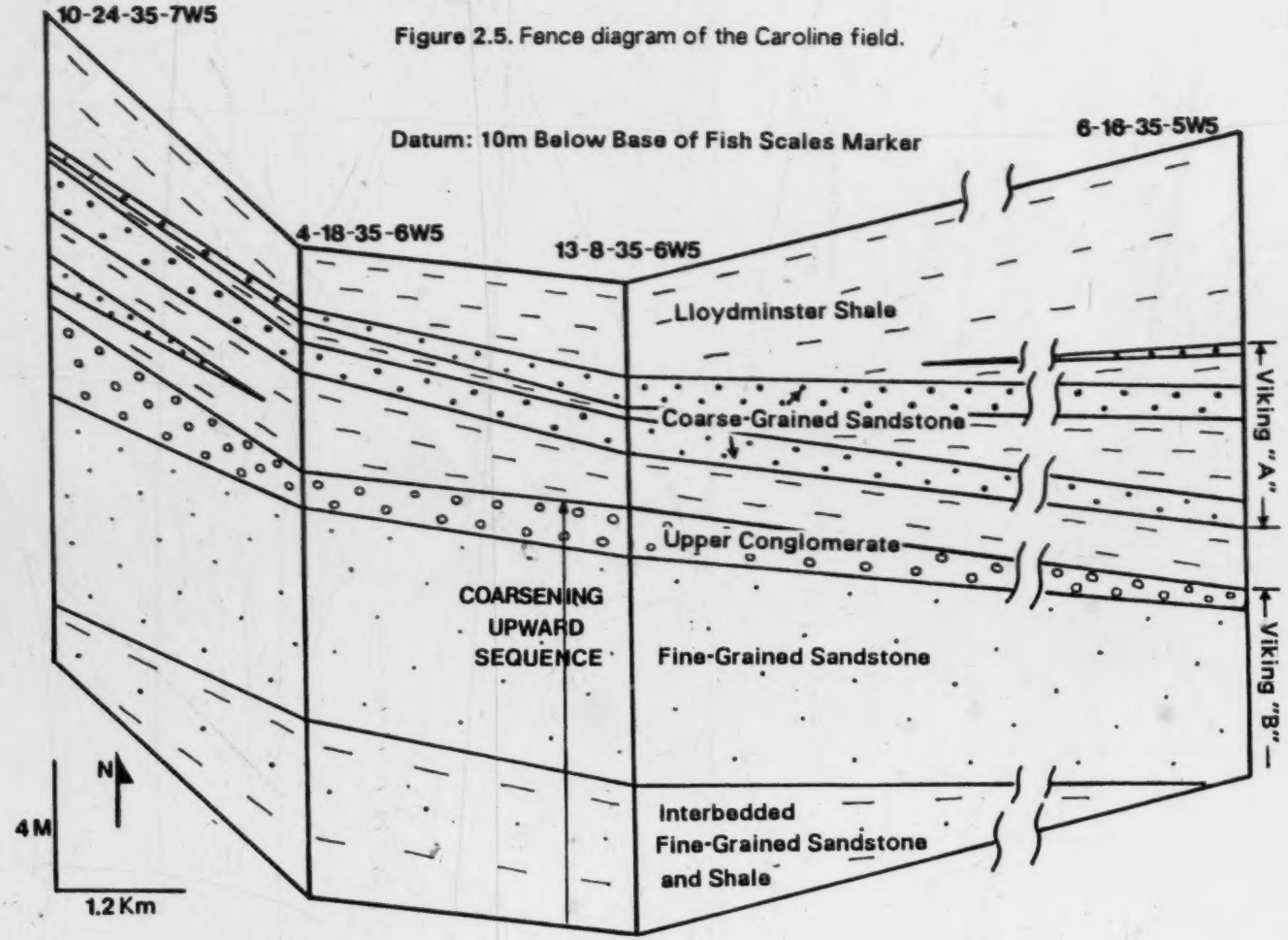

Figure 2.5. Fence diagram of the Caroline field.

III. RESULTS OF MINERALOGY & ANALYTICAL GEOCHEMISTRY

A. Mineralogy of Shales

Shales interbedded with the Viking Formation were analyzed in order to determine mineralogical variations with depth. An important reaction that occurs during burial diagenesis of shales is the illitization of smectite layers in illite/smectite (Perry and Hower, 1970; Boles and Franks, 1979). By studying the compositions of illite/smectite in the Viking shales the extent of illitization can be determined and this may reveal the maximum temperatures reached during burial.

The mineralogy of shales interbedded with the Viking Formation is given in Table 3.1. In all samples clay minerals are a major phase; other phases present include quartz and feldspar. Illite (60-85%) is the dominant clay mineral with lesser amounts of illite/smectite (5-25%), kaolin group minerals (t-20%), chlorite (t-10%) and smectite (nd-5%).

Nature of Illite/Smectite

The percentage of smectite in the illite/smectite decreases with depth (Figure 3.1). The percentage of smectite layers can be determined from the positions of the (001) and (002) basal diffractions (I/S (001) and (002), Figure 3.1).At shallow depths these diffractions are near 13.6 Å (001) and 5.29 Å (002) (Figure 3.1A and 3.1B) and

TABLE 3.1. MINERALOGY of SHALES

SAMPLE NUMBER	DEPTH m	SIZE μm	PHASES			RELATIVE % CLAYS					IS CLAYS (SRODON;1984)	
			Q	F	C	IS	SM	CL	I	K	%SM	ORDERING
16-9-42-4W5												
M85	1936.1	<2	M	nd	M	5	nd	5	80	10	32	Random-IS
		<0.2	t	nd	M	10	nd	5	85	t	39	Random-IS
4-12-42-5W5												
M79	1985.1	<2	t	nd	M	15	nd	5	60	20	34	Random-IS
		<0.2	t	nd	M	25	nd	t	70	5	35	Random-IS
16-19-34-2W5												
MG1	2052.9	<2	t	nd	M	15	nd	10	65	10	22	IS
		<0.2	nd	nd	M	15	nd	5	75	5	29	IS
10-13-35-4W5												
MG94	2174.5	<2	mM	nd	M	10	5	10	65	10	27	IS
		<0.2	nd	nd	M	15	nd	5	80	t	30	IS
7-28-25-4W5												
M72	2711.5	<2	m	nd	M	5	nd	10	80	5	16	IS-ISII
		<0.2	nd	nd	M	10	nd	5	85	t	14	IS-ISII
11-30-30-5W5												
M627	2977.6	<2	t	t	M	10	nd	10	65	15	19	IS-ISII
		<0.2	t	nd	M	15	nd	10	75	mt	17	IS-ISII

Figure 3.1. Nature of illite / smectite in shales, <0.2 μm size-fraction, Na^+ saturated - glycolated (25°C).

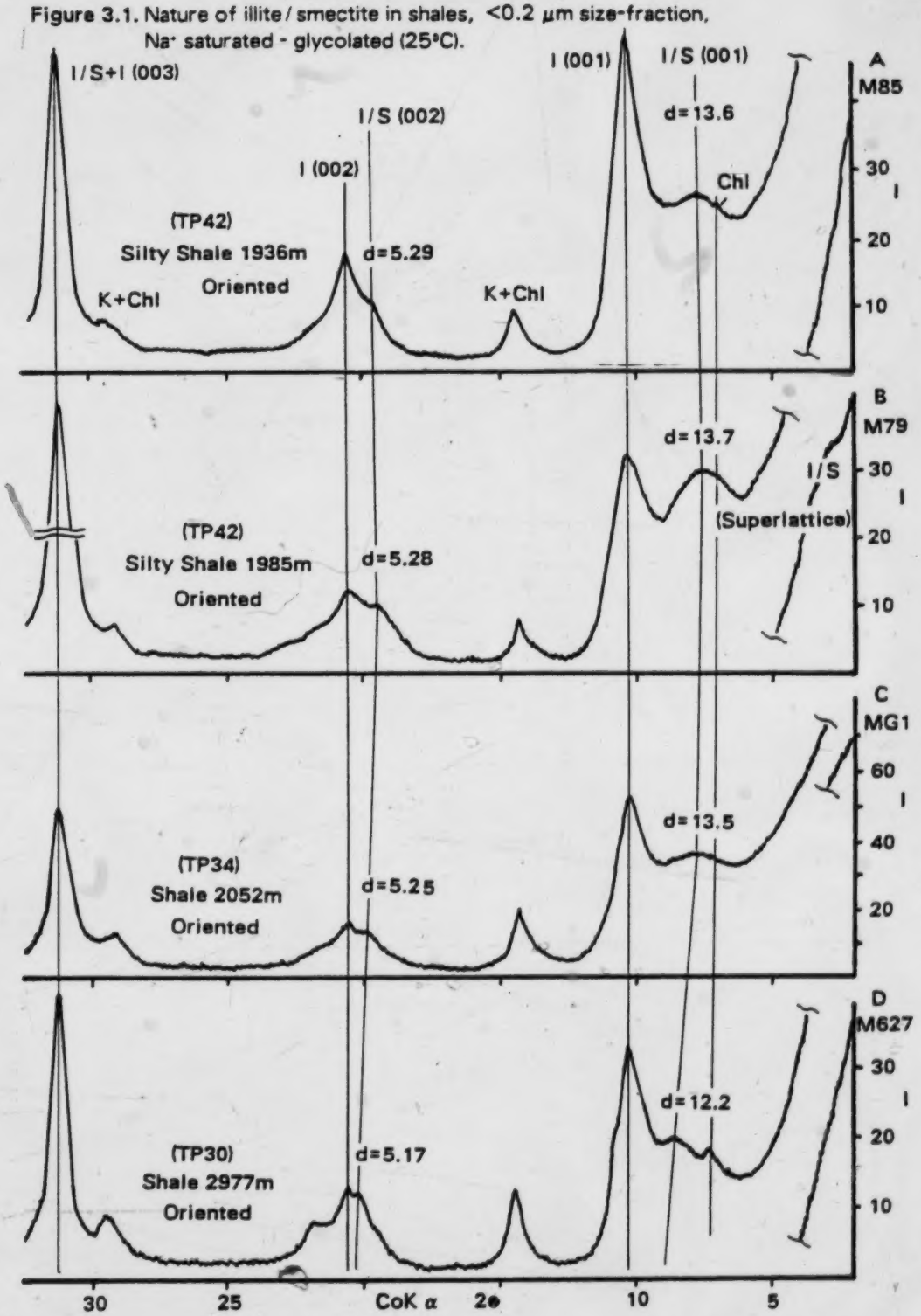

correspond to an illite-glycol smectite with 30-35% smectite layers (Reynolds and Hower, 1970). There is a decrease in the values of these diffractions with depth to a minimum of 12.2 Å (001) and 5.17 Å (002) (Figure 3.1D) reflecting <20% smectite layers (Reynolds and Hower, 1970)

The percentage of smectite layers was also determined by comparing the values of the (002) and (003) diffractions to computer calculated data for various percent smectite layers (Srodon, 1984; Table 3.1). The results show that at shallow depths there are between 32 and 39% smectite layers (e.g., samples M85 & M79, Table 3.1) and at maximum depths between 14 and 19% smectite layers remain (e.g., samples M72 & M627, Table 3.1). Srodon (1984) indicated that the percentage of smectite layers is usually underestimated if abundant discrete illite is present, as in the case of the shales studied (Figure 3.1 and Table 3.1).

A more precise identification of the interstratification was determined by plotting the (001) diffractions values on a plot of different, theoretical illite/smectite types (Srodon, 1984). On the basis of this plot, Srodon (1984) indicated that a continuous series of interstratification types exists including randomly interstratified, I-S ordered (alternating layers of illite and smectite), and ISII ordered (repeating units consisting of illite-smectite-illite-illite). In the Viking Formation, illite/smectites found at depths less than 2000m have interstratifications that are between random and IS ordered.

At depths greater than 2500m interstratification approaches ISII ordering (Table 3.1).

The composition of illite/smectite in the Viking shales may provide useful information concerning maximum temperatures of burial. Shales interbedded with the Viking have illite/smectite compositions that range between ≃35% smectite layers at 2Km depth and ≃15% smectite layers at ≃3Km depth; a change from random to ordered interstratification is also present at ≃2Km depth (Table 3.1). These variations probably reflect different stages of smectite diagenesis, assuming all shale samples had similar starting compositions. The relationship between illite/smectite composition in shales, burial depth and temperature has been studied extensively in the Gulf Coast area (e.g., Perry and Hower, 1970; Perry et al., 1976; Boles and Franks, 1979). These studies indicate that there is a decrease in smectite layers from about 70% at 1Km (60°C) to about 10-30% smectite layers at >4Km (>170°C) and the change from random to ordered interstratification occurs at approximately 2Km (100°C) (Boles, 1981). If shales in the Viking had similar starting illite/smectite compositions as in the Gulf Coast shales then temperatures in excess of 100°C were probably also reached in the Viking.

B. Detrital Mineralogy of Sandstones and Conglomerates

The detrital mineralogy of the Viking sandstones and conglomerates was studied in order to classify the rocks and determine any variations in source during deposition. Three main rock types have been examined: conglomerates, coarse-grained sandstones and fine-grained sandstones. The detrital minerals in these rocks consist of chert, quartz, feldspar, rock fragments (mainly shale), and dolomite (Tables 3.2 & 3.3).

Conglomerates

The conglomerates are dominated by chert (45-80%) and contain lesser amounts of quartz (3-26%), rock fragments (nd-18%), and feldspar (6-12%, Viking "A"; t-5%, Viking "B"); conglomerates also have the highest porosity values of all the lithologies studied (t-16%)' (Table 3.2). Conglomerates contain many different varieties of chert including micro, macro and polycrystalline grains that commonly show relict limestone textures (Plate 3.1A). Conglomerates are usually cemented by small pore-lining quartz crystals (chert cement) and pore spaces are commonly filled by authigenic kaolin group minerals (Plate 3.1A). Compaction of the conglomerates has resulted in numerous sutured chert contacts (Plate 3.1B) and in the deformation of shale rock fragments (Plate 3.1C). Some conglomerates also contain a clay-rich matrix comprised mostly of kaolin

---

'Porosities were determined by point counting and probably are minimum estimates

group minerals (Plate 3.1D). The origin of these kaolin group minerals in uncertain but they are probably detrital and were either deposited along with the conglomerate or infiltrated after deposition. This detrital matrix commonly contains authigenic pyrite and quartz and, in some places, appears to have been replaced by well crystallized authigenic kaolin group minerals (Plate 3.1D & 3.1E).

Coarse-Grained Sandstones

The coarse-grained sandstones are dominated by chert (18-65%) and quartz (5-48%), and contain lesser amounts of rock fragments (nd-14%) and feldspar (2-30%, Viking "A"; t-4%, Viking "B"); porosity values are normally high (t-14%) (Table 3.2). Detrital clays, mainly kaolin group minerals, are common and, in some places, may have inhibited the growth of quartz cement (Plate 3.1F). Coarse-grained sandstones containing abundant detrital quartz are usually well cemented by extensive quartz overgrowths (Plate 3.2A). Detrital quartz is usually unstrained, contains few inclusions and has well rounded outlines (Plate 3.2A). Boundaries between quartz grains are commonly convexo-concave but may be the result of mergence of quartz overgrowths within pore spaces (Plate 3.2B). Biotite is a common accesory phase and is usually compacted around quartz and chert (Plate 3.2B). Porosity has been enhanced in some of these rocks by the dissolution of chert and feldspar (Plate 3.2A & 3.2B).

Fine-Grained Sandstones

The fine-grained sandstones are dominated by quartz (34-60%) and contain lesser amounts of rock fragments (3-24%), chert (5-19%) and feldspar (nd-5%, Viking "B"). Very little visible porosity is seen in these rocks (t-4%) because of extensive quartz overgrowths (Plate 3.2C). Detrital dolomite is common (nd-12%) and, in some samples, is replaced by ankerite (Plate 3.2D & 3.2E). Shale matrix (shale rock fragments) is usually compacted around quartz and chert grains (Plate 3.2F). Muscovite commonly occurs as an accesory phase and is usually degraded along its edges (Plate 3.2F).

Classification

The bulk mineralogy of the Viking Formation is summarized in Figure 3.2. The classification scheme (Figure 3.2) follows the argument of Blatt et al. (1980, p. 370-372) and separates chert and quartz from feldspar and unstable rock fragments (including shale matrix). This form of classification places emphasis on the relative stability of framework grains where quartz + chert > feldspar > unstable rock fragments (Blatt et al., 1980). For the Viking, this classification helps to separate the reservoir rocks (conglomerates and coarse-grained sandstones) from the non-reservoir rocks (fine-grained sandstones) (Figure 3.2).

The presence of quartz, chert, shale rock fragments and dolomite suggests that the source was predominantly

Figure 3.2. Classification of bulk mineralogy

(Data from Table 3.2; results normalized to 100%).

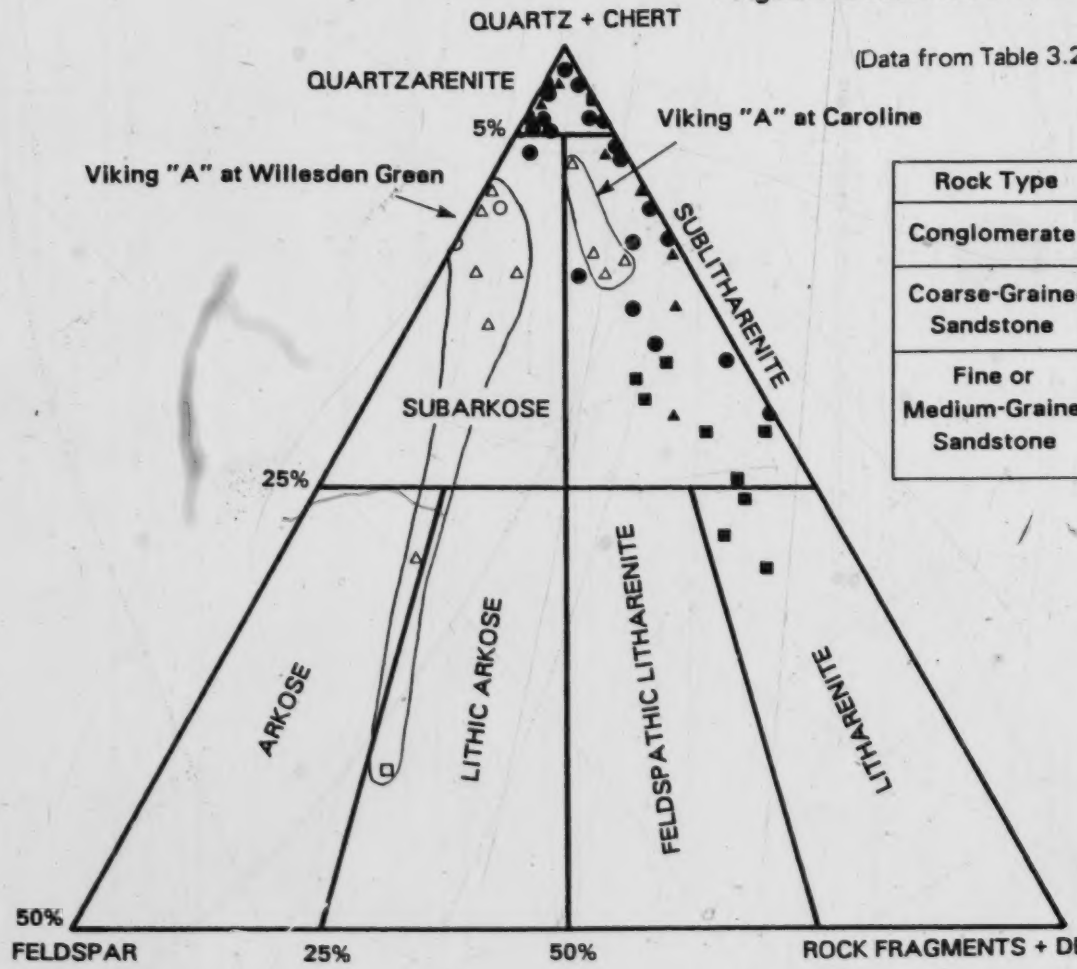

Legend

Rock Type	Viking "A"	Viking "B"
Conglomerate	○	●
Coarse-Grained Sandstone	△	▲
Fine or Medium-Grained Sandstone	□	■

sedimentary in origin (i.e., from the West); plutonic rocks would have provided a source for the feldspar.

Viking "B" rocks contain low percentages of detrital feldspar and consist mainly of quartzarenites, sublitharenites and litharenites depending on the amount of detrital clays present (Figure 3.2). The Viking "A" rocks at Gilby and Willesden Green contain a high feldspar content and consist of subarkoses, arkoses, and lithicarkoses (Figure 3.2). The Viking "A" rocks at Caroline have a lower feldspar content and consists mostly of sublitharenites. The higher feldspar content in the Viking "A" rocks relative to the Viking "B" rocks reflects a change in source for the younger Viking "A" deposits.

TABLE 3.2. PETROGRAPHIC ANALYSIS OF SANDSTONES AND CONGLOMERATES

SAMPLE NUMBER	ROCK TYPE	DEPTH (m)	DETRITAL MINERALS (%)				AUTHIGENIC MINERALS (%)						ϕ (%)	ROCK CLASS (FOLK;1968)
			Ch	Q	F	RF	Q	K	Sid	Cal	Dol	Ank		
GILBY														
4-3-42-4W5														
M87	Congl.	1909.0	76	7	2	nd	4	4	nd	nd	nd	nd	7	Quartzarenite
M88	F.Sst.	1910.0	19	45	4	24	7	t	nd	nd	nd	nd	t	Sublitharenite
11-24-42-6W5														
M80	Congl.	2121.0	73	7	t	6	5	2	nd	nd	nd	nd	7	Sublitharenite
M81	C.Sst.	2122.0	50	35	t	t	9	2	nd	nd	nd	nd	3	Quartzarenite
M82	F.Sst.	2123.0	10	60	1	20	5	t	nd	nd	3	t	1	Sublitharenite
10-9-41-3W5														
M45	Congl.	1923.0	70	10	1	t	2	3	2	nd	nd	2	10	Quartzarenite
M46	C.Sst.	1935.0	51	23	1	nd	7	7	nd	nd	nd	nd	11	Quartzarenite
6-25-40-2W5														
M100	Congl.	1776.0	67	6	3	nd	11	5	nd	nd	nd	nd	8	Quartzarenite
M102	C.Sst.	1778.0	25	44	4	14	8	5	nd	nd	nd	nd	t	Sublitharenite
6-2-40-3W5														
M104	Congl.	1904.0	60	12	4	nd	4	4	nd	nd	nd	t	16	Quartzarenite
3-17-40-4W5														
M48A	Congl.	2156.0	66	8	10	nd	3	2	nd	nd	nd	3	7	Subarkose
M50	Congl.	2157.0	65	5	3	6	5	t	2	nd	nd	2	12	Quartzarenite

TABLE 3.2. (CONTINUED)

SAMPLE NUMBER	ROCK TYPE	DEPTH (m)	DETRITAL MINERALS (%)				AUTHIGENIC MINERALS (%)						ϕ (%)	ROCK CLASS (FOLK;1968)
			Ch	Q	F	RF	Q	K	Sid	Cal	Dol	Ank		
6-15-40-5W5														
M106A	C.Sst.	2145.7	35	40	6	t	3	t	nd	nd	nd	2	13	Subarkose
M107	Congl.	2129.1	71	21	4	t	3	1	nd	nd	nd	t	t	Quartzarenite
14-9-39-2W5														
M15	C.Sst.	1904.0	60	14	2	nd	9	4	nd	nd	nd	nd	11	Quartzarenite
WILLESDEN GREEN														
5-6-41-6W5														
M93	C.Sst.	2293.0	25	48	1	4	14	1	nd	nd	nd	nd	7	Quartzarenite
M94	Congl.	2294.0	64	14	t	t	5	3	nd	nd	nd	nd	14	Quartzarenite
M97	F.Sst.	2299.0	18	47	nd	3	25	3	nd	nd	t	nd	4	Quartzarenite
3-27-40-6W5														
M114A	C.Sst.	2230.0	46	18	12	3	14	1	nd	nd	nd	t	6	Subarkose
M117	Congl.	2236.0	65	3	t	18	8	1	nd	nd	nd	5	t	Sublitharenite
3-31-40-6W5														
M191	Congl.	2276.0	45	26	1	9	14	t	nd	nd	nd	t	5	Sublitharenite
M192	M.Sst.	2278.0	21	42	1	8	18	1	nd	nd	nd	t	9	Sublitharenite
10-31-40-6W5														
M184	Congl.	2273.0	80	5	t	5	4	2	nd	nd	nd	nd	4	Sublitharenite
M185	M.Sst.	2275.0	6	50	3	16	15	t	nd	nd	nd	t	9	Sublitharenite
M186	C.Sst.	2277.0	43	23	t	6	14	2	nd	nd	nd	nd	12	Sublitharenite

TABLE 3.2. (CONTINUED)

SAMPLE NUMBER	ROCK TYPE	DEPTH (m)	DETRITAL MINERALS (%)				AUTHIGENIC MINERALS (%)						ϕ (%)	ROCK CLASS (FOLK;1968)
			Ch	Q	F	RF	Q	K	Sid	Cal	Dol	Ank		
7-29-40-6W5														
M180A	Congl.	2257.0	72	10	7	1	4	2	nd	nd	nd	t	4	Subarkose
M181A	M.Sst.	2258.0	18	21	23	8	22	t	nd	nd	nd	2	6	Subarkose
M182A	C.Sst.	2259.0	40	14	16	5	14	1	nd	nd	nd	t	10	Subarkose
FERRIER														
2-32-37-3W5														
M28	Congl.	1980.0	70	10	1	17	2	t	nd	nd	nd	t	t	Quartzarenite
M29	F.Sst.	1981.5	3	32	1	t	nd	nd	63	nd	t	nd	t	Quartzarenite
6-3-37-5W5														
M07	Congl.	2289.0	63	9	2	1	9	4	nd	nd	nd	nd	12	Quartzarenite
M11	F.Sst.	2295.0	4	37	2	1	2	nd	54	nd	t	nd	t	Quartzarenite
4-19-39-5W5														
M55	C.Sst.	2198.0	50	25	2	11	1	10	nd	nd	nd	t	1	Sublitharenite
M56	Congl.	2199.0	60	10	4	1	8	4	nd	nd	nd	1	12	Quartzarenite
M57	F.Sst.	2201.0	8	23	4	3	nd	nd	60	nd	nd	nd	2	Quartzarenite
6-1-39-7W5														
M122	Congl.	2393.0	70	10	3	t	3	4	nd	nd	nd	t	10	Quartzarenite
M124	F.Sst.	2404.0	13	25	5	2	nd	nd	55	nd	t	nd	t	Subarkose
2-30-38-7W5														
M139	Congl.	2534.0	66	15	5	6	3	3	1	nd	nd	nd	1	Subarkose
M141	F.Sst.	2537.0	20	44	4	10	2	t	20	nd	nd	nd	t	Sublitharenite

TABLE 3.2. (CONTINUED)

SAMPLE NUMBER	ROCK TYPE	DEPTH (m)	DETRITAL MINERALS (%)				AUTHIGENIC MINERALS (%)						ϕ (%)	ROCK CLASS (FOLK;1968)
			Ch	Q	F	RF	Q	K	Sid	Cal	Dol	Ank		
CAROLINE														
7-32-34-6W5														
M250A	C.Sst.	2710.0	50	22	2	7	13	5	nd	nd	nd	nd	1	Sublitharenite
M251A	C.Sst.	2712.0	33	26	3	9	19	6	nd	nd	nd	nd	4	Sublitharenite
4-18-35-6W5														
M219A	C.Sst.	2730.0	39	30	2	2	16	6	nd	nd	nd	1	4	Quartzarenite
M221	Congl.	2734.0	73	9	t	3	9	1	nd	nd	nd	nd	5	Sublitharenite
M224	F.Sst.	2739.0	13	46	3	10	20	t	nd	nd	8	t	t	Sublitharenite
6-16-35-5W5														
M216A	C.Sst.	2465.0	46	17	5	3	14	2	nd	nd	nd	3	10	Subarkose
M217	Congl.	2467.0	70	9	t	2	10	3	nd	nd	nd	3	3	Quartzarenite
M218	F.Sst.	2468.0	15	38	3	18	14	t	nd	nd	12	t	t	Sublitharenite
13-8-35-6W5														
M199A	C.Sst.	2720.0	34	28	3	6	20	5	nd	nd	nd	t	4	Sublitharenite
M202	Congl.	2725.0	63	9	1	7	9	7	nd	nd	nd	nd	4	Sublitharenite
M204	F.Sst.	2727.0	17	39	5	18	12	t	nd	nd	7	t	2	Sublitharenite

TABLE 3.2. (CONTINUED)

SAMPLE NUMBER	ROCK TYPE	DEPTH (m)	DETRITAL MINERALS (%)				AUTHIGENIC MINERALS (%)						ϕ (%)	ROCK CLASS (FOLK;1968)
			Ch	Q	F	RF	Q	K	Sid	Cal	Dol	Ank		
OTHERS														
6-36-29-26W4														
M511	F.SSt.	1540.0	6	56	3	14	11	nd	nd	nd	8	t	2	Sublitharenite
14-30-29-28W4														
M523	Congl.	1872.2	69	14	t	3	8	2	nd	nd	2	t	2	Quartzarenite
M526	Congl.	1874.5	70	9	t	5	6	4	nd	nd	4	t	2	Sublitharenite
6-18-31-2W5														
M629A	C.Sst.	2195.6	33	24	7	1	18	3	nd	nd	nd	2	12	Subarkose
M631A	C.Sst.	2199.8	45	18	6	t	15	1	nd	12	nd	nd	3	Subarkose
M634	Congl.	2202.8	64	9	3	9	9	2	nd	nd	nd	t	4	Sublitharenite
M636	F.Sst.	2204.0	19	37	4	10	21	t	nd	nd	7	t	2	Sublitharenite

TABLE 3.3. X-RAY DIFFRACTION ANALYSIS OF SANDSTONES AND CONGLOMERATES

SAMPLE NUMBER	ROCK TYPE	DEPTH m	SIZE μm	% FINES	PHASES PRESENT								RELATIVE % CLAYS				
					Py	Sid	Cal	Dol	Ank	Q	F	C	IS	SM	CL	I	K
GILBY																	
4-3-42-4W5																	
M87	Congl.	1909.0	5-20	2.0	nd	mt	nd	nd	nd	M	t	mM	t	nd	t	5	95
			2-5	1.0	nd	t	nd	nd	nd	M	t	mM	mt	nd	mt	15	80
			<2	0.5	nd	t	nd	nd	nd	M	t	mM	10	nd	5	45	40
M88	F.Sst.	1910.0	5-20	5.5	nd	t	nd	nd	nd	M	m	mM	20	nd	5	60	15
			2-5	2.0	nd	nd	nd	nd	nd	M	mt	mM	20	nd	5	50	25
			<2	4.0	nd	nd	nd	nd	nd	M	t	M	10	nd	5	55	30
11-24-42-6W5																	
M80	Congl.	2121.0	5-20	3.8	t	t	nd	nd	nd	M	t	mt	nd	nd	nd	55	45
			2-5	1.8	t	t	nd	nd	nd	M	mt	m	nd	nd	15	55	30
			<2	1.4	nd	t	nd	nd	nd	M	m	mM	nd	10	20	50	20
M81	C.Sst.	2122.0	5-20	3.8	nd	t	nd	nd	nd	M	t	mM	nd	nd	nd	5	95
			2-5	1.7	nd	t	nd	nd	nd	M	t	mM	nd	nd	nd	5	95
			<2	0.5	nd	nd	nd	nd	nd	M	mt	mM	nd	nd	15	25	60
M82	F.Sst.	2123.0	5-20	5.8	nd	nd	nd	nd	nd	M	m	mM	20	nd	5	65	10
			2-5	3.2	nd	t	nd	nd	nd	M	m	mM	20	nd	5	60	15
			<2	2.0	nd	nd	nd	nd	nd	M	t	M	10	nd	10	70	10
10-9-41-3W5																	
M45	Congl.	1923.0	5-20	1.0	t	mt	nd	nd	nd	M	mt	mM	nd	nd	nd	5	95
			2-5	1.4	nd	t	nd	nd	nd	M	mt	mM	10	nd	5	25	60
			<2	1.3	nd	t	nd	nd	nd	M	t	M	nd	20	10	40	30

TABLE 3.3. (CONTINUED)

SAMPLE NUMBER	ROCK TYPE	DEPTH m	SIZE µm	% FINES	PHASES PRESENT								RELATIVE % CLAYS				
					Py	Sid	Cal	Dol	Ank	Q	F	C	IS	SM	CL	I	K
M46	C.Sst.	1935.0	5-20	4.9	nd	t	nd	nd	nd	M	t	mM	nd	nd	nd	5	95
			2-5	3.3	nd	t	nd	nd	nd	M	t	mM	mt	nd	nd	10	90
			<2	3.9	nd	nd	nd	nd	nd	M	nd	M	10	nd	mt	30	60
10-10-40-1W5																	
M12	Congl.	1681.0	5-20	1.5	t	t	nd	nd	nd	M	mt	m	10	nd	10	55	25
			2-5	0.3	nd	nd	nd	nd	nd	mM	t	M	10	nd	10	60	20
			<2	3.2	t	t	nd	nd	nd	m	t	M	10	5	10	55	20
M13	C.Sst.	1682.0	5-20	0.4	m	m	nd	nd	nd	M	mt	mt	20	nd	10	60	10
			2-5	0.2	nd	nd	nd	nd	nd	M	t	mM	35	nd	10	55	t
			<2	3.8	nd	nd	nd	nd	nd	m	nd	M	20	10	t	60	10
3-17-40-4W5																	
M48A	Congl.	2156.0	BULK	-	nd	nd	nd	nd	m	M	mM	t	-	-	-	-	-
			5-20	1.4	mt	m	nd	nd	nd	M	m	m	nd	nd	nd	20	80
			2-5	0.6	t	t	nd	nd	nd	M	m	m	nd	nd	nd	35	65
			<2	1.2	nd	nd	nd	nd	nd	M	m	M	nd	35	5	40	20
M50	C.Sst.	2157.0	BULK	-	t	nd	nd	nd	m	M	mM	t	-	-	-	-	-
			5-20	2.7	t	t	nd	nd	nd	M	t	mM	10	nd	5	15	70
			2-5	1.1	nd	nd	nd	nd	nd	M	t	M	15	nd	5	20	60
			<2	1.1	nd	t	nd	nd	nd	M	mt	M	5	20	15	35	25
14-9-39-2W5																	
M15	C.Sst.	1904.0	5-20	2.3	nd	nd	nd	nd	nd	M	m	mM	5	nd	nd	15	80
			2-5	1.7	nd	nd	nd	nd	nd	M	m	M	10	nd	nd	30	60
			<2	3.0	nd	nd	nd	nd	nd	M	t	M	5	10	5	50	30

TABLE 3.3. (CONTINUED)

SAMPLE NUMBER	ROCK TYPE	DEPTH m	SIZE µm	% FINES	PHASES PRESENT								RELATIVE % CLAYS				
					Py	Sid	Cal	Dol	Ank	Q	F	C	IS	SM	CL	I	K
M16	M.Sst.	1904.3	5-20	0.5	nd	t	nd	nd	nd	M	m	mM	nd	nd	nd	t	100
			2-5	0.5	nd	t	nd	nd	nd	M	m	mM	nd	nd	t	5	95
			<2	2.0	nd	t	nd	nd	nd	M	m	M	nd	10	5	15	70
M18	Congl.	1905.0	5-20	1.8	nd	t	nd	nd	nd	M	mt	mM	10	nd	5	25	60
			2-5	1.4	nd	t	nd	nd	nd	M	t	mM	20	nd	10	35	35
			<2	1.6	nd	t	nd	nd	nd	mM	t	M	10	20	15	35	20
6-15-40-5W5																	
M106	C.Sst.	2145.7	BULK	-	t	t	nd	nd	t	M	M	m	-	-	-	-	-
WILLESDEN GREEN																	
5-6-41-6W5																	
M93	C.Sst.	2293.0	5-20	2.0	nd	nd	nd	nd	nd	M	m	m	nd	nd	nd	25	75
			2-5	0.1	nd	nd	nd	nd	nd	M	mt	m	nd	nd	10	30	60
			<2	1.4	nd	nd	nd	nd	nd	M	t	mM	5	10	10	50	25
M94	Congl.	2294.0	5-20	0.9	nd	t	nd	nd	nd	M	nd	mM	nd	nd	5	35	60
			2-5	0.2	nd	t	nd	nd	nd	M	t	mM	nd	nd	nd	25	75
			<2	0.9	nd	t	nd	nd	nd	M	t	M	5	5	5	60	25
M97	F.Sst.	2299.0	5-20	1.9	nd	t	nd	nd	nd	M	m	m	nd	nd	nd	75	25
			2-5	0.2	nd	nd	nd	nd	nd	M	mt	m	10	nd	5	40	45
			<2	1.7	nd	nd	nd	nd	nd	M	t	m	10	nd	15	55	20

TABLE 3.3. (CONTINUED)

SAMPLE NUMBER	ROCK TYPE	DEPTH m	SIZE μm	% FINES	PHASES PRESENT								RELATIVE % CLAYS				
					Py	Sid	Cal	Dol	Ank	Q	F	C	IS	SM	CL	I	K
3-27-40-6W5																	
M114A	C.Sst.	2230.0	5-20	2.0	f	t	nd	nd	nd	M	mM	mM	nd	nd	mt	5	90
			2-5	1.0	t	mt	nd	nd	nd	M	mM	mM	nd	nd	5	15	80
			<2	1.0	nd	mt	nd	nd	nd	M	mM	mM	nd	nd	30	25	45
M117	Congl.	2236.0	BULK	-	m	nd	nd	nd	t	M	t	t	-	-	-	-	-
			5-20	1.5	nd	t	nd	nd	nd	M	t	mM	nd	nd	nd	mt	95
			2-5	1.0	nd	t	nd	nd	nd	M	t	mM	t	nd	t	10	90
			<2	1.0	nd	nd	nd	nd	nd	M	m	mM	10	nd	15	30	45
3-31-40-6W5																	
M191	Congl.	2276.0	5-20	0.9	nd	t	nd	nd	nd	M	t	mM	t	nd	t	mt	95
			2-5	0.6	nd	t	nd	nd	nd	M	t	mM	5	nd	mt	20	75
			<2	0.5	nd	nd	nd	nd	nd	M	t	M	10	mt	5	60	25
M192	M.Sst.	2278.0	5-20	1.3	nd	t	nd	nd	nd	M	mt	m	nd	nd	10	40	50
			2-5	0.1	nd	nd	nd	nd	nd	M	t	mM	5	nd	10	20	65
			<2	1.5	nd	nd	nd	nd	nd	M	t	m	nd	nd	20	35	45
7-29-40-6W5																	
M181	M.Sst.	2258.0	BULK	-	nd	t	nd	nd	m	M	M	t	-	-	-	-	-
FERRIER																	
11-21-36-2W5																	
M06	Congl.	1900.0	5-20	1.6	nd	nd	nd	nd	nd	M	mt	mM	5	nd	5	10	80
			2-5	0.5	nd	t	nd	nd	nd	M	mt	mM	15	nd	10	20	55
			<2	2.0	nd	mt	nd	nd	nd	M	t	M	10	mt	20	35	35

TABLE 3.3. (CONTINUED)

SAMPLE NUMBER	ROCK TYPE	DEPTH m	SIZE µm	% FINES	PHASES PRESENT								RELATIVE % CLAYS				
					Py	Sid	Cal	Dol	Ank	Q	F	C	IS	SM	CL	I	K
M01	M.Sst.	1902.0	5-20	7.5	nd	mM	nd	nd	nd	M	m	mM	5	nd	5	25	65
			2-5	1.7	nd	t	nd	nd	nd	M	m	mM	5	nd	5	10	80
			<2	5.3	nd	t	nd	nd	nd	mM	mt	M	5	nd	10	35	50
M04	M.Sst.	1903.0	5-20	11.4	m	m	nd	nd	nd	M	mM	mM	nd	nd	nd	35	65
			2-5	1.9	nd	nd	nd	nd	nd	M	m	m	nd	nd	10	50	40
			<2	5.1	m	m	nd	nd	nd	M	mM	M	10	nd	10	55	25
2-32-37-3W5																	
M28	Congl.	1980.0	5-20	2.5	nd	t	nd	nd	nd	M	t	mM	10	nd	10	25	55
			2-5	0.5	nd	t	nd	nd	nd	M	mt	mM	10	nd	10	25	55
			<2	3.0	nd	t	nd	nd	nd	M	t	mM	10	nd	20	35	35
M29	F.Sst.	1981.5	BULK	-	t	M	nd	nd	nd	M	t	t	-	-	-	-	-
M30	F.Sst.	1987.0	5-20	10.0	nd	t	nd	nd	nd	M	mt	mM	10	nd	5	60	25
			2-5	5.0	nd	nd	nd	nd	nd	M	m	mM	15	nd	5	55	25
			<2	7.0	t	t	nd	nd	nd	mM	t	M	15	nd	10	65	10
			<0.2	-	nd	nd	nd	nd	nd	nd	nd	M	20	nd	10	70	t
6-3-37-5W5																	
M07	Congl.	2289.0	5-20	0.6	nd	m	nd	nd	nd	M	m	M	nd	nd	nd	t	100
			2-5	0.4	nd	t	nd	nd	nd	M	t	M	nd	nd	nd	5	95
			<2	0.9	nd	nd	nd	nd	nd	M	mt	M	mt	mt	5	15	75
M02	F.Sst.	2290.0	5-20	8.8	nd	M	nd	nd	nd	M	m	mM	nd	nd	5	55	40
			2-5	3.5	nd	M	nd	nd	nd	M	mM	mM	nd	nd	5	45	50
			<2	6.0	t	t	nd	nd	nd	M	mt	M	5	nd	10	55	30
M11	F.Sst.	2295.0	5-20	-	t	mt	nd	nd	nd	M	m	mM	nd	nd	5	65	30
			2-5	-	m	m	nd	nd	nd	M	mM	m	nd	nd	nd	70	30
			<2	-	mt	mt	nd	nd	nd	M	mt	M	10	nd	15	70	5

TABLE 3.3. (CONTINUED)

SAMPLE NUMBER	ROCK TYPE	DEPTH m	SIZE µm	% FINES	PHASES PRESENT								RELATIVE % CLAYS				
					Py	Sid	Cal	Dol	Ank	Q	F	C	IS	SM	CL	I	K
7-14-37-6W5																	
M09	Congl.	2379.0	5-20	2.0	nd	t	nd	nd	nd	M	m	mM	10	nd	mt	20	70
			2-5	1.0	nd	t	nd	nd	nd	M	m	M	30	nd	10	45	15
			<2	1.9	nd	t	nd	nd	nd	M	t	M	15	5	10	55	15
M03	F.Sst.	2381.0	5-20	10.2	nd	m	nd	nd	nd	M	mM	mM	nd	nd	5	25	70
			2-5	2.0	nd	m	nd	nd	nd	M	mM	mM	10	nd	5	20	65
			<2	6.0	nd	m	nd	nd	nd	mM	mt	M	20	nd	10	40	30
			<0.2	-	nd	nd	nd	nd	nd	nd	nd	M	30	nd	10	55	5
M08	F.Sst.	2387.0	5-20	7.4	nd	t	nd	nd	nd	M	m	m	nd	nd	5	45	50
			2-5	0.5	nd	t	nd	nd	nd	M	mM	mM	10	nd	5	35	50
			<2	5.5	nd	mt	nd	nd	nd	M	mt	M	10	nd	40	45	5
10-20-37-7W5																	
M10	F.Sst.	2598.0	5-20	6.8	t	t	nd	nd	nd	M	m	m	nd	nd	5	45	50
			2-5	0.8	t	t	nd	nd	nd	M	mt	m	nd	nd	nd	40	60
			<2	6.0	nd	mt	nd	nd	nd	M	t	M	5	nd	15	50	30
M05	F.Sst.	2611.0	5-20	8.0	t	m	nd	nd	nd	M	m	m	nd	nd	nd	55	45
			2-5	2.0	t	m	nd	nd	nd	M	mM	mM	nd	nd	nd	45	55
			<2	3.2	nd	m	nd	nd	nd	M	mM	M	10	nd	15	65	10
4-19-39-5W5																	
M56	Congl.	2199.0	5-20	0.8	t	nd	nd	nd	nd	M	m	mM	nd	nd	nd	t	100
			2-5	0.2	nd	nd	nd	nd	nd	M	m	mM	nd	5	nd	20	75
			<2	1.5	nd	t	nd	nd	nd	M	mt	M	nd	15	5	45	35
M57	F.Sst.	2201.0	5-20	7.4	nd	t	nd	nd	nd	M	m	mM	15	nd	nd	50	35
			2-5	2.5	nd	t	nd	nd	nd	M	m	mM	15	nd	5	50	30
			<2	3.8	t	t	nd	nd	nd	mM	t	M	10	nd	10	60	20

TABLE 3.3. (CONTINUED)

SAMPLE NUMBER	ROCK TYPE	DEPTH m	SIZE μm	% FINES	PHASES PRESENT								RELATIVE % CLAYS				
					Py	Sid	Cal	Dol	Ank	Q	F	C	IS	SM	CL	I	K
6-1-39-7W5																	
M122	Congl.	2393.0	5-20	0.3	nd	m	nd	nd	nd	M	mt	M	nd	nd	nd	t	100
			2-5	0.3	nd	t	nd	nd	nd	M	m	M	nd	nd	nd	10	90
			<2	1.2	nd	nd	nd	nd	nd	M	mt	M	nd	20	5	45	30
M125	F.Sst.	2404.0	5-20	7.7	nd	t	nd	nd	nd	M	m	mM	25	nd	5	45	25
			2-5	1.5	nd	t	nd	nd	nd	M	mM	M	40	nd	nd	45	15
			<2	4.0	nd	nd	nd	nd	nd	m	t	M	25	nd	5	55	15
2-30-38-7W5																	
M139	Congl.	2534.0	5-20	1.1	nd	t	nd	nd	nd	mM	t	M	t	nd	t	5	95
			2-5	0.8	nd	t	nd	nd	nd	M	mt	mM	5	t	5	10	80
			<2	0.8	nd	t	nd	nd	nd	M	m	M	nd	nd	20	30	50
M141	F.Sst.	2537.0	BULK	-	t	M	nd	nd	nd	M	m	t	-	-	-	-	-
			5-20	6.3	mt	mM	nd	nd	nd	M	m	m	nd	nd	15	55	30
			2-5	2.8	mM	M	nd	nd	nd	M	m	m	nd	nd	nd	5	95
			<2	2.4	M	M	nd	nd	nd	M	m	M	15	nd	5	55	25
CAROLINE																	
10-24-35-7W5																	
M39A	C.Sst.	2732.0	5-20	4.0	nd	mt	nd	nd	nd	M	t	M	5	nd	nd	10	85
			2-5	1.2	nd	t	nd	nd	nd	M	mt	mM	5	nd	t	15	80
			<2	3.3	nd	t	nd	nd	nd	M	mt	M	5	nd	5	30	60
M40	Congl.	2734.0	5-20	2.6	nd	m	nd	nd	nd	M	mt	M	t	nd	t	10	90
			2-5	1.5	nd	t	nd	nd	nd	M	mt	M	10	nd	5	30	55
			<2	3.9	nd	t	nd	nd	nd	mM	mt	M	10	mt	5	60	25

TABLE 3.3. (CONTINUED)

SAMPLE NUMBER	ROCK TYPE	DEPTH m	SIZE μm	% FINES	PHASES PRESENT								RELATIVE % CLAYS				
					Py	Sid	Cal	Dol	Ank	Q	F	C	IS	SM	CL	I	K
M42	F.Sst.	2737.0	5-20	7.5	nd	m	nd	nd	nd	M	m	mM	5	nd	nd	35	60
			2-5	4.5	nd	mt	nd	nd	nd	M	m	mM	mt	nd	nd	30	65
			<2	8.0	nd	t	nd	nd	nd	m	mt	M	10	nd	5	55	30
7-32-34-6W5																	
M250A	C.Sst.	2710.0	5-20	1.0	nd	m	nd	nd	nd	M	m	M	nd	nd	t	mt	95
			2-5	0.7	nd	mt	nd	nd	nd	M	m	M	mt	nd	mt	5	90
			<2	1.6	nd	t	nd	nd	nd	M	m	M	5	nd	20	15	60
M252A	C.Sst.	2717.0	5-20	1.5	nd	mt	nd	nd	nd	M	m	mM	5	nd	t	5	90
			2-5	1.5	nd	t	nd	nd	nd	M	mM	mM	5	nd	mt	30	65
			<2	1.5	nd	t	nd	nd	nd	M	m	M	10	nd	15	35	40
M253	F.Sst.	2719.1	BULK	-	t	t	nd	m	m	M	m	m	-	-	-	-	-
4-18-35-6W5																	
M220	C.Sst.	2734.0	5-20	0.9	nd	m	n	nd	nd	M	m	M	nd	nd	t	t	95
			2-5	0.9	nd	mt	nd	nd	nd	M	m	M	nd	nd	mt	5	90
			<2	0.7	nd	t	nd	nd	nd	M	m	M	5	nd	15	25	55
M224	F.Sst.	2739.0	5-20	4.6	nd	t	nd	nd	nd	M	m	mM	15	nd	5	55	25
			2-5	1.3	nd	t	nd	nd	nd	M	m	mM	15	nd	10	45	30
			<2	1.8	nd	mt	nd	nd	nd	m	mt	M	10	nd	10	65	15
13-8-35-6W5																	
M199A	C.Sst.	2720.0	5-20	1.2	nd	m	nd	nd	nd	M	mt	M	nd	nd	nd	t	100
			2-5	2.0	nd	t	nd	nd	nd	M	m	M	nd	nd	t	5	95
			<2	1.5	nd	t	nd	nd	nd	M	mM	M	nd	nd	25	15	60

TABLE 3.3. (CONTINUED)

SAMPLE NUMBER	ROCK TYPE	DEPTH m	SIZE µm	% FINES	PHASES PRESENT								RELATIVE % CLAYS				
					Py	Sid	Cal	Dol	Ank	Q	F	C	IS	SM	CL	I	K
M202	Congl.	2725.0	5-20	1.0	nd	m	nd	nd	nd	M	m	M	nd	nd	t	t	100
			2-5	0.7	nd	mt	nd	nd	nd	M	m	mM	5	nd	5	5	85
			<2	1.2	nd	t	nd	nd	nd	M	mt	M	5	5	20	30	40
M204	F.Sst.	2727.0	5-20	6.8	nd	mt	nd	nd	nd	M	m	mM	5	nd	nd	25	70
			2-5	0.8	nd	t	nd	nd	nd	M	m	mM	5	nd	5	30	60
			<2	4.2	nd	t	nd	nd	nd	m	m	M	10	nd	5	55	30
			<0.2	-	nd	nd	nd	nd	nd	nd	nd	M	30	nd	5	65	t
6-16-35-5W5																	
M216A	C.Sst.	2465.0	5-20	0.9	nd	t	nd	nd	nd	M	m	mM	nd	nd	nd	t	100
			2-5	0.5	nd	t	nd	nd	nd	M	m	mM	nd	nd	nd	20	80
			<2	1.8	nd	nd	nd	nd	nd	M	m	M	nd	5	10	50	35
M217	Congl.	2467.0	5-20	1.8	nd	m	nd	nd	nd	M	mt	mM	t	nd	t	5	90
			2-5	1.0	nd	t	nd	nd	nd	M	mt	mM	10	nd	5	30	55
			<2	1.1	nd	nd	nd	nd	nd	M	mt	M	10	nd	5	50	35
M218	F.Sst.	2468.0	BULK	-	nd	t	nd	m	nd	M	m	m	-	-	-	-	-
			5-20	7.7	nd	mt	nd	nd	nd	M	m	mM	nd	nd	mt	25	70
			2-5	1.2	nd	t	nd	nd	nd	M	m	mM	5	nd	mt	30	65
			<2	5.6	nd	nd	nd	nd	nd	m	t	M	10	nd	mt	55	35
OTHERS																	
6-36-29-26W4																	
M509	Congl.	1534.0	5-20	5.0	nd	nd	nd	nd	nd	M	m	mM	15	nd	5	60	20
			2-5	4.0	nd	nd	nd	nd	nd	M	m	M	25	nd	5	55	15
			<2	5.0	nd	t	nd	nd	nd	mM	t	M	10	nd	5	55	30

TABLE 3.3. (CONTINUED)

SAMPLE NUMBER	ROCK TYPE	DEPTH m	SIZE µm	% FINES	PHASES PRESENT								RELATIVE % CLAYS				
					Py	Sid	Cal	Dol	Ank	Q	F	C	IS	SM	CL	I	K
M511	F.Sst.	1540.0	BULK	-	nd	t	nd	t	t	M	m	t	-	-	-	-	-
			5-20	-	nd	t	nd	nd	nd	M	mM	mM	5	nd	5	20	70
			2-5	-	nd	nd	nd	nd	nd	M	m	M	5	nd	5	25	65
			<2	-	nd	t	nd	nd	nd	m	t	M	15	nd	5	35	45
			<0.2	-	nd	nd	nd	nd	nd	nd	nd	M	25	nd	10	60	5
14-30-31-28W4																	
M523	Congl.	1872.0	5-20	2.0	nd	t	nd	nd	nd	M	mt	mt	nd	nd	nd	65	35
			2-5	1.0	nd	t	nd	nd	nd	M	mM	m	10	nd	5	55	30
			<2	1.5	nd	nd	nd	nd	nd	M	t	M	15	nd	10	60	15
M524	Congl.	1873.0	5-20	3.0	nd	t	nd	nd	nd	M	m	m	nd	nd	10	60	30
			2-5	3.0	nd	t	nd	nd	nd	M	m	m	10	nd	5	55	30
			<2	3.5	nd	nd	nd	nd	nd	M	m	M	15	nd	5	55	25
M526	Congl.	1875.0	5-20	-	t	t	nd	nd	nd	M	mt	m	nd	nd	5	40	55
			2-5	-	nd	nd	nd	nd	nd	M	m	m	10	nd	5	40	45
			<2	-	nd	nd	nd	nd	nd	M	mt	M	15	nd	10	45	30
2-13-29-2W5																	
M597	F.Sst.	2177.0	5-20	3.3	nd	nd	nd	nd	nd	M	m	M	10	nd	5	55	30
			2-5	4.0	nd	nd	nd	nd	nd	M	m	M	15	nd	5	40	40
			<2	4.2	nd	nd	nd	nd	nd	m	m	M	10	nd	5	40	45
			<0.2	-	nd	nd	nd	nd	nd	nd	nd	M	20	nd	10	65	5
6-36-30-2W5																	
M605	C.Sst.	2093.0	5-20	1.3	nd	nd	nd	nd	nd	M	m	mt	nd	nd	nd	5	95
			2-5	0.4	nd	nd	nd	nd	nd	M	mM	m	nd	nd	nd	40	60
			<2	2.3	nd	nd	nd	nd	nd	M	m	M	15	nd	20	50	15

TABLE 3.3. (CONTINUED)

SAMPLE NUMBER	ROCK TYPE	DEPTH m	SIZE µm	% FINES	PHASES PRESENT								RELATIVE % CLAYS				
					Py	Sid	Cal	Dol	Ank	Q	F	C	IS	SM	CL	I	K
M606	Congl.	2094.0	5-20	2.0	nd	t	nd	nd	nd	M	m	mM	10	nd	10	60	20
			2-5	1.8	nd	t	nd	nd	nd	M	mM	mM	20	nd	5	55	20
			<2	4.5	nd	nd	nd	nd	nd	mM	mt	M	15	nd	20	55	10
M613	F.Sst.	2117.0	5-20	4.9	nd	nd	nd	nd	nd	M	m	m	10	nd	5	60	25
			2-5	1.4	nd	t	nd	nd	nd	M	m	mM	15	nd	5	65	15
			<2	7.0	nd	nd	nd	nd	nd	mM	mt	M	10	nd	10	70	10
6-18-31-2W5																	
M629A	C.Sst.	2196.0	5-20	3.7	t	t	nd	nd	nd	M	m	m	nd	nd	nd	35	65
			2-5	0.8	nd	t	nd	nd	nd	M	m	m	nd	nd	5	45	50
			<2	5.0	nd	nd	nd	nd	nd	M	m	M	nd	25	10	55	10
M631A	C.Sst.	2200.0	BULK	-	t	t	M	nd	nd	M	t	nd	-	-	-	-	-
			5-20	2.0	t	t	m	nd	nd	M	m	mM	nd	nd	mt	10	85
			2-5	1.5	t	t	nd	nd	nd	M	m	mM	5	nd	5	25	65
			<2	2.5	nd	t	nd	nd	nd	M	mM	M	10	nd	20	45	25
M634	Congl.	2203.0	5-20	-	nd	t	nd	nd	nd	M	mM	mM	15	nd	5	40	40
			2-5	-	nd	nd	nd	nd	nd	M	mM	M	20	nd	5	45	30
			<2	-	nd	nd	nd	nd	nd	M	m	M	25	nd	5	55	15
7-7-29-22W4																	
M500	F.Sst.	1280.0	BULK	-	nd	t	nd	mM	t	M	mM	m	-	-	-	-	-
M502	F.Sst.	1288.1	BULK	-	t	nd	nd	m	m	M	t	t	-	-	-	-	-

TABLE 3.3. (CONTINUED)

SAMPLE NUMBER	ROCK TYPE	DEPTH m	SIZE µm	% FINES	PHASES PRESENT								RELATIVE % CLAYS				
					Py	Sid	Cal	Dol	Ank	Q	F	C	IS	SM	CL	I	K
14-30-31-28W4																	
M519	F.Sst.	1866.0	BULK	-	nd	t	nd	m	mM	M	mM	m	-	-	-	-	-
11-7-39-26W4																	
M556	C.Sst.	1548.4	BULK	-	t	t	nd	nd	mM	M	t	t	-	-	-	-	-
6-24-32-3W5																	
M24/3	Congl.	2200.0	BULK	-	t	t	nd	nd	mM	M	t	m	-	-	-	-	-
10-24-33-8W5																	
M660	F.Sst.	3101.0	BULK	-	t	M	nd	nd	nd	M	m	mM	-	-	-	-	-
16-1-46-4W5																	
M726	Congl.	1734.0	BULK	-	t	nd	mM	nd	nd	M	t	t	-	-	-	-	-

PLATE 3.1

A. Photomicrograph of a Viking "B" conglomerate showing detrital chert (Ch), quartz (Q), authigenic quartz (AQ) and kaolin group minerals (AK). Chert grains show relict limestone textures, such as crinoid stems and sponges spicules (arrows) (Willesden Green field, well # 13-19-40-6W5, sample # M189, depth = 2257.8m, plane polars, dark blue = porosity, field of view = 2.7 X 2.7mm).

B. Photomicrograph of a Viking "B" conglomerate showing the dissolution of chert (Ch) along sutured grain contacts (arrow) and within grains (Willesden Green field, well # 5-6-41-6W5, sample # M94, depth = 2294.3m, plane polars, dark blue = porosity, field of view = 2.7 X 2.7mm).

C. Photomicrograph of a Viking "A" conglomerate showing the compaction of a detrital shale rock fragment (RF) around chert (Ch), quartz (Q) and feldspar (F) (Willesden Green field, well # 7-29-40-6W5, sample # M180, depth = 2257.0m, plane polars, dark blue = porosity, field of view = 2.7 X 2.7mm).

D. Photomicrograph of a Viking "B" conglomerate showing detrital kaolin group minerals (K) surrounding chert (Ch). The matrix is very extensive and inhibited quartz cementation. The matrix also contains authigenic (Py) and authigenic kaolin group minerals (AK) (Ferrier field, well # 2-32-37-3W5, sample # M28, depth = 1980.0m, plane polars, field of view = 2.7 X 2.7mm).

E. Photomicrograph of Viking "B" conglomerate showing authigenic kaolin group minerals (AK) growing within the detrital kaolin group minerals (K). Abundant quartz (Q) is also present (Ferrier field, well # 2.32-37-3W5, sample # M28, depth = 1980.0m, plane polars, dark brown = hydrocarbon staining, field of view = 1 X 1mm).

F. Photomicrograph of a Viking "B" coarse-grained sandstone showing detrital kaolin group minerals (K) that contain pyrite (Py) and siderite (Sid) (Gilby field, well # 3-17-40-4W5, sample # M50, depth = 2157.0m, plane polars, field of view = 1 X 1mm).

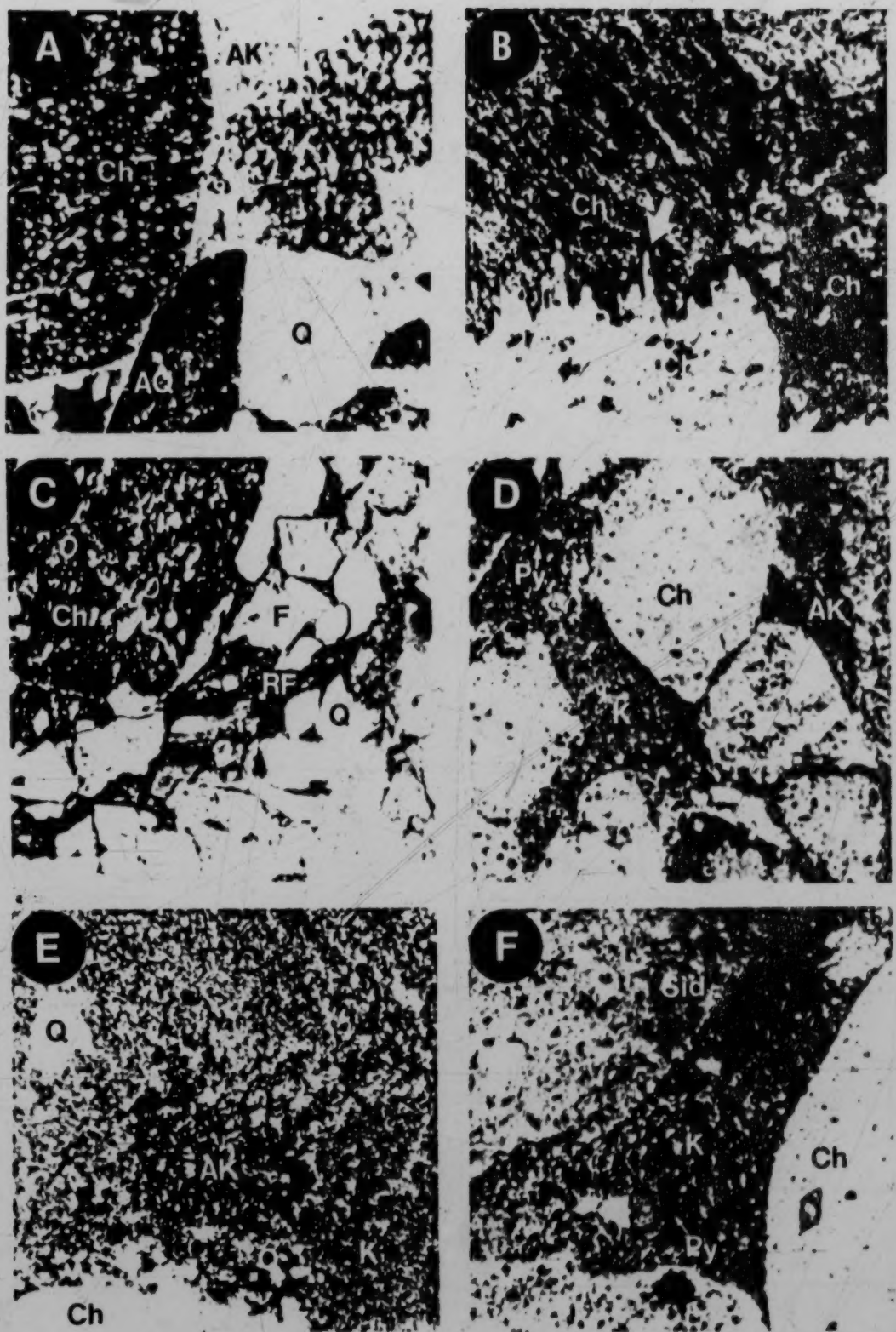
A
AK
Ch
Q
AQ
B
Ch
Ch
C
Ch
F
RF
Q
D
Py
Ch
AK
K
E
Q
AK
K
Ch
F
Sid
K
Ch
Py

PLATE 3.2

A. Photomicrograph of a Viking "B" medium-grained sandstone showing detrital quartz (Q), chert (Ch) and a shale rock fragment (RF). Complete quartz overgrowths (AQ) occur on detrital quartz. The dissolution of chert has created oversized pores (white arrows) (Willesden Green field, well # 3-31-40-6W5, sample # M192, depth = 2278.0m, plane polars, dark blue = porosity, field of view = 2.7 X 2.7mm).

B. Photomicrograph of a Viking "A" medium or coarse-grained sandstone showing detrital feldspar (F), biotite (Bt), quartz (Q) and chert (Ch). Lithification has occurred primarily through quartz cementation (AQ) and contacts between detrital quartz are commonly convexo-concave (black arrow). The dissolution of detrital feldspar (large arrow) and feldspar overgrowths (AF) are also seen (arrow) (Willesden Green field, well # 7-29-40-6W5, sample # M181, depth = 2258.0m, X polars, field of view = 1 X 1 mm).

C. Photomicrograph of a Viking "B" fine-grained sandstone showing detrital quartz (Q), chert (Ch) and dolomite (Dol). The formation of quartz overgrowths (AQ) completely occludes porosity in some areas (Caroline field, well # 6-16-35-5W5, sample # M218, depth = 2468.0m, plane polars, field of view = 1 X 1 mm).

D. Photomicrograph of a Viking "B" fine-grained sandstone showing the replacement of detrital dolomite (Dol) by ankerite (Ank)(stained blue) (Well # 14-30-31-28W4, sample # M519, depth = 1866.0m, plane polars, field of view = 0.64 X 0.64mm).

E. Photomicrograph of a Viking "B" fine-grained sandstone showing euhedral ankerite overgrowths (Ank) on detrital dolomite cores (Dol). The formation of ankerite completely filled remaining pore space. Small granular crystals of siderite (Sid) lining grain surfaces are also seen (Caroline field, well # 6-16-35-5W5, sample # M218, depth = 2468.0m, X polars, field of view = 0.64 X 0.64mm).

F. Photomicrograph of a Viking "B" fine-grained sandstone showing detrital shale matrix (RF). Muscovite (high-birefringent mineral) has altered mostly to illite (arrow) (Caroline field, well # 6-16-35-5W5, sample # M218, depth = 2468.0m, X polars, field of view = 0.64 X 0.64m).

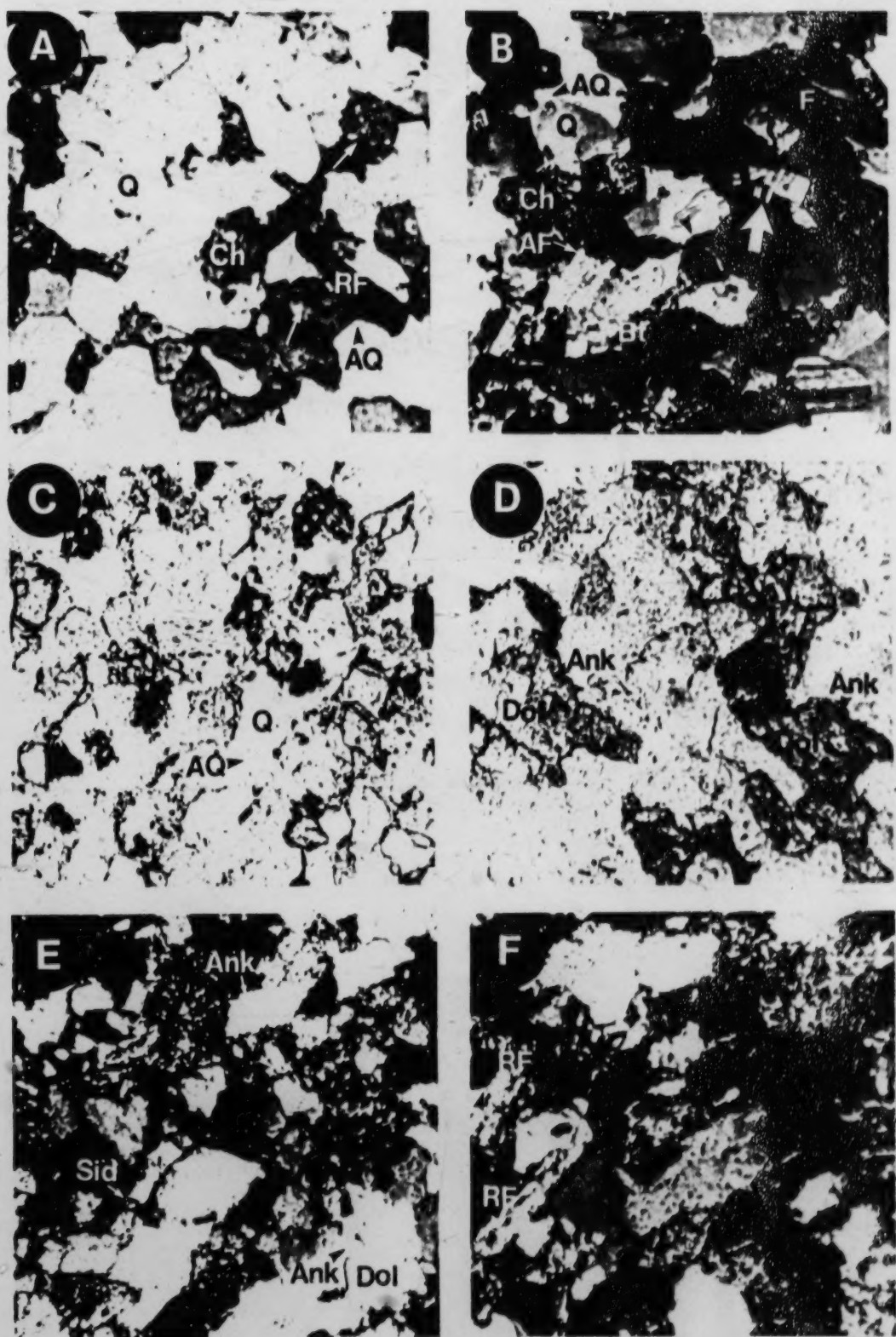
A
Q
Ch
RF
AQ
B
AQ
Q
F
Ch
AF
Br
C
Q
AQ
D
Ank
Dol
Ank
E
Ank
Sid
Ank
Dol
F
RF
RF

C. Authigenic Mineralogy of Sandstones and Conglomerates

Authigenic minerals in the sandstones and conglomerates were studied in order to determine their abundance and to establish the relative timing of mineral empalcement. The authigenic minerals observed in the Viking Formation are glauconite, pyrite, chlorite, siderite, quartz, feldspar, Fe-calcite, ankerite, kaolinite group minerals, illite, illite/smectite and smectite (Tables 3.2 & 3.3).

Glauconite

Glauconite is usually present in amounts <5% at Willesden Green, Gilby and Joffre and is usually not detected in fields to the south (i.e., Caroline). Glauconite occurs as large rounded grains (Plate 3.3A) and as material compacted between more competent grains (Plate 3.3B). Glauconite commonly shows dissolution or shrinkage porosity that occurred after quartz cementation (Plate 3.3A & 3.4C). Shrinkage porosity, associated with glauconite, is a common feature of the Viking sandstones at Provost, east-central Alberta (Foscolos et al., 1982). EDAX analysis of glauconite indicates that it contains Si, Al, K, Ca and Fe (Plate 3.4D). Many glauconite grains also show replacement by pyrite (Plate 3.3B & 3.4E).

Pyrite

Pyrite is found in trace amounts in most samples. It usually occurs as large euhedral aggregates (Plate 3.3C)

that commonly show complex twinning (Plate 3.4A). Aggregates of smaller crystals (framboids) are also present (Plate 3.4B). Pyrite occurs as a replacement of glauconite (Plate 3.4E) and is also found within some detrital clay matrices (Plate 3.1D). Some pyrite formed early, predating chlorite (Plate 3.4G) and siderite (Plate 3.3E). Some pyrite also formed late, postdating quartz cementation (Plate 3.3C & 3.4A).

Chlorite

Chlorite occurs in trace amounts in most samples and usually comprises t-40% of the <2μm size-fraction (Table 3.3). Authigenic chlorite occurs most commonly as well crystallized plates or rosettes (Plate 3.4G, 3.5A) and as interlocking aggregates that appear amorphous (Plate 3.5B). Chlorite is commonly enveloped by later cements, such as quartz (Plate 3.5C & 3.5E) and siderite (Plate 3.5D & 3.5F). EDAX analysis of chlorite indicates that it is Fe-rich (Plate 3.5G)

X-ray diffraction analysis of chlorite suggests that it is chamosite (Figure 3.3). The lower intensity of the chlorite 001 peak (14.2Å) relative to the 002 (7.1Å) and 004 (3.5Å) is characteristic of chamosite (Brindley, 1951). Heating to 550°C greatly increases the intensity of the 001 diffraction (Figure 3.3), a feature also indicative of Fe-rich chlorites (Brown and Brindley, 1980).

Figure 3.3. X-ray diffraction analysis of chlorite.

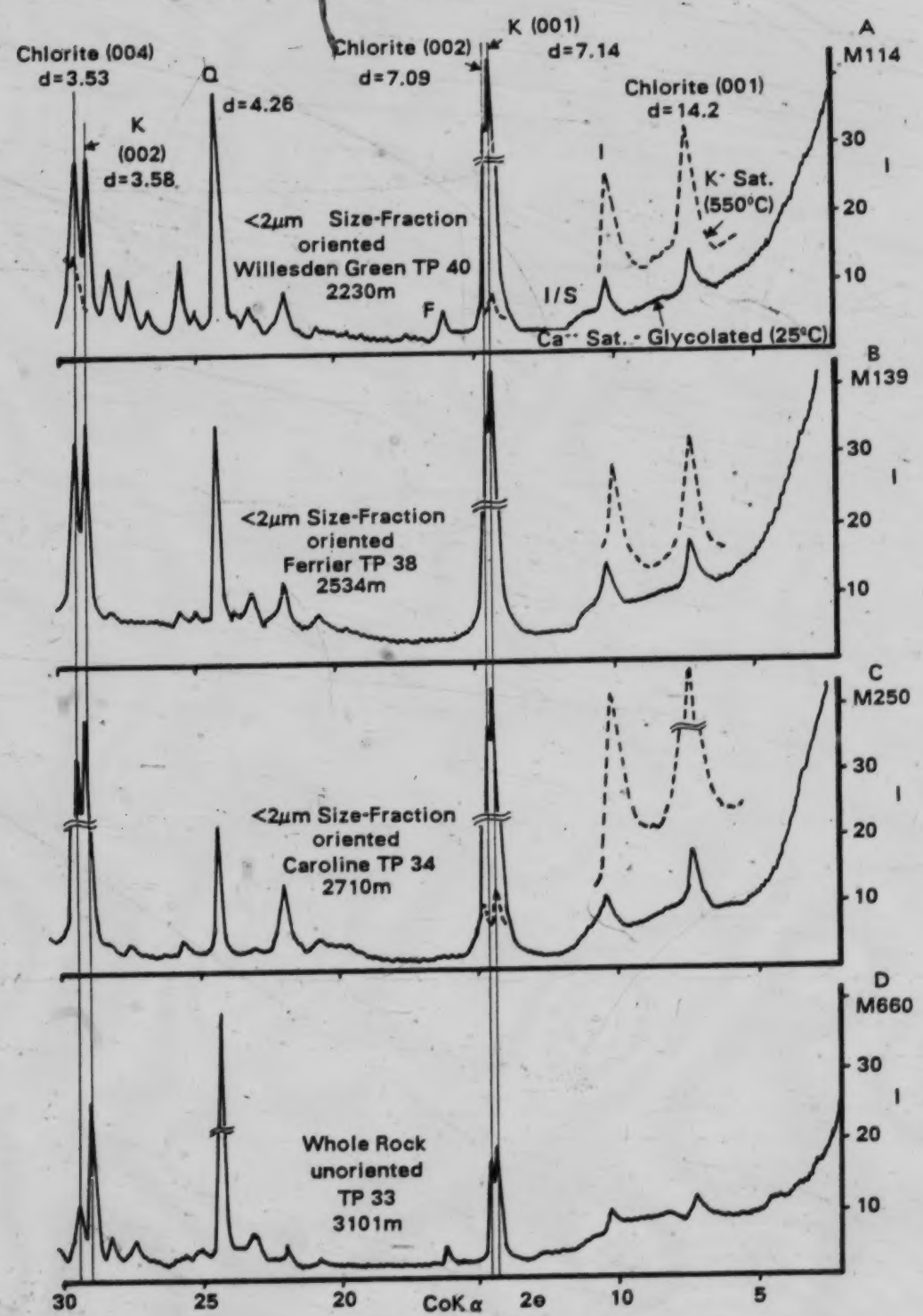

The replacement of detrital kaolin group minerals by chlorite is common and has been documented in sample M139 (Plate 3.6). Intermediate stages of replacement are characterized by alternating layers of kaolinite group minerals and poorly crystallized "pseudo-chlorite" (Plate 3.6C & 3.6E). EDAX analysis of the "pseudo-chlorite" indicates it contains Si, Al and Fe and probably represents a 1:1 layered, Fe-rich clay mineral, such as berthierine. In some places the chlorite appears well crystallized (Plate 3.6F); EDAX analysis indicates it contains minor Mg (Plate 3.6G). This phase is probably chamosite. Since XRD patterns for berthierine overlap with those of chamosite, precise identification is not possible. However, the occurrence of minor amounts of Fe in partially altered detrital kaolin group minerals (Plate 3.6F & 3.6H) suggests that the intermediate phase exists.

Siderite

Siderite is a common cement ranging between t-2% in the coarse-grained sandstones and conglomerates and up to 63% in some fine-grained sandstones (Table 3.2). Siderite usually occurs as pore-lining crystals that formed before quartz cementation (Plate 3.3D). Some siderite occurs as radiating crystals with relict pyrite cores (Plate 3.3E); similar textural features have been observed by Gautier (1983) in the Cretaceous Gammon Shale of northwestern United States. Samples containing a high volume percent siderite normally

preserve uncompacted sedimentary textures (Plate 3.3F). Large rhombohedral crystals of siderite are also present (Plate 3.5D); they commonly envelope earlier cements, such as chamosite (Plate 3.5F). Siderite also replaces detrital dolomite and, in some places, this may have inhibited ankeritization (Plate 3.7A).

Quartz

Quartz is the most abundant cement in all rock types ranging between 3-25% in the fine and coarse-grained sandstones and between 2-14% in the conglomerates (Table 3.2). Complete quartz overgrowths usually form around detrital quartz (Plate 3.7C, 3.8A) and, in many samples, the mergence of overgrowths resulted in the destruction of porosity (Plate 3.7D). Small, prismatically terminated crystals are common on chert grains (Plate 3.7E, 3.8A). Thomas and Oliver (1979) indicated that the growth of quartz in Viking conglomerates was probably inhibited because the random orientation of c-axes in chert grains inhibits nucleation.

The timing of most quartz cements is late and it commonly envelops earlier phases, such as chamosite (Plate 3.5C & 3.5E) and siderite (Plate 3.3D). Some authigenic quartz appears to have formed with the chamosite (Plate 3.6F).

Feldspar

Feldspar cement is usually present in minor amounts in lithologies containing abundant detrital feldspar (e.g., Viking "A" rocks). Authigenic feldspar usually occurs as optically discontinuous overgrowths around detrital feldspar (Plate 3.7F). Authigenic feldspar also occurs as small tabular crystals growing on host grains (Plate 3.8B & 3.8C). EDAX analysis indicates that most overgrowths are albite (Plate 3.8B, 3.8C & 3.8D). The timing of authigenic feldspar appears to be late and commonly overlaps with quartz cements (Plate 3.8C).

Fe-Calcite

Fe-calcite (d_{104} = 3.03 Å) is uncommon but comprised up to 12% of one rock (sample # M631, Table 3.2). Fe-calcite crystallized after quartz and, in some places, completely fills pore space (Plate 3.9A). Fe-calcite also occurs as a replacement of detrital feldspar; much of the Fe-calcite cement contains small feldspar inclusions (Plate 3.9B).

Ankerite

Discrete ankerite (d_{104} = 2.90 Å) occurs mainly in the coarse-grained sandstones and conglomerates and is present in amounts up to 5% (Table 3.2). Discrete ankerite occurs as euhedral, pore-filling crystals that formed after quartz cementation (Plate 3.8D, & 3.9C). Ankerite also occurs as a replacement of detrital feldspar (Plate 3.9D). EDAX analysis

of ankerite indicates it is Ca-rich (Plate 3.8G).

Ankerite also occurs as a replacement of detrital dolomite in the fine-grained sandstones (Figure 3.4). Samples that show only minor ankeritization usually contain a large unreacted dolomite core (d_{104} = 2.88) and a small Fe-dolomite or ankerite rim (d_{104} = 2.90) (Figure 3.4A and Plate 3.2E & 3.8F). Intermediate stages of ankeritization are characterized by equal quantities of dolomite (d_{104} = 2.89) and ankerite (d_{104} = 2.92) (Figure 3.4B and Plate 3.7B). Extensive ankeritization is characterized by a small Fe-rich dolomite core (d_{104} = 2.89) and a large ankerite component (d_{104} = 2.92) (Figure 3.4C and Plate 3.2D).

Kaolin Group Minerals

Kaolin group minerals are abundant in the coarse-grained sandstones and conglomerates (nd-10%) and are a minor component in the fine-grained sandstones (nd-2%) (Table 3.2). Most of these clays are present in the 5-20μm size-fraction and decrease in abundance in the 2-5μm (t-95%) and <2μm (5-60%) size-fractions (Table 3.3). Detrital kaolin group minerals occur as extensive pore-fillings in many conglomerates and coarse-grained sandstones (Plate 3.10A &3.10E). Detrital kaolin group minerals are usually greater than 10μm in diameter and have corroded and compacted edges (Plate 3.11A & 3.11B). Many detrital crystals are also enveloped by quartz cements (Plate 3.11D). Authigenic kaolin group minerals also occur as extensive pore-fillings (Plate

Figure 3.4. Degree of ankeritization of Viking dolomites.

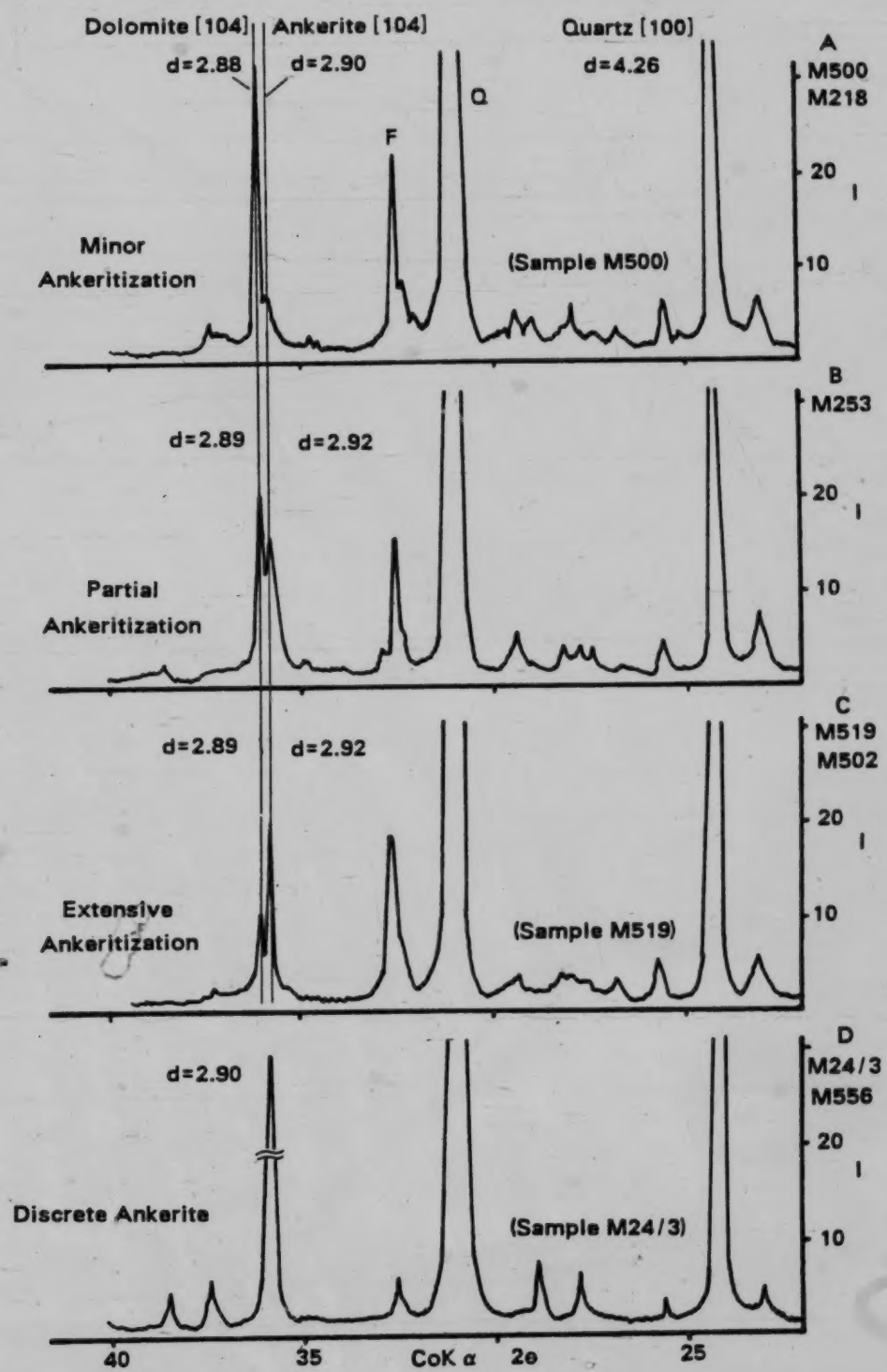

3.9E & 3.10C) and, in some places, appear to have formed as a replacement of detrital kaolin group minerals (Plate 3.10B, 3.10F & 3.11E). The authigenic phase usually occurs as well defined crystals, 10-20μm in diameter, with psuedohexagonal outlines and booklet-like stacking (Plate 3.11E & 3.11F).

X-ray diffraction analysis indicates that the kaolin group minerals are comprised of dickite and kaolinite (Figure 3.5). Samples that contain mostly authigenic kaolin group minerals (e.g., samples M119 & M122, Plate 3.9C & 3.10E) are comprised mostly of dickite (Figure 3.5A & 3.5B). XRD patterns obtained for dickite usually show very sharp and intense peaks characteristic of a well crystallized phase. Samples that contain both authigenic and detrital kaolin group minerals (e.g., samples M139 & M45, Plate 3.10A, 3.10B & 3.10D) contain both dickite and kaolinite (Figure 3.5C). In XRD, dickite shows well developed crystallinity while the kaolinite has broad, low intensity peaks characteristic of a poorly crystallized phase. Samples that contain a high percentage of detrital kaolin group minerals(e.g., samples M191 & M81, Plate 3.10E, 3.10F, 3.11A & 3.11C) contain a high percentage of kaolinite (Figure 3.5D).

Illite

The coarse-grained rocks contain few detrital clays; most of the illite seen in XRD is probably authigenic

Figure 3.5. X-ray diffraction analysis of kaolin group minerals
([hkl] data from Bailey, 1980).

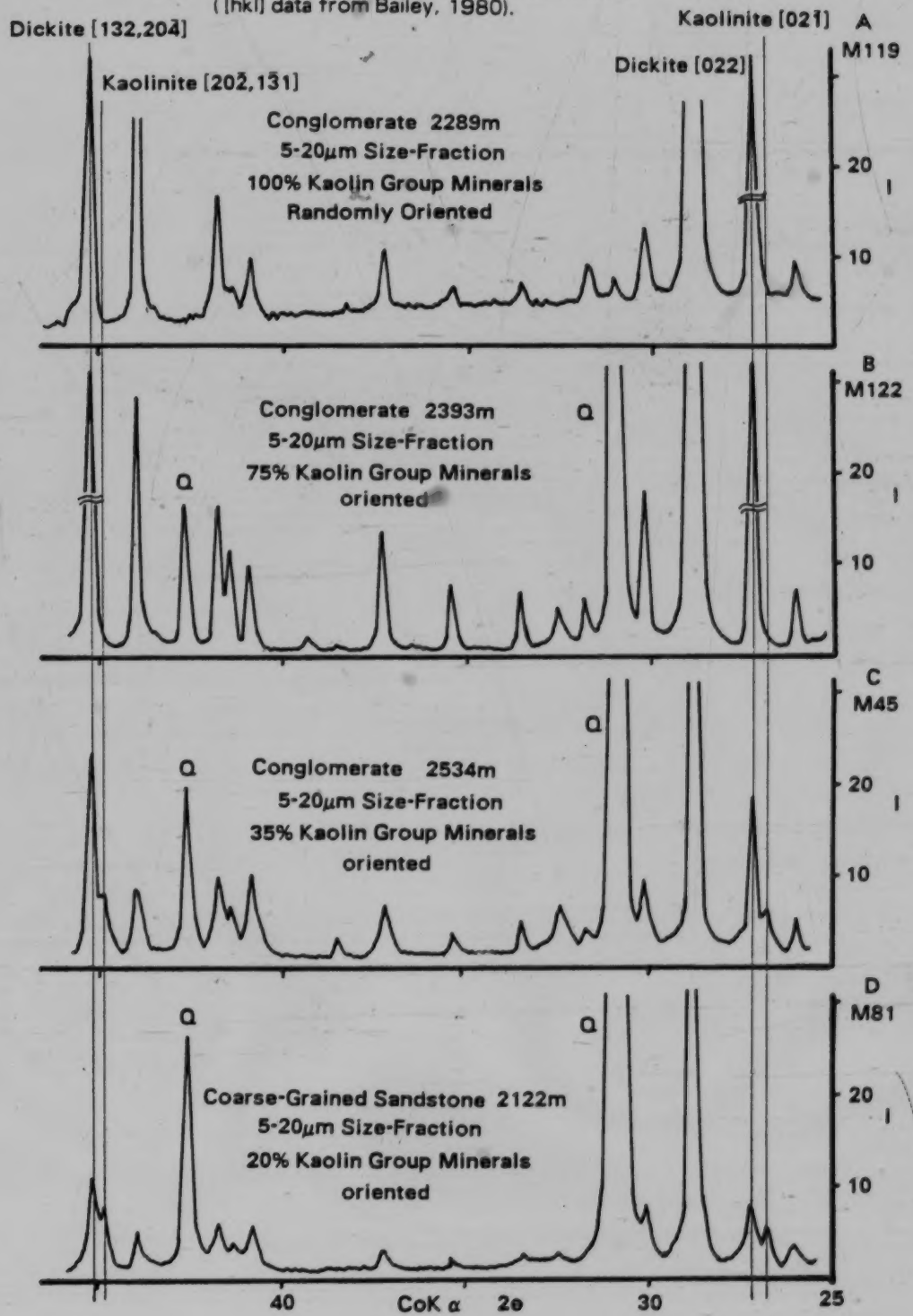

(Figure 3.6). Authigenic illite usually occurs as lath-like crystals lining grain surfaces and previously formed phases, such as quartz and ankerite (Plate 3.11G, 3.11H & 3.12G). Illite and illite/smectite can have similar morphologies and can be difficult to distinguish (Plate 3.12F).

Illite/Smectite

Illite/smectite occurs in trace amounts in most rocks and usually comprises nd-25% of the <2μm size-fraction. A detrital origin for some of these clays cannot be ruled out; however authigenic illite/smectite is common in all rocks. It usually occurs as interlocking networks of crystals ("honeycombs") that line grain surfaces (Plate 3.12A). Individual crystals usually contain lath-like projections that may be mistaken for illite in SEM (Plate 3.12F). EDAX analysis of illite/smectite suggests that they contain a high illite (K^+) content (Plate 3.12H).

The nature of the interstratification and the percentage of smectite layers does not vary with depth in either the fine or coarse-grained rocks (Figure 3.6 & 3.7). The values of the I/S (001) and (002) basal diffractions are constant within these sandstones and do not show a continuous decrease with depth. At shallow burial these values are 12.7 to 13.3Å (001) and 5.22 to 5.28Å (002) (Figure 3.6A and 3.7A). At maximum burial similar values are seen: 12.2 to 12.8Å (001) and 5.21 to 5.23Å (002) (Figure 3.6D & 3.7D).

Figure 3.6. Nature of clay minerals in coarse-grained rocks, <2.0 μm size-fraction Ca⁺⁺ saturated - glycolated (25°C).

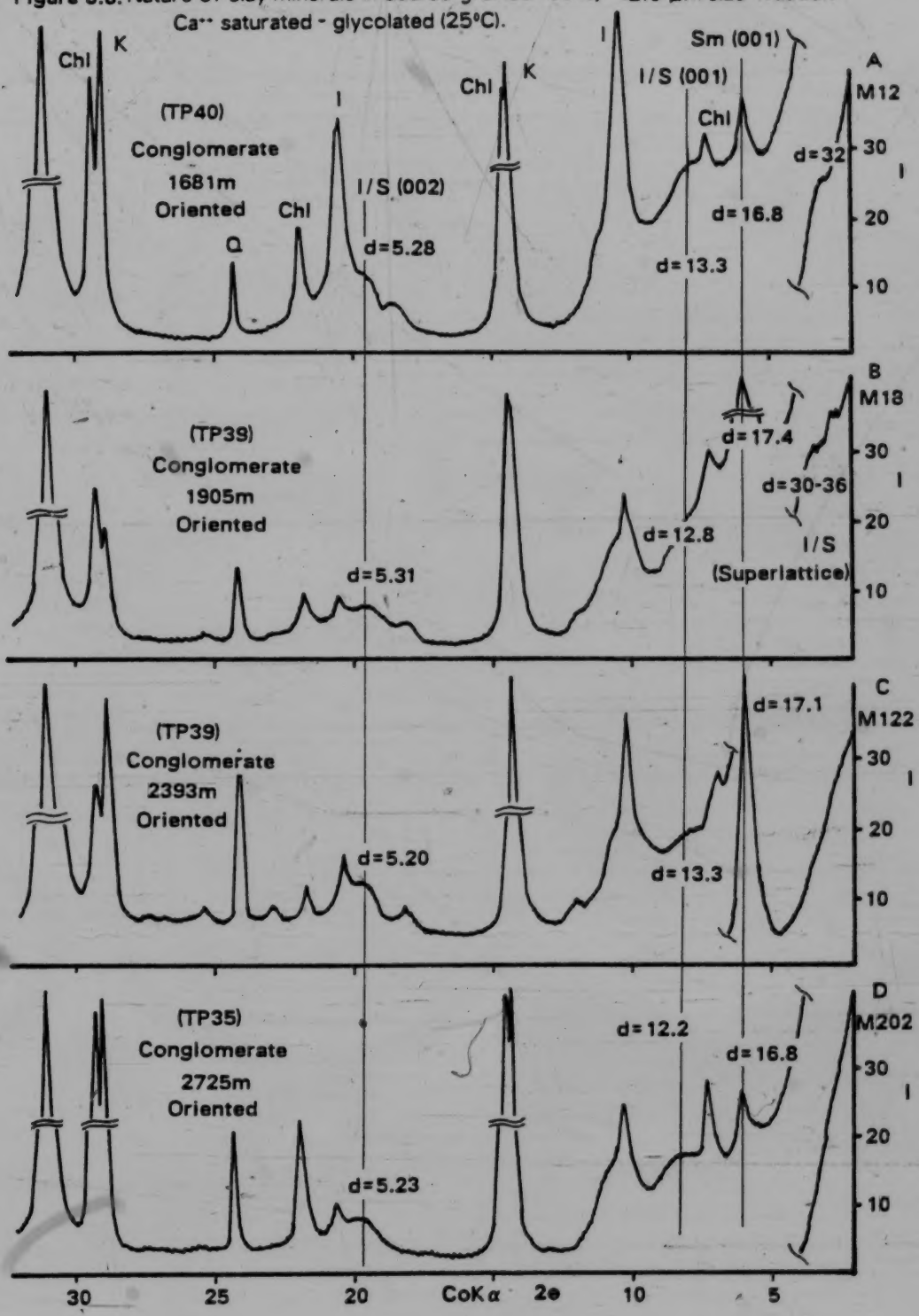

Figure 3.7. Nature of illite / smectite in the fine-grained sandstones, <0.2 μm size-fraction Na^+ saturated - glycolated (25°C).

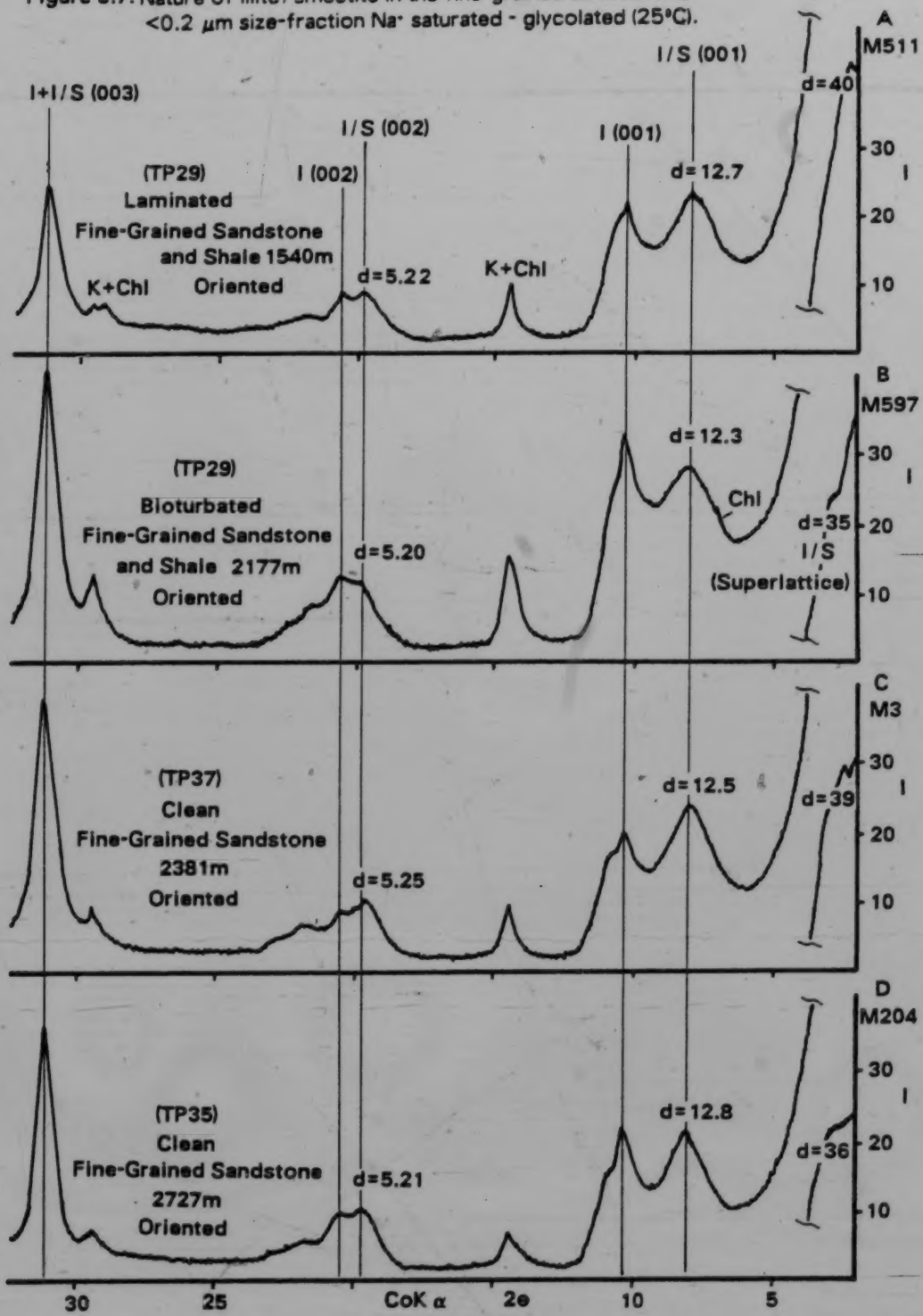

A comparison of the I/S (001), (002), and (003) basal diffraction values to computer generated data for illite/smectite (Srodon, 1984) also shows similar results as above (Table 3.4). The percentage of smectite layers is consistent between 22 and 29% and the ordering is predominantly IS-type. The well developed ordering of these phases is also illustrated by the appearance of superlattice diffractions between 30 and 40 Å (Figures 3.6 & 3.7).

The lack of variation in percent smectite layers and ordering of the illite/smectite in the sandstones contrasts with the illite/smectite in the shales. In the shales, the decrease in percent smectite layers and increase in ordering with depth may reflect the conversion of smectite to illite, similar to the illitization reactions reported in shales of the Gulf Coast (e.g., Boles and Franks, 1979). In the sandstones, illite/smectite found at shallow and at greater burial depths are similar in composition indicating that the dominant control on their formation was fluid chemistry rather than temperature.

Illite/smectite appears to be one of the last phases to form. It occurs as extensive coatings on siderite and chamosite (Plate 3.12E), authigenic kaolin group minerals (Plate 3.11G), and ankerite (Plate 3.12G). The crystallization of illite/smectite appears to have occurred at the same time as illite and smectite.

TABLE 3.4. PERCENT SMECTITE IN ILLITE/SMECTITE IN SANDSTONES

SAMPLE NUMBER	ROCK TYPE	DEPTH (m)	SIZE (μm)	% SMECTITE	ORDERING
6-36-29-26W4					
M511	F.Sst.	1540.0	<2.0	25	IS
			<0.2	25	IS
2-32-37-3W5					
M30	F.Sst.	1987.0	<2.0	24	IS
			<0.2	24	IS
2-13-29-2W5					
M597	F.Sst.	2177.0	<2.0	22	IS>IIS
			<0.2	22	IS>IIS
7-14-37-6W5					
M3	F.Sst.	2381.0	<2.0	29	IS>IIS
			<0.2	29	IS>IIS
13-8-35-6W5					
M204	F.Sst.	2727.0	<2.0	23	IS
			<0.2	23	IS

Smectite

Smectite occurs in trace amounts in the coarse-grained sandstones and conglomerates and has not been detected in the fine-grained sandstones (Table 3.3). Smectite is found mainly in the <2μm size-fraction where it varies from nd-25% (Table 3.3). Smectite usually show a strong 17Å basal diffraction upon glycolation and has been found in all fields including Gilby, Willesden Green, Ferrier and Caroline (Figure 3.6).

Most of the smectite present is probably authigenic. Authigenic smectite usually occurs as honeycomb-networks of crystals that line grain surfaces (Plate 3.12B). EDAX analysis of smectite indicates the dominant cations are Ca, Mg and Fe (Plate 3.12D). The timing of smectite formation appears to be late and postdates quartz and albite cements (Plate 3.12C).

PLATE 3.3

A. Photomicrograph of a Viking "B" coarse-grained sandstone showing large, pellet-shaped glauconite grains (Gl) undergoing dissolution. Dissolution postdates quartz cementation as shown by the relict outline of the glauconite grain (arrows) (Gilby field, well # 10-10-40-1W5, sample # M13, depth = 1682.0m, plane polars, dark blue = porosity, field of view = 1 X 1 mm).

B. Photomicrograph of a Viking "B" coarse-grained sandstone showing the compaction of glauconite (Gl) and its replacement by pyrite (Py) (Willesden Green field, well # 10-10-40-1W5, sample # M13, depth = 1682.0m, plane polars, dark blue = porosity, field of view = 1 X 1 mm).

C. Photomicrograph of a Viking "B" conglomerate showing clusters of pyrite crystals (Py) lining chert (Ch). The dissolution of chert is apparent with secondary pore spaces filled with pyrite (white arrow). Pyrite also occurs as extensive pore-fillings that appear to postdate quartz cementation (AQ) (dark arrow) (Willesden Green field, well # 5-6-41-6W5, sample # M94, depth = 2294.3m, plane polars, dark blue = porosity, field of view = 1 X 1 mm).

D. Photomicrograph of a Viking "B" coarse-grained sandstone showing detrital quartz (Q) lined by early authigenic siderite (Sid). The siderite has been enveloped by quartz overgrowths (AQ) (Caroline field, well # 2-25-35-7W5, sample # M233, depth = 2727.0m, plane polars, dark blue = porosity, field of view = 1 X 1 mm).

E. Photomicrograph of a Viking "B" coarse-grained sandstone showing how early pyrite (Py) may have served as a nucleation site for authigenic siderite (Sid) (Caroline field, well # 2-25-35-7W5, sample # M233, depth = 2727.0m, X polars, field of view = 0.64 X 0.64mm).

F. Photomicrograph of a Viking "B" fine-grained sandstone showing extensive siderite cement (Sid). Siderite either formed as a replacement of detrital grains or crystallized before significant compaction (Carbon field, well # 7-7-29-22W4, sample # M503, depth = 1289.0m, X polars, field of view = 0.64 X 0.64 mm).

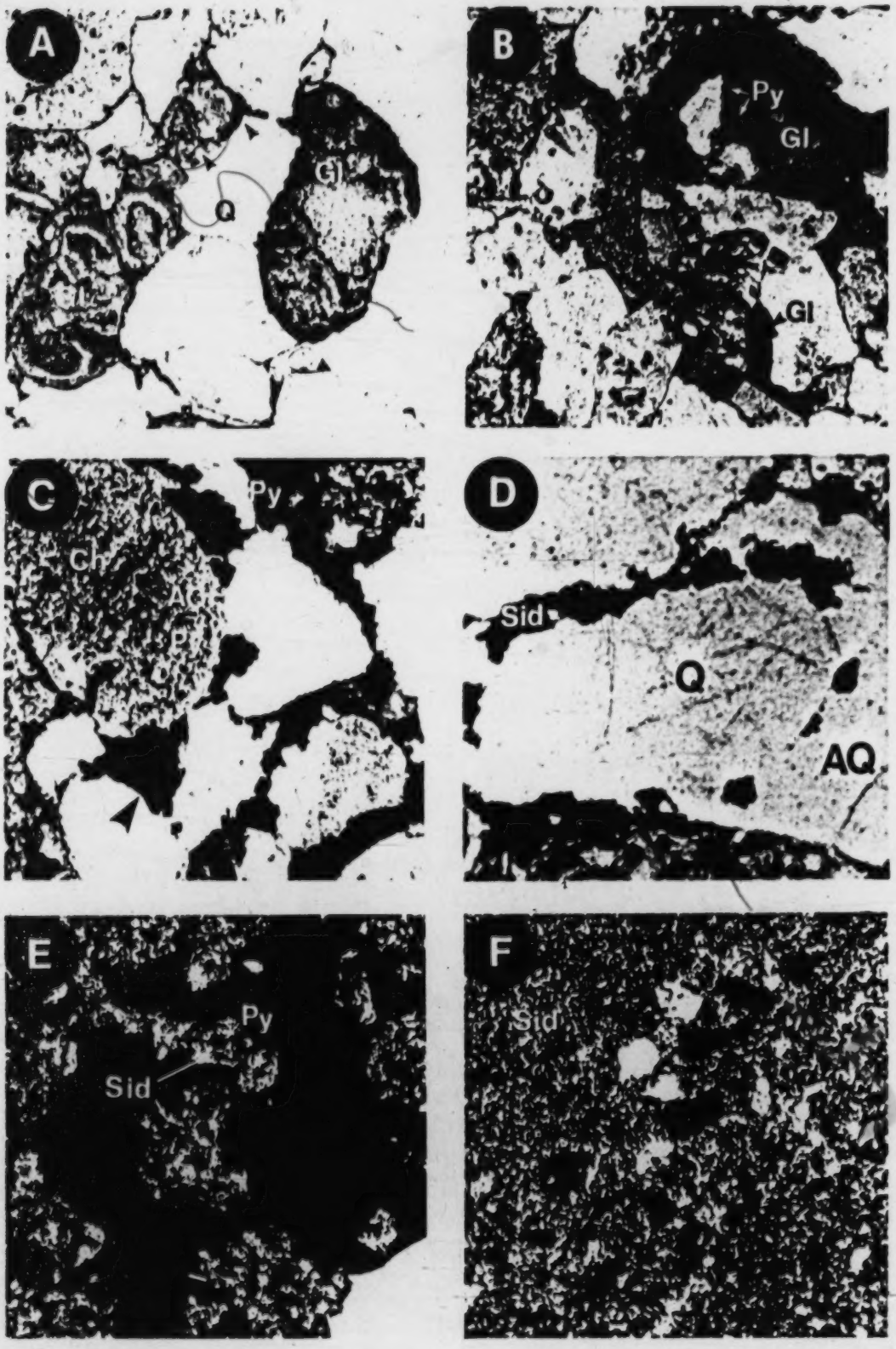
A
Gl
Q
B
Py
Gl
Gl
C
Py
Ch
Ac
P
D
Sid
Q
AQ
E
Py
Sid
F
Sid

PLATE 3.4

A. Scanning electron photomicrograph of a Viking "B" conglomerate showing quartz overgrowths (AQ) and pyrite (Py). The pyrite appears to be growing on top of the authigenic quartz (Willesden Green field, well # 5-6-41-6W5, sample # M94, depth = 2294.0m).

B. Scanning electron photomicrograph of a Viking "A" coarse-grained sandstone showing authigenic quartz (AQ) and framboidal pyrite (Py). The pyrite appears to be growing on the authigenic quartz (Caroline field, well # 13-8-35-6W5, sample M199, depth = 2720.0m).

C. Scanning electron photomicrograph of a Viking "B" coarse-grained sandstone showing the dissolution of glauconite (Gl). An energy dispersive X-ray analysis (EDAX) of the glauconite (Photomicrograph D) indicates that it contains Si, Al, K, Ca and Fe [1] (Joffre field, well # 11-7-39-26W4, sample # M556, depth = 1548.4m).

E. Scanning electron photomicrograph of a Viking "B" coarse-grained sandstone showing the surface of a glauconite grain and its replacement by pyrite (Py). An EDAX of the glauconite surface (Photomicrograph F) indicates that Fe and S are present (Joffre field, well # 11-7-39-26W4, sample # M556, depth = 1548.4m).

G. Scanning electron photomicrograph of a Viking "B" conglomerate showing poorly crystallized pyrite (Py) with a chlorite (Chl) rosette growing on its surface. An EDAX of the chlorite (Photomicrograph H) indicates it is Fe-rich (Willesden Green field, well # 3-31-40-6W5, sample # M191, depth = 2276.0m).

---

[1]Au and Ag, commonly present on EDAX, were introduced during sample preparation

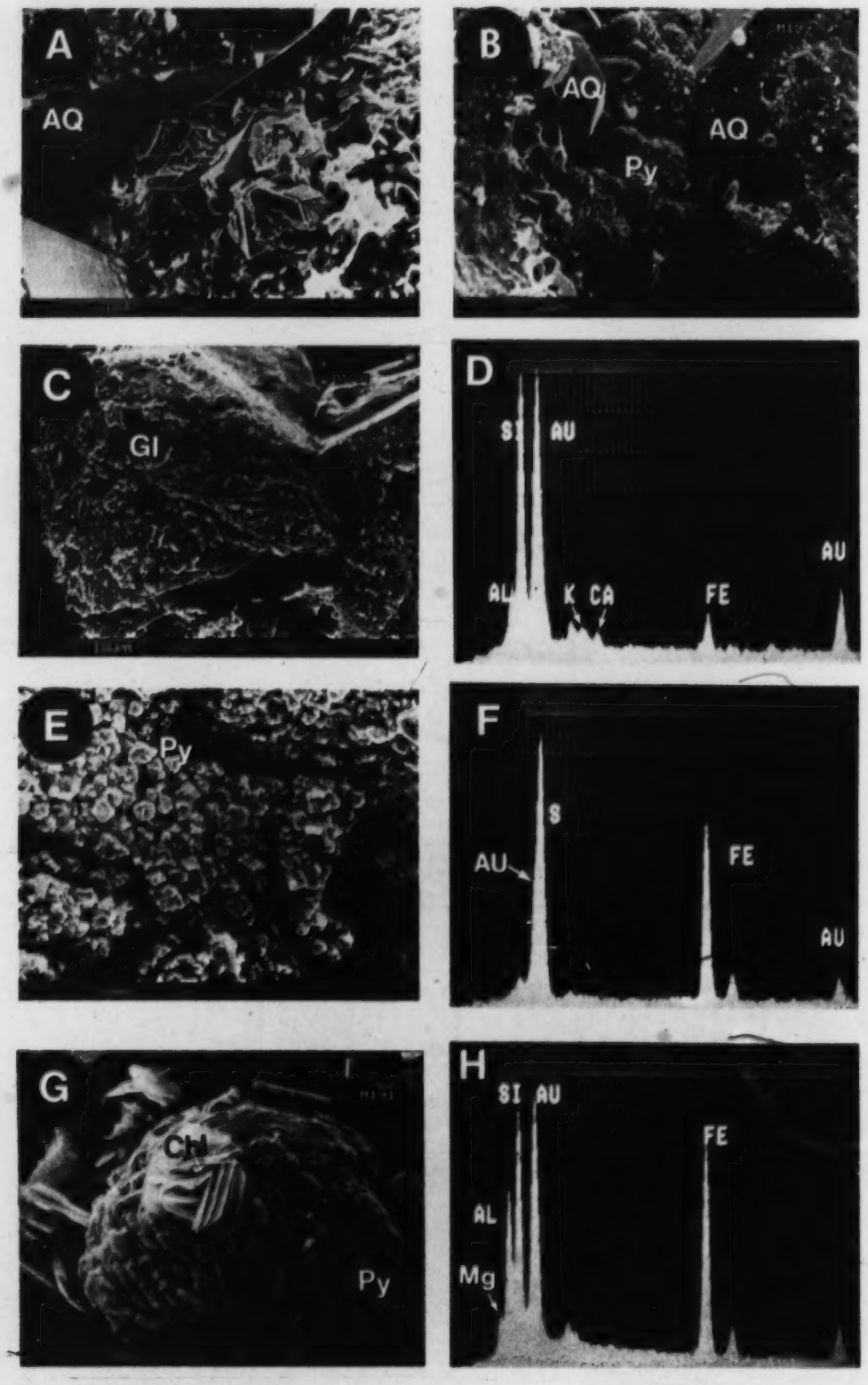
A
AQ
Py
B
AQ
AQ
Py
C
Gl
D
SI
AU
AU
AL
K CA
FE
E
Py
F
S
AU
FE
AU
G
Chl
Py
H
SI AU
FE
AL
Mg

PLATE 3.5

A. Scanning electron photomicrograph of a Viking "B" coarse-grained sandstone showing well crystallized, platy chlorite (Chl) lining grain surfaces (Gilby field, well # 3-27-40-6W5, sample # M114, depth = 2230.0m).

B. Scanning electron photomicrograph of a Viking "A" coarse-grained sandstone showing poorly crystallized chlorite (Chl) and authigenic quartz (AQ). (Caroline field, well # 7-32-34-6W5, sample # M250, depth = 2710.0m).

C. Scanning electron photomicrograph of a Viking "A" conglomerate showing authigenic chlorite (Chl) that is being enveloped by authigenic quartz (AQ) (Gilby field, well # 11-24-42-6W5, sample # M80, depth = 2121.0m).

D. Scanning electron photomicrograph of a Viking "B" medium-grained sandstone showing authigenic chlorite (Chl), siderite (Sid), quartz (AQ) and kaolin group minerals (AK). Siderite can be seen enveloping chlorite (arrow) (well # 10-24-33-8W5, sample # M660, depth = 3101.0m).

E. Scanning electron photomicrograph of a Viking "A" conglomerate showing a well crystallized chlorite (Chl) rosette which is being enveloped by authigenic quartz (AQ). An EDAX of the chlorite (Photomicrograph G) indicates it is Fe-rich (Gilby field, well # 11-24-42-6W5, sample # M80, depth = 2121.0m).

F. Scanning electron photomicrograph of a Viking "B" fine-grained sandstone showing early chlorite (Chl) that is being replaced by siderite (Sid) (arrow). An EDAX of the siderite (Photomicrograph H) indicates that it contains minor Mg, Ca & Mn; the Si may reflect chlorite contamination (Gilby field, well # 2-30-38-7W5, sample # M141, depth = 2537.0m).

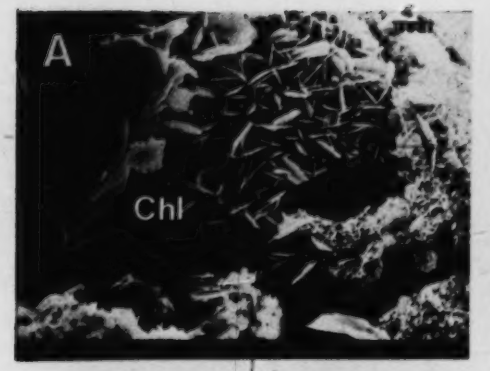
A
Chl

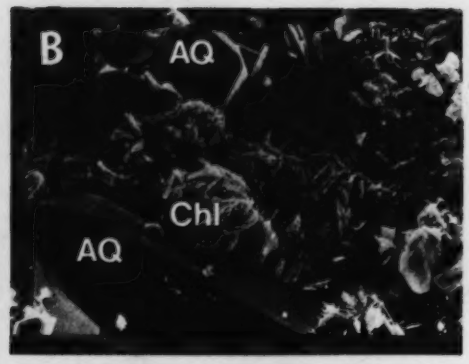
B
AQ
Chl
AQ

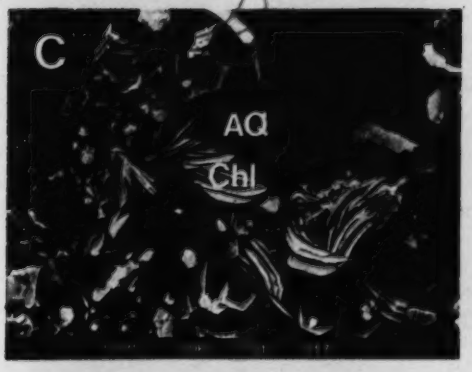
C
AQ
Chl

D
Chl
Sid
AK
AQ

E
Chl
AQ

F
Chl
Sid

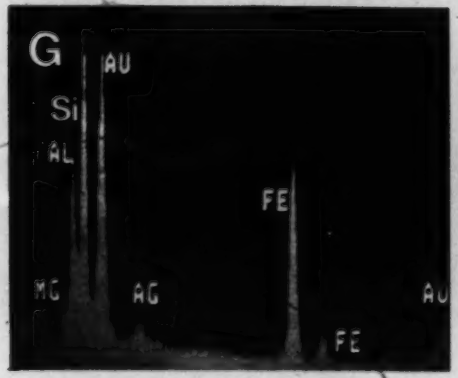
G
AU
Si
AL
FE
MG
AG
AU
FE

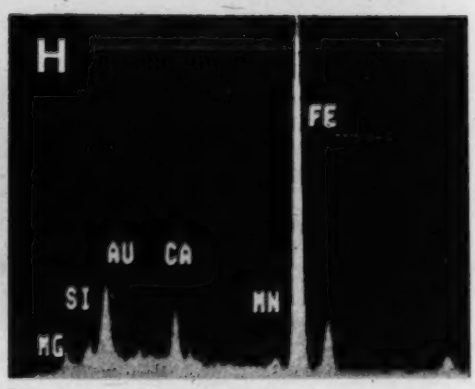
H
FE
AU CA
SI
MN
MG

PLATE 3.6

A. Scanning electron photomicrograph of a Viking "B" conglomerate showing kaolin group minerals (AK). Some of these crystals are enveloped by authigenic quartz (arrow) and may be detrital (Ferrier field, well # 2-30-38-7W5, sample # M139, depth = 2534.0m).

B. Scanning electron photomicrograph showing details of kaolin group minerals in Photomicrograph A. Crystals are well formed with psuedohexagonal outlines and are stacked into booklets. Individual crystals range between 10 and 20 microns in diameter.

C. Scanning electron photomicrograph of Viking "B" conglomerate showing detrital kaolin group minerals (K) and its replacement by chlorite (Chl). The chlorite can be seen replacing certain layers within the stacked booklet (black arrow). An EDAX of the chlorite (Photomicrograph D) indicates it is Fe-rich (Ferrier field, well # 2-30-38-7W5, sample # M139, depth = 2534.0m).

E. Scanning electron photomicrograph showing details of chlorite in Photomicrograph C. The nature of the intergrowths reflects the layer by layer replacement of kaolin group minerals (K) by chlorite (Chl).

F. Scanning electron photomicrograph of a Viking "B" conglomerate showing detrital kaolin group minerals (K) and well crystallized authigenic chlorite (Chl). In some kaolinite group mineral booklets thin chlorite interlayers (arrow) are visible. Authigenic quartz (AQ) can be seen growing within and around some of the chlorite. An EDAX of the chlorite (Photomicrograph G) indicates it is Fe-rich but also contains Mg. An EDAX of the kaolin group minerals (Photomicrograph H) indicates it contains minor Fe (Ferrier field, well # 2-30-38-7W5, sample # M139, depth = 2534.0m).

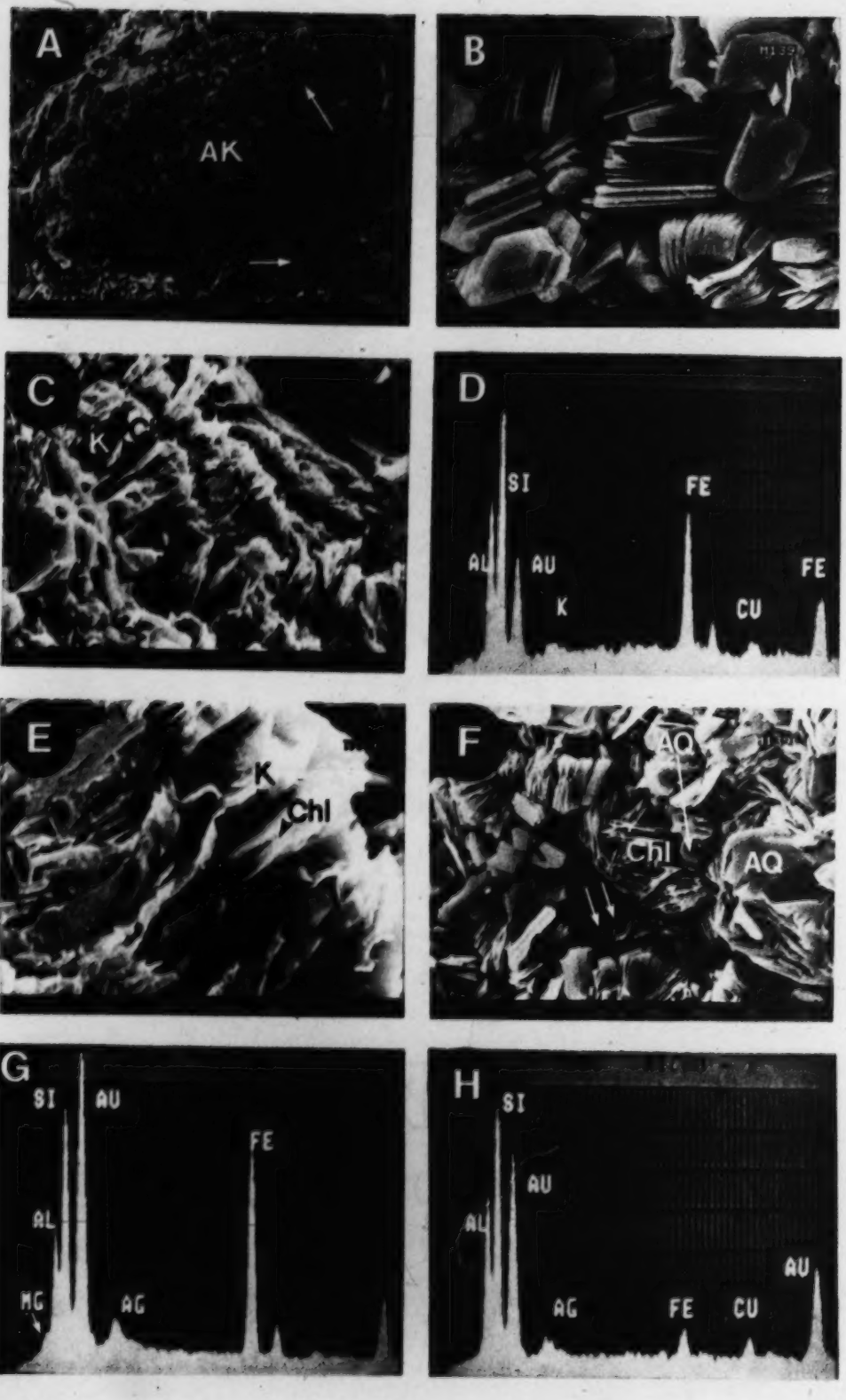
A
AK
B
C
K
D
SI
FE
AL
AU
K
CU
FE
E
K
Chl
F
AQ
Chl
AQ
G
SI
AU
FE
AL
MG
AG
H
SI
AU
AL
AU
AG
FE
CU

PLATE 3.7

A. Photomicrograph of a Viking "B" fine-grained sandstone showing the replacement of dolomite (Dol) by authigenic siderite (Sid). The formation of siderite may have inhibited ankeritization of the dolomite (Caroline field, well # 10-24-35-7W5, sample # M42, depth = 2737.0m, X polars, field of view = 0.64 X 0.64 mm).

B. Photomicrograph of a Viking "B" fine-grained sandstone showing extensive ankeritization (Ank) (stained blue) of detrital dolomite (Dol). Detrital dolomite cores (Dol) show pitted surfaces reflecting mechanical abrasion. Authigenic pyrite (Py) is also seen growing within some carbonate grains (Caroline field, well # 7-32-34-6W5, sample # M253, depth = 2719.1m, plane polars, field of view = 0.64 X 0.64 mm).

C. Photomicrograph of a Viking "B" coarse-grained sandstone showing complete overgrowths of quartz (AQ) on detrital quartz (Q). The dissolution of chert has created secondary porosity that has been filled with bitumen (stained black). Dissolution occurred after quartz cementation as shown by the irregular outline left by the quartz overgrowth (white arrow). (Willesden Green field, well # 5-6-41-6W5, sample # M93, depth = 2293.0m, plane polars, dark blue = porosity, field of view = 1 X 1 mm).

D. Photomicrograph of a Viking "B" coarse-grained sandstone showing extensive quartz cementation. Complete overgrowths on many grains end in triple junctions within pore spaces (arrows) (Willesden Green field, well # 5-6-41-6W5, sample # M93, depth = 2293.0m, X polars, field of view = 2.7 X 2.7 mm).

E. Photomicrograph of a Viking "B" conglomerate showing numerous, small quartz crystals (AQ) lining chert (Ch) (Gilby field, well # 11-24-42-6w5, sample # M80, depth = 2121.0m, plane polars, dark blue = porosity, field of view = 1 X 1 mm).

F. Photomicrograph of a Viking "A" coarse-grained sandstone showing optically discontinous feldspar overgrowths (AF) on detrital feldspar (F) (Gilby field, well # 6-15-40-5W5, sample # M106, depth = 2145.7m, X polars, field of view = 1 X 1 mm).

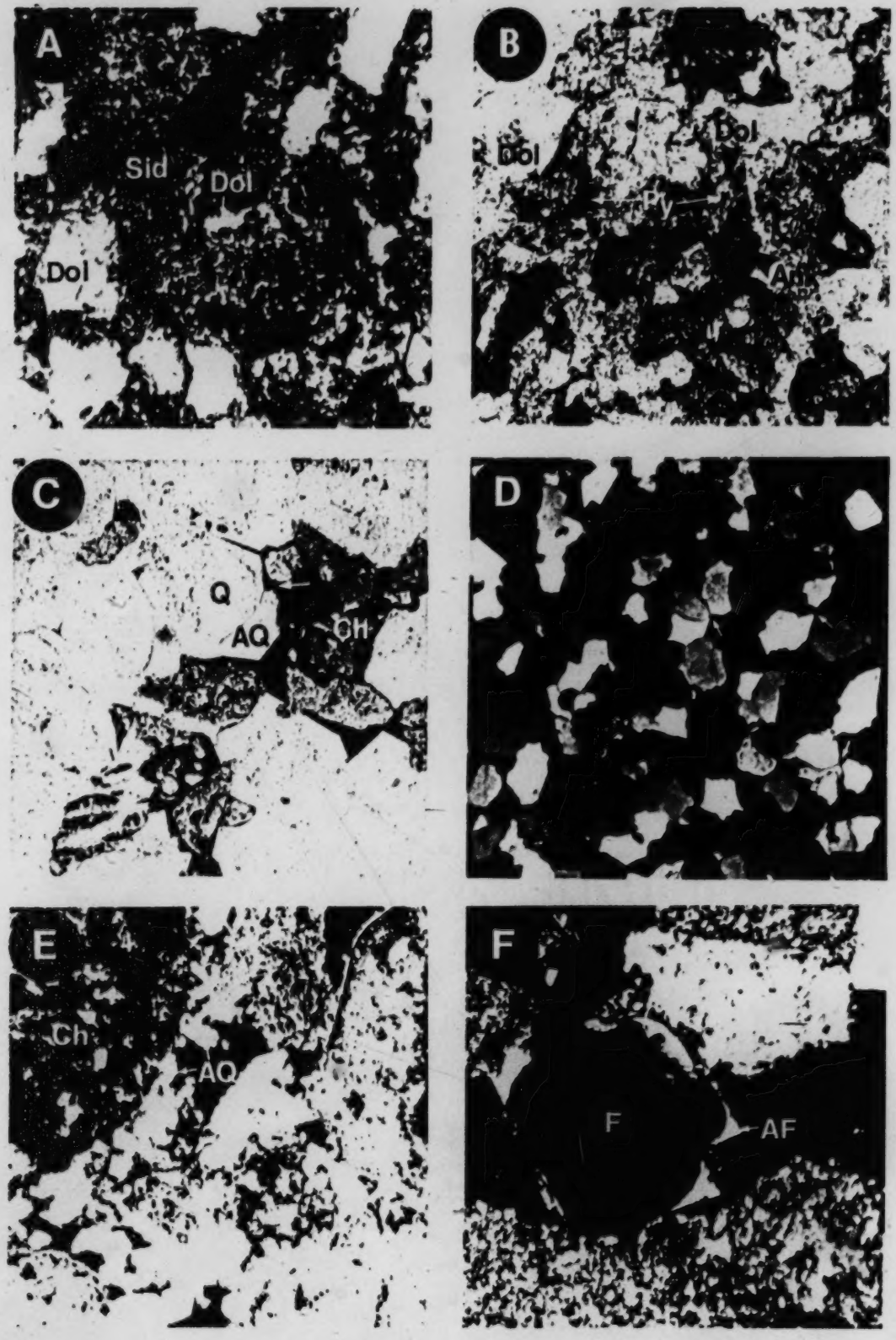
A
Sid
Dol
Dol
B
Dol
Dol
Py
Ank
C
Q
AQ
Ch
D
E
Ch
AQ
F
F
AF

PLATE 3.8

A. Scanning electron photomicrograph of a Viking "B" conglomerate showing large, complete quartz overgrowths (AQ) and smaller, pore-lining authigenic quartz (AQ) (Gilby field, well # 14-9-39-2W5, sample # M18, depth = 1905.0m).

B. Scanning electron photomicrograph of a Viking "A" coarse-grained sandstone showing pore-lining authigenic quartz (AQ) and pore-filling authigenic kaolin group minerals (AK). Individual kaolin group minerals range between 5 and 20 microns in diameter and are stacked into booklets. Authigenic feldspar (AF) are also seen growing on detrital feldspar. An EDAX of the authigenic feldspar (not shown) indicates it is albite. (Caroline field, well # 6-16-35-5W5, sample # M216, depth = 2465.0m).

C. Scanning electron photomicrograph of a Viking "A" coarse-grained sandstone showing authigenic feldspar (AF) partly enveloping authigenic quartz (AQ) (arrow). An EDAX of the feldspar (not shown) indicates it is albite (Caroline field, well # 6-16-35-5W5, sample # M216, depth = 2465.0m).

D. Scanning electron photomicrograph of a Viking "A" coarse-grained sandstone showing abundant authigenic quartz (AQ), ankerite (Ank), and feldspar (AF). The ankerite partly envelopes the authigenic quartz (arrow). An EDAX of the authigenic feldspar (not shown) indicates it is albite. An EDAX of the ankerite (Photomicrograph E) indicates it is Ca-rich (Caroline field, well # 6-16-35-5W5, sample # M216, depth = 2465.0m).

F. Scanning electron photomicrograph of a Viking "B" fine-grained sandstone showing an ankerite overgrowth (Ank) on a detrital dolomite core (Dol). An EDAX of the ankerite (location #2) (Photomicrograph G) indicates it is Fe-rich; the dolomite core contains minor amounts of Fe (location #1) (Caroline field, well # 6-16-35-5W5, sample # M218, depth = 2468.0m).

H. Scanning electron photomicrograph of the 5-20 microns size-fraction from sample # M45. Authigenic quartz (AQ), broken off detrital grains during disaggregation, was concentrated in this size-fraction. Kaolin group minerals (K) are also present.

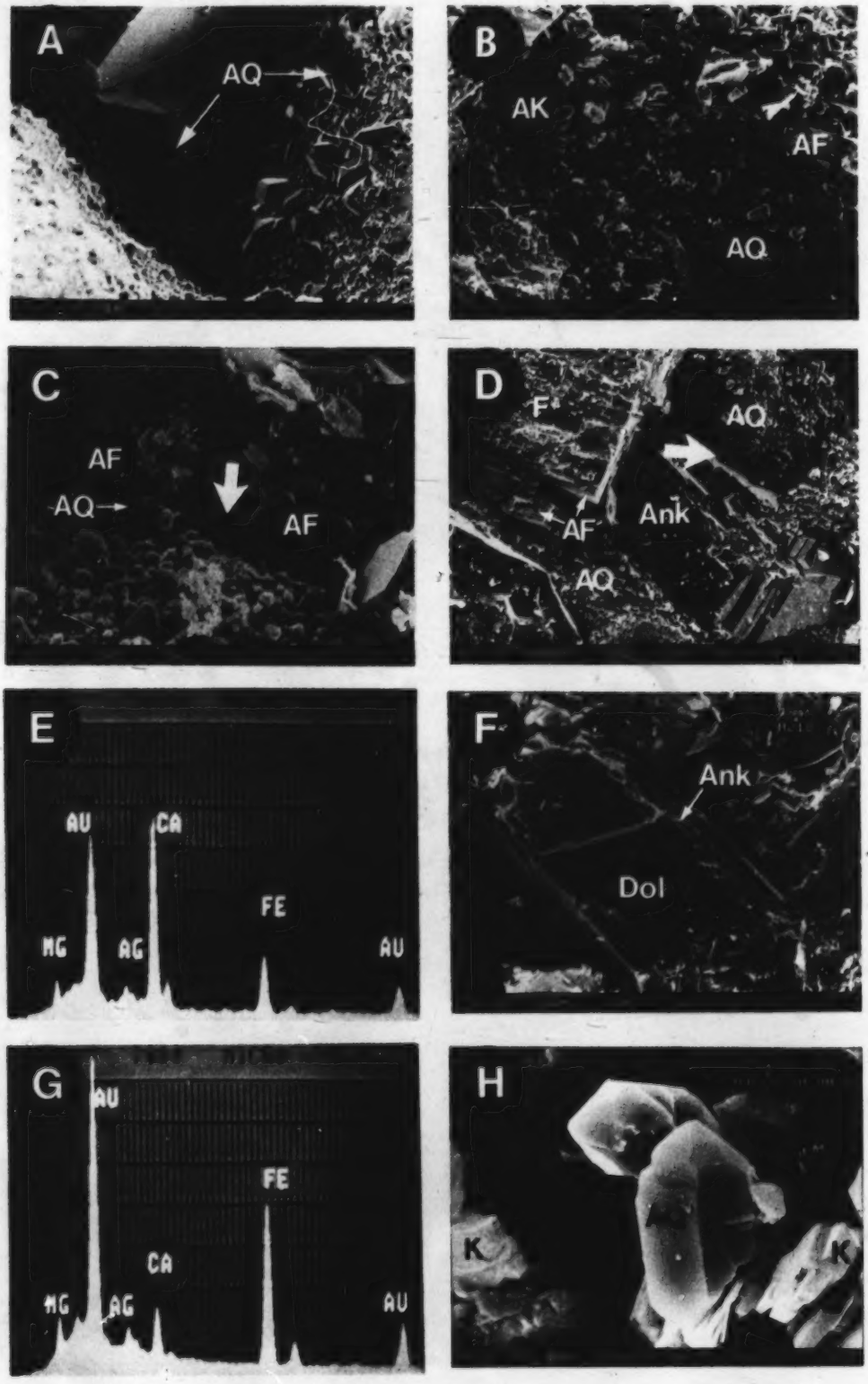
A
AQ
B
AK
AF
AQ
C
AF
AQ
AF
D
F
AQ
AF
Ank
AQ
E
AU
CA
FE
MG
AG
AU
F
Ank
Dol
G
AU
FE
CA
MG
AG
AU
H
K
K

PLATE 3.9

A. Photomicrograph of a Viking "A" coarse-grained sandstone showing authigenic quartz (AQ); detrital grain boundaries are marked by small gaps where nucleation was inhibited (arrow). Fe-calcite (Cal) fills remaining pore space (well # 6-18-31-2W5, sample # M631, depth = 2199.8m, plane polars, field of view = 1 X 1 mm).

B. Photomicrograph of a Viking "A" coarse-grained sandstone showing authigenic calcite (Cal) and detrital feldspar (F). Small lath-like inclusions of feldspar are seen within some calcite cements suggesting replacement (arrow) (well # 6-18-31-2W5, sample # M631, depth = 2199.8m, X polars, field of view = 1 X 1 mm).

C. Photomicrograph of a Viking "A" conglomerate showing authigenic ankerite (Ank) (stained light blue) and sideritized chert (Sid). The formation ankerite was late and is seen enveloping authigenic quartz (AQ) (Gilby field, well # 3-17-40-4W5, sample # M48, depth = 2156.0m, plane polars, dark blue = porosity, field of view = 1 X 1 mm).

D. Photomicrograph of a Viking "B" conglomerate showing ankerite (Ank) replacing detrital feldspar (F); small feldspar laths are present within the ankerite (arrow). Replacement occurred after quartz cementation (AQ) (Harmattan field, well # 6-24-32-3W5, sample # M24/3, depth = 2200.0m, X polars, field of view = 0.64 X 0.64 mm).

E. Photomicrograph of a Viking "B" conglomerate showing authigenic pore-filling kaolin group minerals (AK) and pore-lining authigenic quartz (AQ) (Ferrier field, 6-1-39-7W5, sample # M122, depth = 2393.0m, plane polars, dark blue = porosity, field of view = 1 X 1 mm).

F. Photomicrograph of a Viking "B" conglomerate showing the partial dissolution of detrital feldspar (F) and its alteration to authigenic kaolin group minerals (AK) (Caroline field, well # 10-24-35-7W5, sample # M40, depth = 2734.0m, plane polars, field of view = 1 X 1 mm).

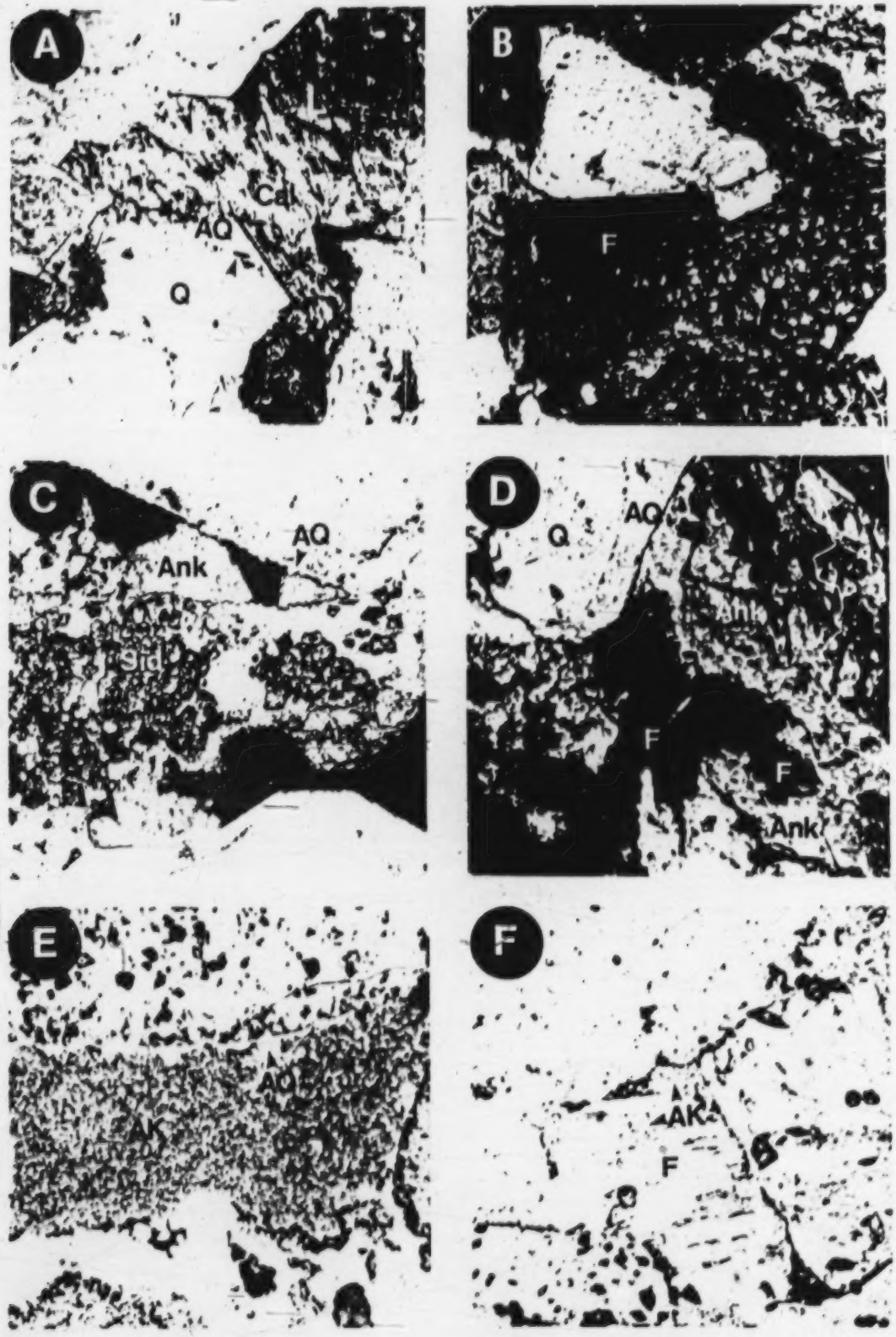
A
L
Cal
AQ
Q
B
Cal
F
C
AQ
Ank
Sid
D
AQ
Q
Ank
F
F
Ank
E
AQ
AK
F
AK
F

PLATE 3.10

A. Photomicrograph of a Viking "B" conglomerate showing chert (Ch) floating in a matrix comprised of detrital kaolin group minerals (K). Dark brown areas contain authigenic kaolin group minerals (arrows). Numerous, small quartz crystals (Q) are also seen withing the matrix (Ferrier field, well # 2-30-38-7W5, sample # M139, depth = 2534.0m, plane polars, field of view = 2.7 X 2.7mm).

B. Photomicrograph showing details authigenic kaolin group minerals (AK) in Photomicrograph A. They appear as large crystals that are stacked into booklets (Dark brown = hydrocarbon staining, field of view = 0.15 X 0.15mm).

C. Photomicrograph of a Viking "B" conglomerate showing extensive pore-filling authigenic kaolin group minerals (AK). Remanents of detrital kaolin group minerals (K) and authigenic quartz (AQ) are also seen (Willesden Green field, well # 14-25-40-7W5, sample # M119, depth = 2289.2m, plane polars, dark blue = porosity, field of view = 1 X 1mm).

D. Photomicrograph of a Viking "B" conglomerate showing detrital kaolin group minerals (K) and pore-lining authigenic quartz (AQ) (Gilby field, well # 10-9-41-3W5, sample # M45, depth = 1923.0m, plane polars, dark blue = porosity, field of view = 1 X 1mm).

E. Photomicrograph of a Viking "B" coarse-grained sandstone showing chert (Ch) and quartz (Q) floating in detrital kaolin group minerals (K). Quartz overgrowths are absent on most grains (Gilby field, well # 11-24-42-6W5, sample # M81, depth = 2122.0m, plane polars, dark blue = porosity, field of view = 0.64 X 0.64mm).

F. Photomicrograph of a Viking "B" conglomerate showing detrital kaolin group minerals (K), siderite (Sid), pyrite (Py), and minor authigenic kaolin group minerals (AK) (Willesden Green field, well # 3-31-40-6W5, sample # M191, depth = 2276.0m, plane polars, dark blue = porosity, field of view = 0.64 X 0.64mm).

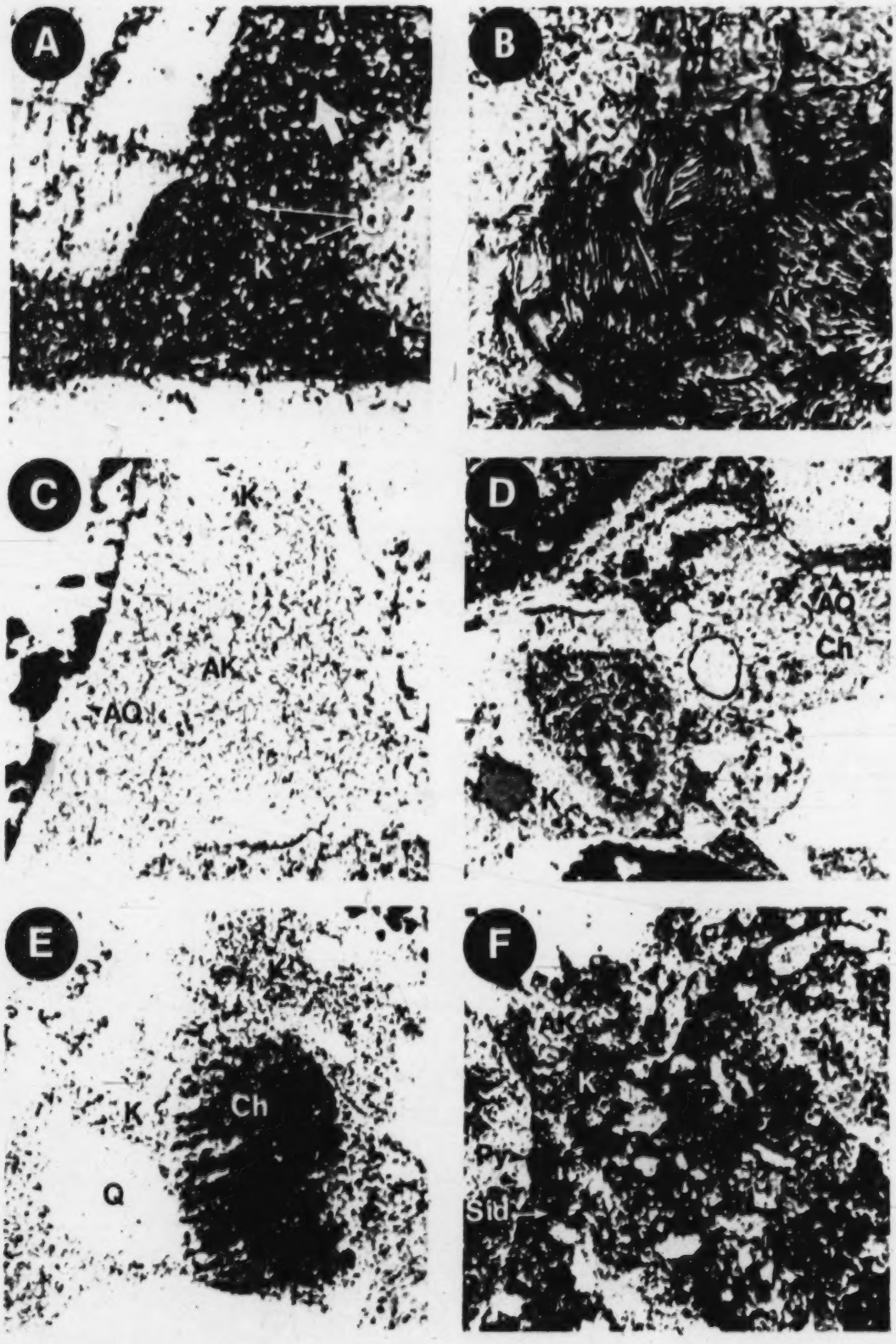
A
K
B
K
C
K
AK
AQ
D
AQ
Ch
K
E
K
Ch
Q
F
AK
K
Py
Sid

PLATE 3.11

A. Scanning electron photomicrograph of a Viking "B" conglomerate showing detrital kaolin group minerals (K) compacted against grain surfaces (Gilby field, well # 11-24-42-6W5, sample # M81, depth = 2122.0m).

B. Scanning electron photomicrograph showing details of the detrital kaolin group minerals in Photomicrograph A. Crystals have corroded edges and appear to be compacted against grain surfaces.

C. Scanning electron photomicrograph of a Viking "B" conglomerate showing detrital kaolin group minerals (K). Crystals have psuedohexagonal outlines but are broken and incomplete (Willesden Green field, well # 3-31-40-6W5, sample # M191, depth = 2276.0m).

D. Scanning electron photomicrograph of a Viking "B" conglomerate showing authigenic quartz (AQ) enveloping detrital kaolin group minerals (K) (Caroline field, well # 6-16-35-5W5, sample # M217, depth = 2467.0m).

E. Scanning electron photomicrograph of a Viking "B" conglomerate showing detrital kaolin group minerals (K) and authigenic kaolin group minerals (AK) (Ferrier field, well # 6-1-39-7W5, sample # M122, depth = 2393.0m).

F. Scanning electron photomicrograph of a Viking "B" conglomerate showing authigenic kaolin group minerals (AK) lining authigenic quartz (AQ). Some of the kaolin group minerals may be detrital and have been enveloped by authigenic quartz (arrows) (Ferrier field, well # 6-1-39-7W5, sample # M122, depth = 2393.0m).

G. Scanning electron photomicrograph of a Viking "A" coarse-grained sandstone showing illite (I) and illite / smectite (IS) lining detrital grains and authigenic kaolin group minerals (AK). Illite occurs as discrete lath-like fibers while illite / smectite is comprised of networks of crystals. (Caroline field, well # 13-8-35-6W5, sample # M199, depth = 2720.0m).

H. Scanning electron photomicrograph of a Viking "B" conglomerate showing authigenic quartz (AQ) and kaolin group minerals (AK) that are lined with illite (I) and illite / smectite (IS) (Gilby field, well # 4-3-42-4W5, sample # M87, depth = 1909.0m).

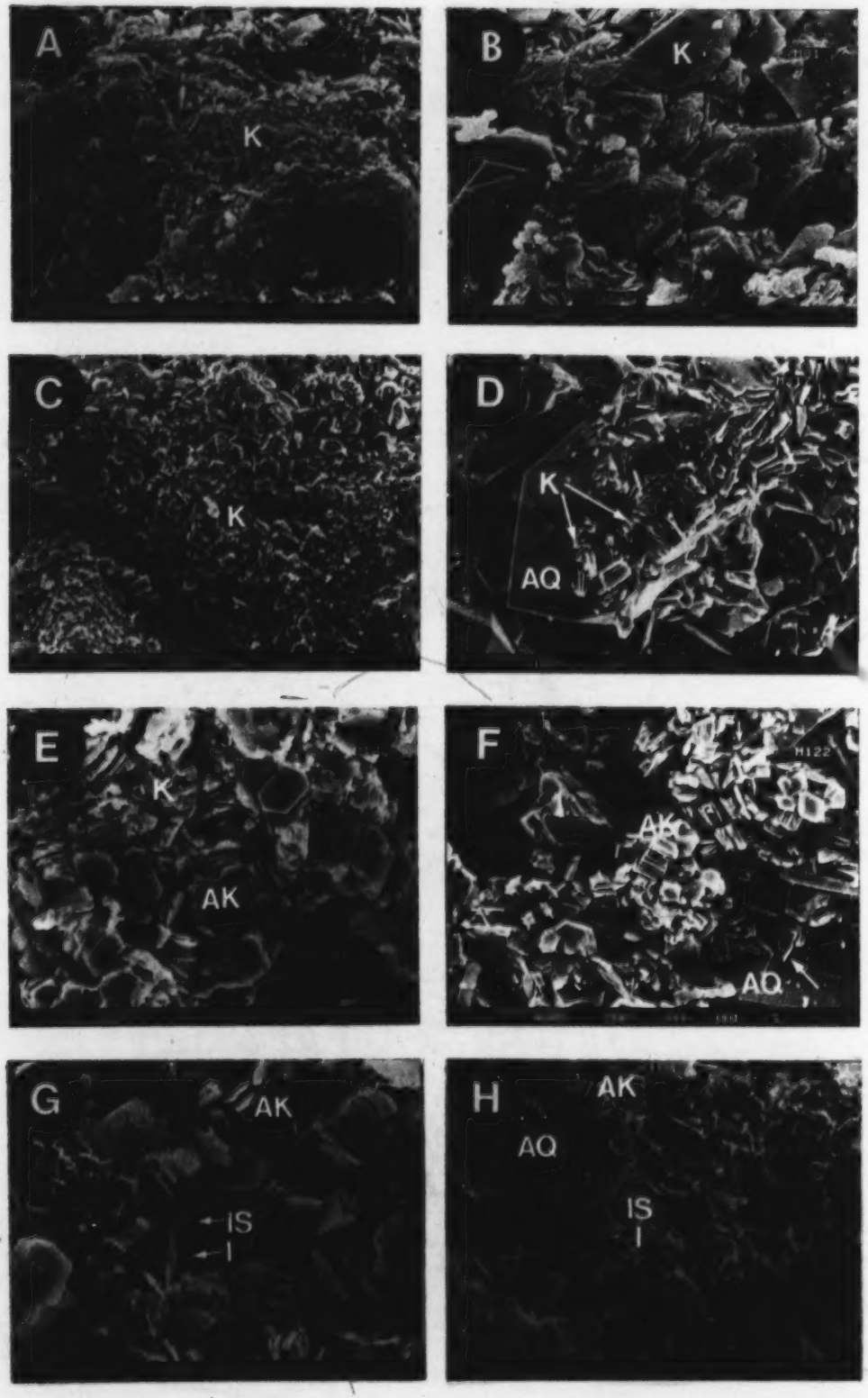
A
K
B
K
C
K
D
K
AQ
E
K
AK
F
AK
AQ
G
AK
IS
I
H
AK
AQ
IS
I

PLATE 3.12

A. Scanning electron photomicrograph of a Viking "A" coarse-grained sandstone showing late pyrite (Py) and pore-lining illite / smectite (IS). The illite / smectite forms interlocking networks of crystals ("honeycombs") that have lath-like projections (Caroline field, well # 4-18-35-6W5, sample # M220, depth = 2734.0m).

B. Scanning electron photomicrograph of a Viking "B" coarse-grained sandstone showing authigenic quartz (AQ) and pore-lining smectite (Sm). The smectite has a honeycomb-like texture, similar to illite / smectite. An EDAX of the smectite (not shown) indicates that the dominant cation is Ca; minor K and Fe are also present (Willesden Green field, well # 5-6-41-6W5, sample # M93, depth = 2293.0m).

C. Scanning electron photomicrograph of a Viking "A" conglomerate showing authigenic feldspar (AF) lined by smectite (Sm). An EDAX of the smectite (Photomicrograph D) indicates the prsence of Fe and Mg. An EDAX of the authigenic feldspar (not shown) indicates it is albite (Gilby field, well# 3-17-40-4W5, sample # M48; depth = 2156.0.).

E. Scanning electron photomicrograph of a Viking "B" fine-grained sandstone showing authigenic chlorite (Chl) and siderite (Sid) that are coated by illite / smectite (IS). The illite / smectite occurs as honeycomb-like crystals that contain lath-like projections (Ferrier field, well # 2-30-38-7W5, sample # M141, depth = 2537.0m).

F. Scanning electron photomicrograph of a Viking "B" fine-grained sandstone showing authigenic illite (I) and illite / smectite (IS). The illite occurs as fibrous crystals while illite / smectite occurs as honeycomb-like crystals with lath-like projections. An EDAX of the illite / smectite (Photomicrograph H) indicates it is Ca and K-rich (Caroline field, well # 6-16-35-5W5, sample # M218, depth = 2468.0m).

G. Scanning electron photomicrograph of a Viking "B" fine-grained sandstone showing ankerite (Ank) lined by illite (I) and illite / smectite (IS) (Ferrier field, well # 6-3-37-5W5, sample # M02, depth = 2290.0m).

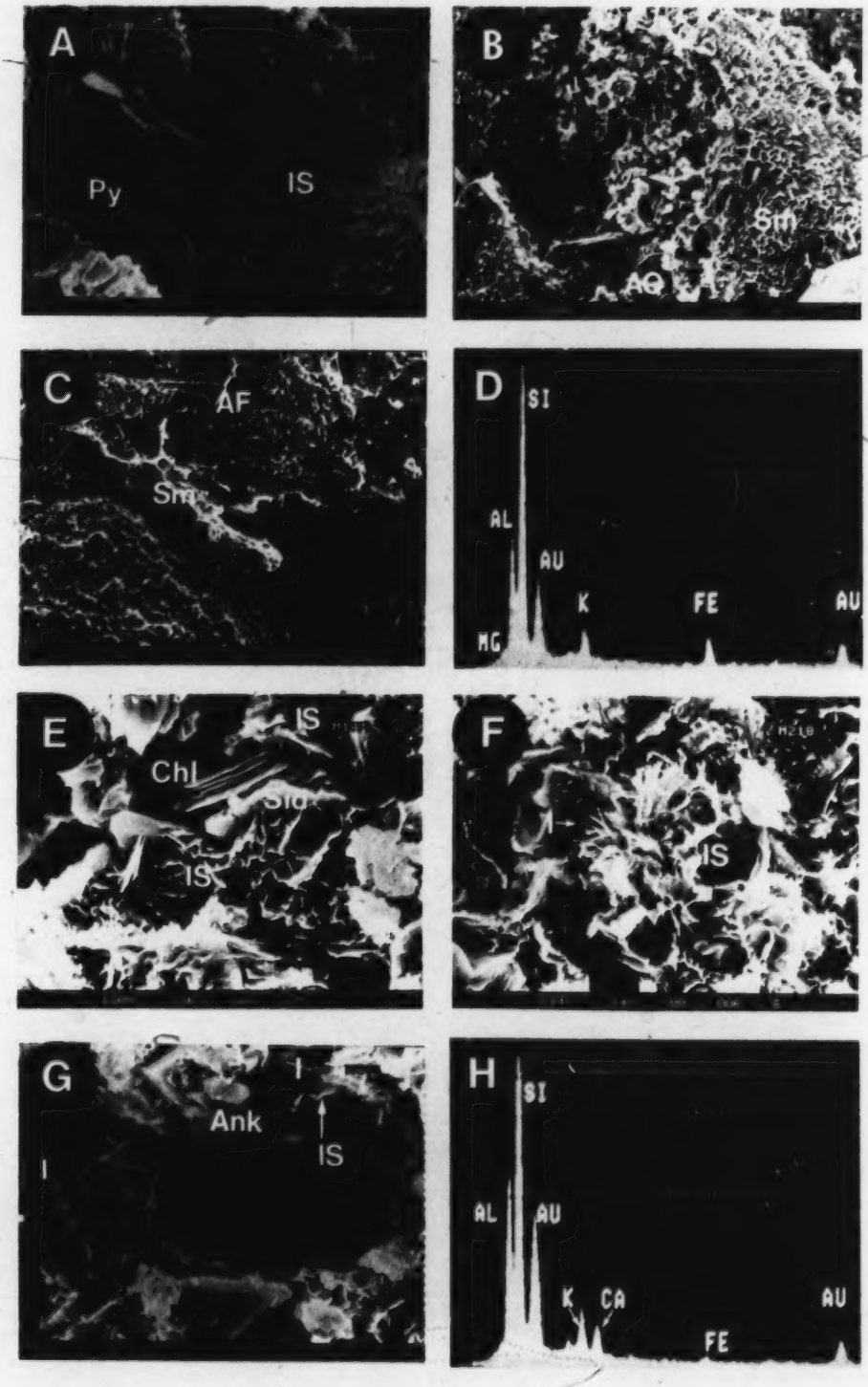
A
Py
IS
B
Sm
AQ
C
AF
Sm
D
SI
AL
AU
K
FE
AU
MG
E
IS
Chl
IS
F
IS
G
Ank
IS
H
SI
AL
AU
K
CA
FE
AU

Paragenetic Sequence

The relative timing of mineral emplacement based on textural evidence (Figure 3.8) is as follows:

1. Glauconite;
2. Pyrite;
3. Chamosite + minor quartz cement;
4. Siderite;
5. Quartz overgrowths;
6. Albite + minor dickite + Fe-calcite + ankerite;
7. Pyrite;
8. Dickite;
9. Illite + illite/smectite + smectite.

This paragenetic sequence applies for the Viking Formation in a general sense but can vary between different areas and between different lithologies. Glauconite is found mainly at Gilby, Joffre, and Willesden Green indicating that it formed in the offshore areas. Early pyrite is common in all rock types and formed shortly after burial in most of the fields studied (Figure 3.8). Chamosite and early authigenic quartz formed after pyrite (Figure 3.8) and, in some samples, may have formed from the replacement of detrital kaolin group minerals. Early chamosite and quartz are usually most abundant in rocks containing abundant detrital kaolin group minerals, such as some conglomerates and coarse-grained sandstones. Siderite cementation occurred after chamosite (Figure 3.8); siderite is found in all rock types but is most abundant in the fine-grained sandstones.

Figure 3.8. Paragenetic sequence.

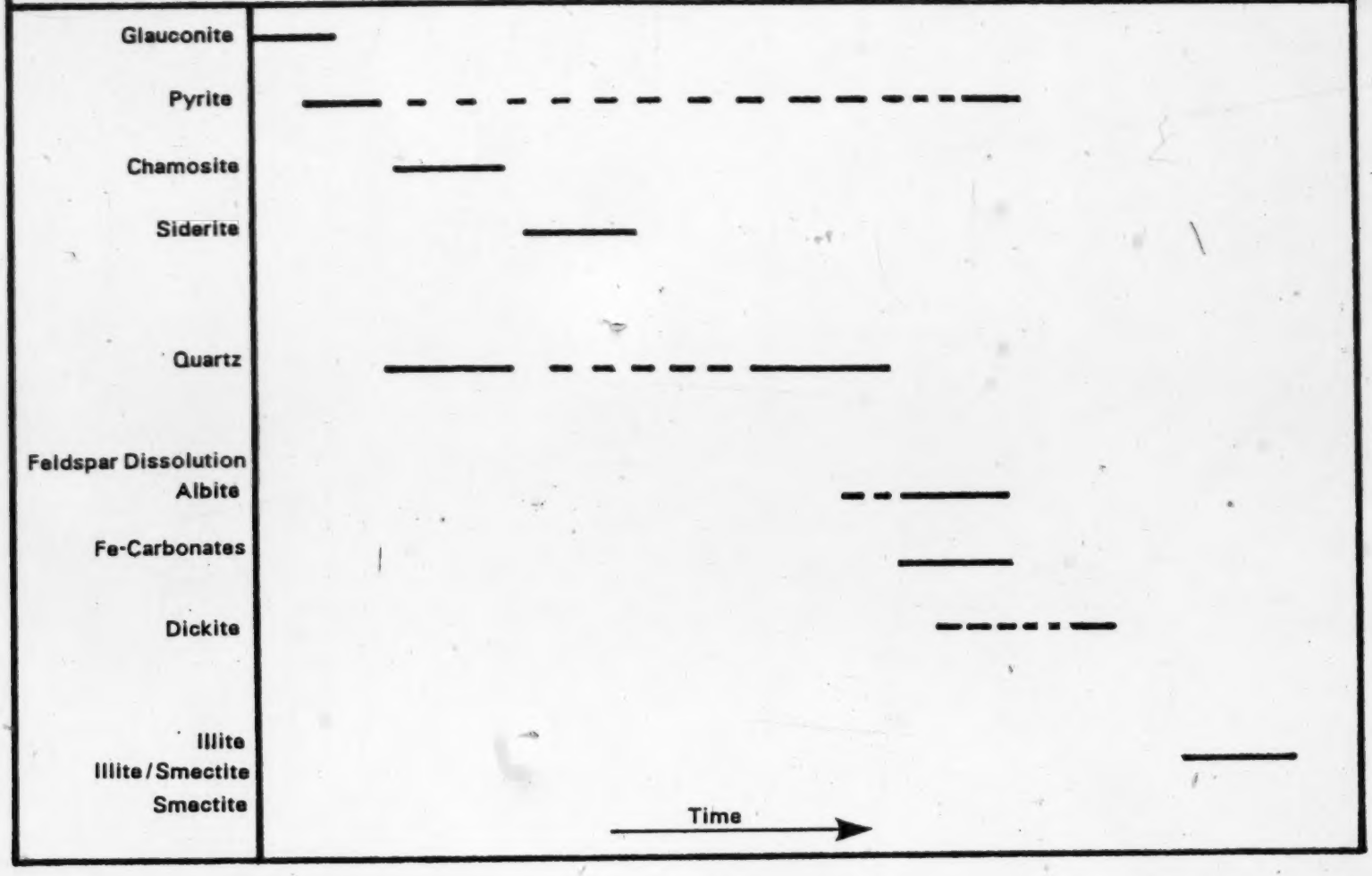

The crystallization of quartz cement occurred after siderite (Figure 3.8). Quartz cementation is most extensive in the fine and coarse-grained sandstones and occurs as overgrowths on detrital quartz. In the chert-pebble conglomerates, quartz cement is less extensive and occurs as small pore-lining crystals. The albitization of detrital feldspar and crystallization of albite, minor dickite, Fe-calcite and ankerite followed quartz cementation (Figure 3.8). Albitization is most extensive in rocks containing abundant detrital feldspar, such as Viking "A" rocks. The crystallization of extensive pore-filling and pore-lining clay minerals occurred late in the diagenetic history (Figure 3.8). Dickite was the first clay mineral to form and is more abundant in the conglomerates and coarse-grained sandstones than in the fine-grained sandstones. The last clay minerals to crystallize were illite, illite/smectite and smectite (Figure 3.8), mainly in the coarse-grained rocks.

D. Stable Isotopes

Stable isotope studies were conducted on certain carbonate and silicate minerals to aid in the interpretation of the diagenetic history. Stable isotope studies are helpful for determining the nature of the fluids and the temperatures present during mineral crystallization. This information can be used with the petrographic data to develop a more complete understanding of the diagenetic history.

Carbonates Minerals

Stable isotopes of carbon and oxygen were obtained for siderite, Fe-calcite, ankerite and mixtures of dolomite and ankerite (Table 3.5). Isotopic compositions for siderite were determined for both 10 day and 3 week extraction times; similar values were obtained indicating that 10 days was sufficient time for complete reaction of these siderites. The average $\delta^{18}O$ (SMOW) values for siderite range between +18.1 and +23.9; the average $\delta^{13}C$ values (PDB) range between -1.5 and -6.33. Siderites having high $\delta^{18}O$ values also have high $\delta^{13}C$ values (e.g., sample M29, Table 3.5); siderites having low $\delta^{18}O$ values generally have low $\delta^{13}C$ values (e.g., sample M660, Table 3.5). Two samples containing Fe-calcite were analyzed; the average $\delta^{18}O$ value was +14.3 and the average $\delta^{13}C$ value was -7.8. The two ankerite samples analyzed had an average $\delta^{18}O$ value of +16.5 and an average $\delta^{13}C$ value of -9.3.

TABLE 3.5. STABLE ISOTOPE RESULTS FOR CARBONATE MINERALS

SAMPLE NUMBER	ROCK TYPE	DEPTH (m)	MINERAL PHASE	EXTR. TIME	$\delta^{13}C$ PDB	$\delta^{18}O$ PDB	$\delta^{18}O$ SMOW
2-32-37-3W5							
M29	F.Sst.	1981.0	SIDERITE	10 dy	-1.9	-6.8	23.9
				3 wk	-1.3	-6.8	23.9
4-19-39-5W5							
M57	F.Sst.	2201.0	SIDERITE	10 dy	-6.3	-7.4	23.3
2-30-38-7W5							
M141	F.Sst.	2537.0	SIDERITE	10 dy	-1.5	-8.6	22.0
10-24-33-8W5							
M660	F.Sst.	3101.0	SIDERITE	10 dy	-4.6	-12.2	18.3
				3 wk	-4.7	-12.6	17.9
16-1-46-4W5							
M726	Congl.	1730.0	Fe-CALCITE	1 hr	-8.4	-16.4	13.9
6-18-31-2W5							
M631A	C.Sst.	2200.0	Fe-CALCITE	1 hr	-7.2	-15.8	14.6
11-7-39-26W4							
M556	C.Sst.	1548.4	ANKERITE	10 dy	-12.4	-13.9	16.6
6-24-32-3W5							
M24/3	Congl.	2200.0	ANKERITE	10 dy	-6.3	-14.0	16.5

TABLE 3.5. CONTINUED

SAMPLE NUMBER	ROCK TYPE	DEPTH (m)	MINERAL PHASE	EXTR. TIME	$\delta^{13}C$ PDB	$\delta^{18}O$ PDB	$\delta^{18}O$ SMOW
14-30-31-28W4							
M519	F.Sst.	1866.0	ANK+DOL	1 hr	-3.5	-13.2	17.3
				10 dy	-1.9	-12.2	18.3
7-32-34-6W5							
M253	F.Sst.	2719.1	ANK±DOL	1 hr	-7.7	-13.4	17.0
				10 dy	-6.0	-11.4	18.9
7-7-29-26W4							
M500	F.Sst.	1280.0	DOL>ANK	1 hr	-	-	-
				10 dy	-5.0	-10.5	20.0
M502	F.Sst.	1288.1	ANK+DOL	1 hr	-4.9	-12.6	17.9
				10 dy	-2.8	-11.6	18.9
6-16-35-5W5							
M218	F.Sst.	2468.0	DOL>>ANK	1 hr	-	-	-
				10 dy	-2.8	-8.5	22.1

Mixtures of detrital dolomite and ankerite were also analyzed. Samples containing mostly detrital dolomite have $\delta^{18}O$ values of +22.0 to +22.1 (Table 3.5); these values are similar to those reported for detrital dolomites found in the Colorado Shales, lying above the Viking Formation (Longstaffe, 1983, 1984). Samples containing greater percentages of ankerite have lower $\delta^{18}O$ values of +18.3 to +18.9 (Table 3.5) (e.g., closer to values obtained for authigenic ankerite).

Silicates Minerals

$\delta^{18}O$ values were determined for 5-20μm samples containing both kaolin group minerals and quartz and for the quartz isolated from this material; these values were then used to calculate the $\delta^{18}O$ values of the kaolin group minerals (Table 3.6). Mineralogical analysis of samples M191 and M81 (Plate 3.10E, 3.10F, 3.11A & 3.11C, and Figure 3.5) indicate that the dominant kaolin group mineral is kaolinite. $\delta^{18}O$ values for these kaolinites were calculated as +28.1 and +28.2 (Table 3.6), typical of detrital clays (Savin and Epstein, 1970a,b; Longstaffe, 1983). Sample M45 contains mostly pore-lining, authigenic quartz (Plate 3.10D) that was dislodged and concentrated in the 5-20μm size-fraction (Plate 3.8H). The $\delta^{18}O$ value of this authigenic quartz is +20.2. Sample M119 contains mostly authigenic dickite (Figure 3.5 and Plate 3.10E) and has an $\delta^{18}O$ value of +12.6. Sample M122 contains 75% dickite and

TABLE 3.6. $\delta^{18}O$ (SMOW) RESULTS FOR SILICATE MINERALS

SAMPLE NUMBER	ROCK TYPE	DEPTH (m)	NATURE OF KAOLINITE	NATURE OF QUARTZ	% KAOL (XRD)	$\delta^{18}O$ BULK	$\delta^{18}O$ QTZ	$\delta^{18}O$ KAOL
14-25-40-7W5								
M119	Congl.	2289.2	Authigenic	-	100	12.6	-	12.6
6-1-39-7W5								
M122	Congl.	2393.0	Authigenic	Authigenic	75	14.4	-	12.4
13-8-35-6W5								
M199A	C.Sst.	2720.0	Auth+Detr	Auth+Detr	45	18.3	-	-
10-9-41-3W5								
M45	Congl.	1923.0	Auth>Detr	Authigenic	35	18.5	20.2	15.4
2-30-38-7W5								
M139	Congl.	2534.0	Detr>Auth	Auth+Detr	35	19.5	-	-
3-31-40-6W5								
M191	Congl.	2276.0	Detrital	Auth+Detr	30	20.5	17.2	28.2
11-24-42-6W5								
M81	C.Sst.	2122.0	Detrital	Auth+Detr	20	20.2	18.2	28.1

25% quartz that is mostly authigenic since abundant pore-lining quartz was observed (Plate 3.9E & 3.11E, and Figure 3.5). An $\delta^{18}O$ value of +20.2 (authigenic quartz from sample M45) was used to calculate the $\delta^{18}O$ of the dickite ($\delta^{18}O$ = +12.4) (Table 3.6). The kaolin group mineral in sample M45 has an $\delta^{18}O$ value of +15.4 suggesting that it contains a large fraction of authigenic dickite. The $\delta^{18}O$ values for the 5-20μm quartz material in samples M191 and M81 are +17.2 and +18.2 (Table 3.6) and probably reflects mixtures of both detrital and authigenic quartz.

Oxygen Isotope Geothermometry

The $\delta^{18}O$ values determined for the authigenic carbonates and silicates were useful for interpreting the $\delta^{18}O$ composition of the fluids and the temperatures involved in crystallization of these minerals. For each mineral $\delta^{18}O$ value a range of possible fluid compositions and temperatures exists (Figure 3.9). These values have been calculated using the following equations:

1. calcite-water, $10^3 \ln\alpha = 2.78(10^6 T^{-2}) - 2.89$ (Friedman and O'Neil, 1977);
2. quartz-water, $10^3 \ln\alpha = 3.38(10^6 T^{-2}) - 3.4$ (Friedman and O'Neil, 1977);
3. kaolinite-water, $10^3 \ln\alpha = 2.5(10^6 T^{-2}) - 2.87$ (Land and Dutton, 1978; from Eslinger, 1971).

$\delta^{18}O$ water-temperature pairs for siderite were determined using the calcite-water equation; for a given

Figure 3.9. Summary of oxygen-isotope results. Curves represent the relationship between $\delta^{18}O$ - mineral (average values), $\delta^{18}O$ - fluid and temperature. Methods used to construct these curves are discussed in text.

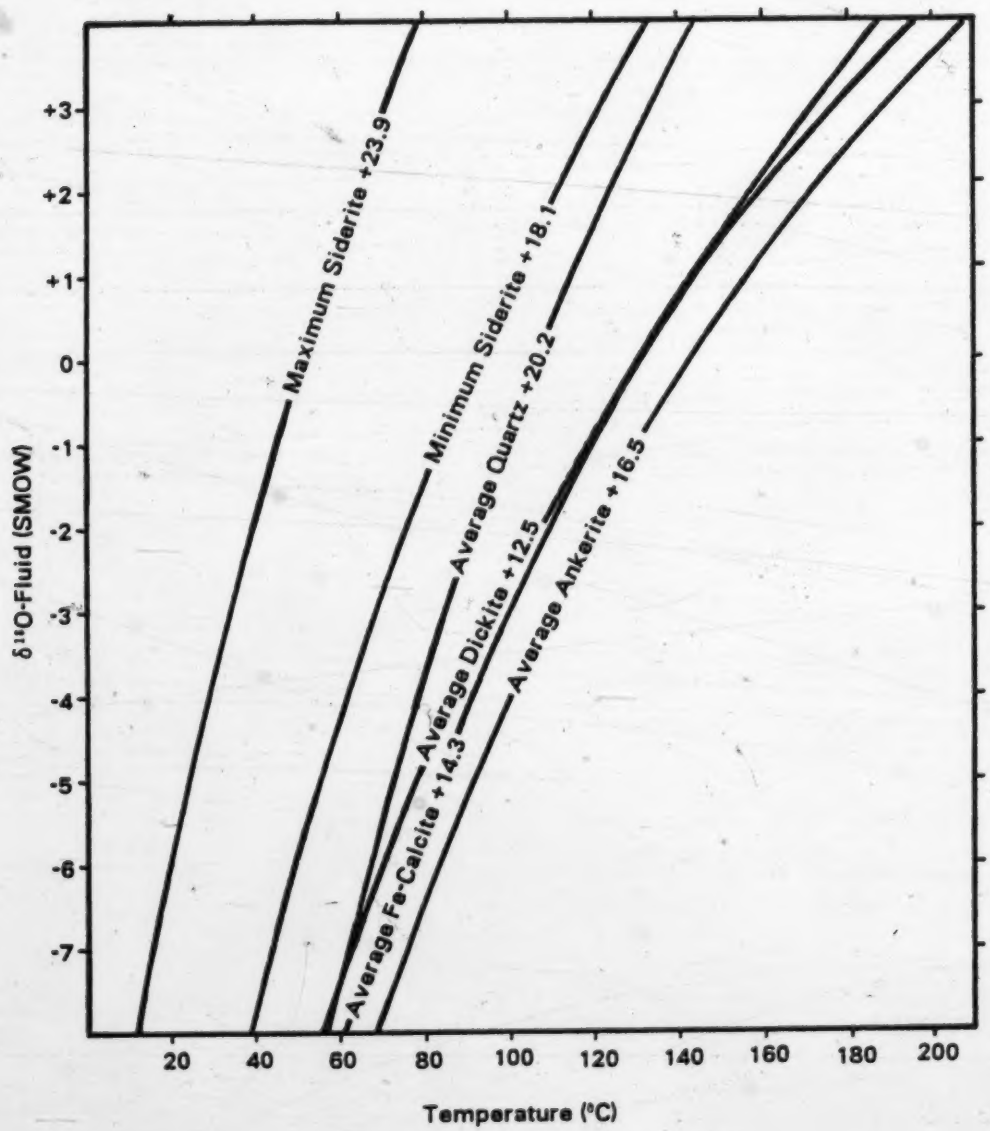

$\delta^{18}O$ - water the temperatures obtained may be underestimated (Gautier, 1982). $\delta^{18}O$ water-temperatures pairs for ankerite were calculated using the dolomite-water equation; although similar in structure it is uncertain how the iron content of ankerite effects the calculations (Dutton and Land, 1985).

In order to construct the fluid-temperature curves in Figure 3.9 reasonable temperature and $\delta^{18}O$ - fluid ranges must be assumed. For the Viking, 0 to 200°C was used to represent the possible range of temperatures reached during diagenesis. Constraints on the fluid compositions include present day formation water $\delta^{18}O$ of approximately -6 (Hitchon, 1969; Schwartz et al., 1981), and an original composition of 0, since seawater was probably the original pore fluid.

E. Microprobe Analysis

Chemical data for siderite, dolomite, Fe-calcite, ankerite and feldspar were obtained by microprobe analysis (Table 3.7). Average compositions (expressed as mol% X 100%) for the carbonates are:

1. Siderite: $(Fe_{7.5}Mg_{1.5}Ca_{0.9}Mn_{0.1})CO_3$;
2. Detrital dolomite: $(Ca_{5.1}Mg_{4.9})CO_3$;
3. Fe-Calcite: $(Ca_{9.9}Fe_{0.1})CO_3$;
4. Ankerite replacing detrital dolomite: $(Ca_{6.1}Mg_{2.5}Fe_{1.4})CO_3$;
5. Discrete ankerite and ankerite replacing feldspar: $(Ca_{5.9}Mg_{2.5}Fe_{1.7})CO_3$.

Feldspars were analyzed near areas showing replacement by ankerite. Three analysis indicated mixtures of feldspar and ankerite (analyses 21, 22 & 26, Table 3.7) and one analysis indicated that the feldspar was albite (analysis 25, Table 3.7).

TABLE 3.7. MICROPROBE RESULTS

SAMPLE & DESCRIPTION	COMPOSITION (MOLE%)
2-30-38-7W5 (M141 F.Sst.)	
1. SIDERITE	$(Fe_{73}Mg_{17}Ca_{9}Mn_{1})CO_3$
2. SIDERITE	$(Fe_{74}Mg_{16}Ca_{9}Mn_{1})CO_3$
3. SIDERITE	$(Fe_{76}Mg_{14}Ca_{9}Mn_{1})CO_3$
4. SIDERITE	$(Fe_{74}Mg_{14}Ca_{10}Mn_{2})CO_3$
7-7-29-22W5 (M500 F.Sst.)	
5. SIDERITE	$(Fe_{76}Mg_{13}Ca_{10}Mn_{1})CO_3$
6. SIDERITE	$(Fe_{77}Mg_{13}Ca_{9}Mn_{1})CO_3$
2-30-38-7W5 (M631A C.Sst.)	
7. CALCITE CORE	$(Ca_{99}Fe_{1})CO_3$
8. CALCITE CORE	$(Ca_{99}Fe_{1})CO_3$
9. CALCITE RIM	$(Ca_{98}Fe_{2})CO_3$
10. CALCITE RIM	$(Ca_{99}Fe_{1})CO_3$
7-32-34-6W5 (M253 F.Sst.)	
11. DOLOMITE CORE	$(Ca_{51}Mg_{49})CO_3$
12. DOLOMITE CORE	$(Ca_{51}Mg_{49})CO_3$
13. ANKERITE RIM	$(Ca_{61}Mg_{25}Fe_{14})CO_3$
14. ANKERITE RIM	$(Ca_{61}Mg_{25}Fe_{14})CO_3$
11-7-39-26W4 (M556 C.Sst.)	
15. ANKERITE CORE	$(Ca_{58}Mg_{25}Fe_{17})CO_3$
16. ANKERITE RIM	$(Ca_{59}Mg_{25}Fe_{16})CO_3$
17. ANKERITE CORE	$(Ca_{61}Mg_{26}Fe_{13})CO_3$
6-24-32-3W5 (M24 / 3 Congl.)	
18. ANKERITE CORE	$(Ca_{57}Mg_{25}Fe_{18})CO_3$
19. ANKERITE CORE	$(Ca_{58}Mg_{24}Fe_{18})CO_3$
20. ANKERITE RIM	$(Ca_{57}Mg_{25}Fe_{18})CO_3$
21. FELDSPAR IN ANK.	Na, Al, Si, Ca, Mg, Fe
22. FELDSPAR IN ANK.	Na, Al, Si, Ca, Mg, Fe
5-30-41-6W5 (M181 C.Sst.)	
23. ANKERITE CORE	$(Ca_{60}Mg_{24}Fe_{16})CO_3$
24. ANKERITE RIM	$(Ca_{58}Mg_{25}Fe_{17})CO_3$
25. FELDSPAR NEAR ANK.	Na, Al, Si
26. FELDSPAR IN ANK.	Na, Al, Si, Ca, Mg, Fe

IV. DIAGENESIS

A. Interpretation of Paragenetic Sequence

The interpretation of the paragenetic sequence of mineral emplacement is an important step towards understanding processes that occurred throughout the diagenetic history. Diagenetic minerals that formed during early burial of the Viking may be similar to minerals that crystallized early in Cretaceous rocks of northwestern United States or similar to minerals crystallizing in shallow buried Gulf Coast sandstones. Changes in fluid chemistry during later stages of diagenesis in the Viking are probably related to uplift and an influx of meteoric water; these changes should be reflected in the types of minerals that formed late in the paragenetic sequence.

The paragenetic sequence in the Viking (Figure 3.8) showed that the types of minerals that crystallized evolved from early iron-rich phases, such as glauconite, pyrite, chamosite and siderite, to quartz. This was followed by a period of albitization and crystallization of Fe-calcite, kaolin group minerals (dickite) and ankerite. Late pyrite cement also formed at this time. Among the last phases to crystallize were the clay minerals beginning with dickite followed by illite, illite/smectite and smectite. Detailed studies of this paragenetic sequence may help to reveal the dominant processes that were active during various stages of diagenesis and may help to determine when the influx of

meteoric water occurred.

Early Iron-Rich Cements

The formation of glauconite, pyrite, chamosite, quartz, and siderite occurred either during deposition or early burial (see Chapter III). The crystallization of most of these phases reflects the formation of a reducing environment with a high iron activity.

The formation of glauconite occurred prior to or during deposition since many grains are highly compacted (e.g., Plate 3.3A). Some of the glauconite also appears as pellet-shaped grains suggesting that it formed through biogenic activity (e.g., Plate 3.3A). The association of gluaconite and biogenic activity is well established; many glauconites appear to have formed from the alteration of clay minerals aggregated as fecal pellets (Burst, 1958; Hower, 1961; McRae, 1972; Pryor, 1975; McConchie et al., 1979; Birch et al., 1976; Bayliss and Syvitski, 1982). Glauconite has also been reported forming as a replacement of non-clay minerals and through the recrystallization of amorphous Fe, Si and Al-rich gels (McRae, 1972; Sorokin and Vlasov, 1979; Harder, 1980). The recrystallization of amorphous gels can better account for the presence of glauconite in coarse, relatively clean sandstones that otherwise show little evidence of biogenic activity (Harder, 1980). In the Viking Formation, the occurrence of glauconite in many clean coarse-grained rocks suggests that some of the

glauconite may have formed through the recrystallization of Fe, Si and Al-rich gels.

The association of glauconite and organic matter is well known and it is likely that during early burial the bacterial decay of organics created the necessary reducing conditions for glauconite formation (McRae, 1972; McConchie et al., 1979). Under reducing conditions detrital Fe-bearing phases will dissolve, mobilizing iron (Berner, 1981). In more oxidizing zones Fe will precipitate as iron hydroxides and through the absorption of Si, Al, K and Mg, derived from the solution or breakdown of other phases, glauconite forms (Sorokin and Vlasov, 1979; Harder, 1980).

In the Viking, glauconite is common in the offshore region (e.g., Gilby and Joffre). Porrenga (1967) showed that glauconite is more common in cool, deep marine environments, while chamosite forms in shallow, warm waters. Harder (1980) indicated that in deeper waters original pore fluids are higher in dissolved silica because of the dissolution of siliceous organisms and high Si saturations favour the formation of glauconite over chamosite.

The crystallization of pyrite occurred after glauconite (e.g., Plate 3.4E) and reflects the introduction of aqueous sulfide. The formation of early sulfides has been documented in many of the Cretaceous shelf sandstones in the northwestern United States and is thought to represent the anoxic decomposition of organic matter (Gautier, 1983). Berner (1981a) indicated that during early burial sulfate

reducing bacteria decompose organic matter and release HS^-. The continued dissolution of oxidized Fe-bearing minerals, such as Fe-oxides or biotite, also occurs under these conditions (Berner, 1981a; Wilson, 1982). In the presence of HS^-, free iron will be readily transformed into pyrite (Berner, 1981b). Much of the early pyrite in the Viking probably originated in this manner with additional iron provided by the breakdown of glauconite.

Chamosite (Fe-chlorite) formed early in the burial history primarily through the replacement of detrital kaolinite. The replacement of detrital kaolinite by chamosite reflects early reducing conditions with high Fe activities. In such an environment kaolinite was probably unstable and Fe was incorporated into its structure forming an Fe-rich, 1:1 layered phase, such as berthierine (e.g., Plate 3.6C). With complete replacement and incorporation of minor Mg, probably from trapped seawater, chamosite formed (e.g., Plate 3.6F). Iijima and Matsumoto (1982) reported berthierine forming through the reduction of detrital kaolinite in the upper Triassic coal measures of Japan and in deeper sections it had also transformed to chamosite.

Sources of iron for the Viking chamosites were probably from detrital Fe-minerals or pyrite. Bhattacharyya (1983) was able to synthesize berthierine by reacting kaolinite with pyrite under reducing conditions. In the synthesis small euhedral quartz crystals were also found with berthierine and were interpreted to have formed from the

excess Si released during the transformation (Bhattacharyya, 1983). A similar association is seen in the Viking: detrital kaolinite / berthierine + chamosite / neoformed quartz (e.g., Plate 3.9F). This may also explain the abundance of small quartz crystals found within some kaolinite matrices (e.g., Plate 3.1E & 3.10A).

The cessation of pyrite formation and the incorporation of Fe into chamosite reflects early changes in pore fluid chemistry. Irwin and Curtis (1977) indicated that marine sulfate levels decline after 10 meters of burial causing bacterial sulfate reduction and early pyrite formation to end. Due to the high oxidizing potential of HS^-, only in its absence can Fe be used in the formation of other Fe-bearing phases (Berner, 1981a). Another possibility is that only a small percentage of organic matter was initally present in the sandstones and was consumed quickly by bacteria. The presence of an intermediate stage of chamosite development (berthierine) and the preservation of abundant detrital kaolinite suggests that conditions for chamosite formation did not last long. This may reflect the depletion of Fe due to a limited supply of detrital Fe-minerals or a change in pore fluid chemistry resulting in the crystallization of a more stable Fe-mineral (e.g., siderite).

The crystallization of siderite reflects the influx of dissolved CO_2 into the pore fluid system. Average $\delta^{13}C$ values for the siderite vary between -1.6 and -4.7; these values are similar to the $\delta^{13}C$ values reported for early

diagenetic siderites found in Cretaceous shales of northwestern United States (Gautier, 1983; Figure 4.1). Early formed carbonates usually have heavier $\delta^{13}C$ values than late carbonates due to a change from bacterially derived CO_2 to inorganically derived CO_2 (Irwin et al., 1977; Figure 4.1).

The release of isotopically heavy carbon occurs at the same time methane generation during initial burial (Rosenfeld and Silverman, 1959; Irwin et al., 1977). The production of early methane is attributed to the bacterial breakdown of organic matter (bacterial fermentation) shortly after the cessation of bacterial sulfate reduction (Irwin et al., 1977; Berner, 1981b; Gautier, 1982). The fermentation process can continue to temperatures of about 60°C where the thermal destruction of the bacteria occurs (Irwin et al., 1977; Surdam et al., 1984) (Figure 4.1). Siderite from the Viking Formation has the highest $\delta^{13}C$ values of all the carbonates studied and probably formed from CO_2 evolved during bacterial fermentation (Figure 4.1).

It is doubtful that the sandstones contained sufficient organic matter to account for the volume of siderite cements seen in some samples (e.g., sample M29, Table 3.2). Most of the CO_2 was probably provided by early methane generation in adjacent shales. With compaction and shale dewatering the CO_2 + methane would have migrated into adjacent sandstones stablizing Fe with respect to siderite.

Figure 4.1. Source of carbon dioxide for Viking carbonates; carbon-isotopic data from Table 3.5 (modified after Irwin et al., 1977; Surdam et al., 1984).

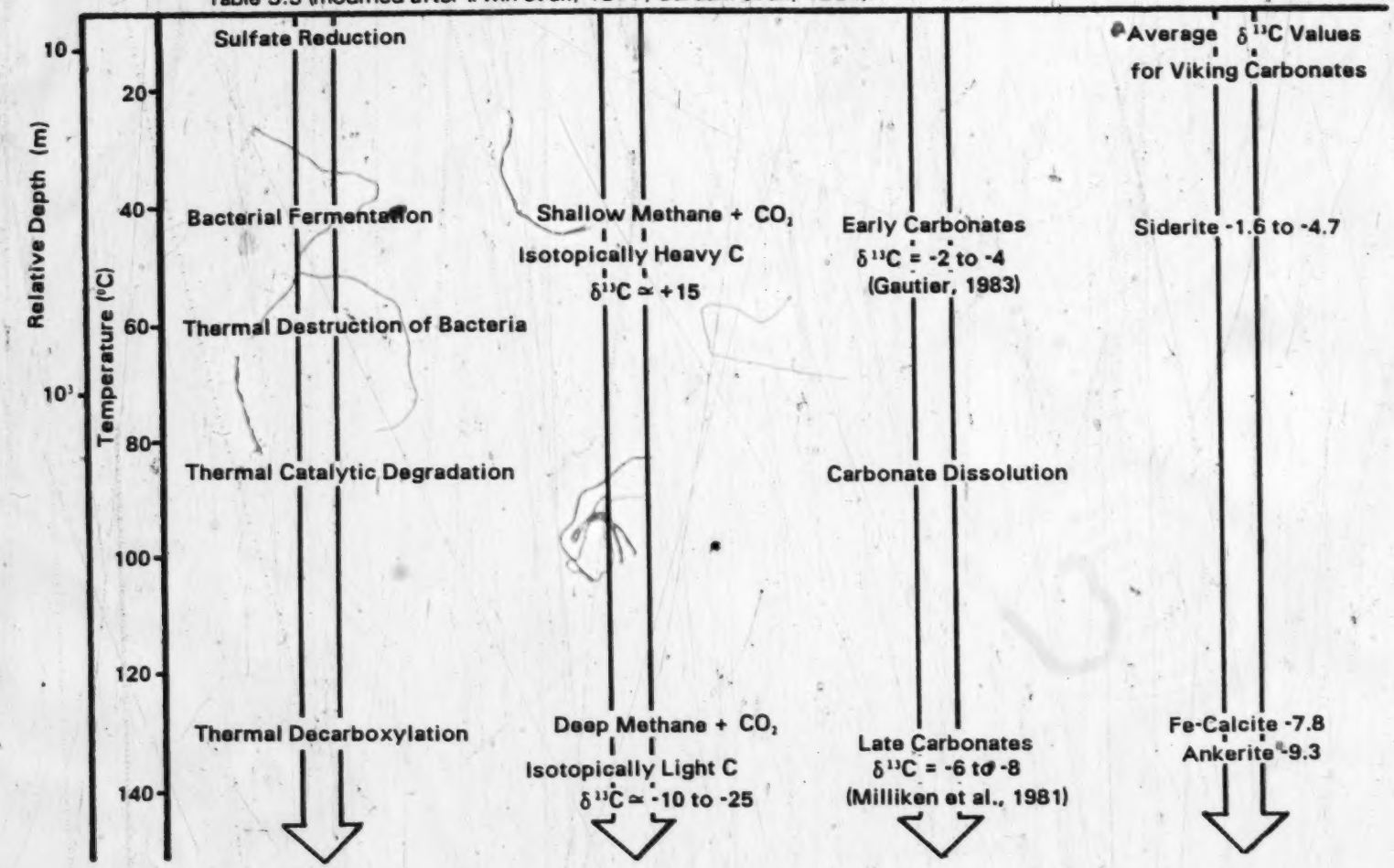

Siderite is very patchy in distribution and tends to selectively replace certain sandstone beds. With compaction, CO_2 generated in the shaly interbeds would have migrated into all the sandstones. Siderite would have crystallized only if reducing conditions existed and if sufficient Fe had been mobilized.

A likely source of Fe for siderite may have been authigenic chamosite. In some samples siderite is seen enveloping chamosite (e.g., Plate 3.8F). Bhattacharyya (1982) indicated that siderite commonly replaces chamosite during the burial diagenesis of ironstones. In the Viking Formation, the introduction of CO_2 would have increased the PCO_2 levels stabilizing Fe with respect to siderite (Garrels and Christ, 1965, p. 161).

The average siderite composition indicates that Mg, Ca and Mn were also available during crystallization (Table 3.7). Mn was probably derived from the dissolution of minor detrital Mn-oxides. Mg and Ca may have been derived from the breakdown of detrital dolomite, clays or organic matter; Irwin (1980) stated that organic matter can be comprised of 2-10% chlorophyll containing up to 2.8 wt% Mg. Additional Ca and Mg may have been provided by the original connate waters and some Mg may have been provided by chamosite.

Quartz Cementation

Quartz cementation is very extensive in the Viking Formation and, where complete overgrowths are present, has

almost completely destroyed original porosity (e.g., Plate 3.7D). Thomas and Oliver (1979) studied regional depth-porosity variations of the Viking in the same area as this study; their results show that compaction and quartz cementation was the dominant mechanism of porosity reduction. They also indicated that most of the Si for quartz overgrowths was probably provided by pressure solution; however the lack of extensive sutured contacts between quartz grains was also noted. Many quartz grain contacts appear convexo-concave (e.g., Plate 3.2A), but where distinct dust rims are visible it is apparent that few detrital grains are actually touching and the contacts are the result of mergence of overgrowths within pore spaces (e.g., Plate 3.7C). Cathodoluminescence studies of extensively quartz cemented sandstones indicate that convexo-concave boundaries, resulting from the mergence of overgrowths, are commonly mistaken for pressure solution contacts (Sibley and Blatt, 1976; Blatt, 1982). The amount of pressure solution that has occurred in the Viking cannot be deduced since cathodoluminescence was not performed. However, the occurrence of sutured chert contacts suggests that some Si for quartz overgrowths may have been provided by pressure solution (e.g., Plate 3.1B).

A number of additional sources for Si have been proposed to account for quartz cementation in quartz-rich sandstones. In the Gulf Coast region the release of Si is commonly associated with the illitization of smectite layers

in illite/smectites during burial of shales (e.g., Boles and Franks, 1979). Other studies of shales in the Gulf Coast indicate that most of the Si is conserved during illitization and a very large quantity of illite/smectite would be needed before any excess Si could be transported into adjacent sandstones (Hower et al., 1976; Yeh and Savin, 1977; Hower, 1981). Considering illite/smectite is a minor component in most Viking shales (e.g., see Table 3.1), it is unlikely that any Si was transported into the sandstones during illitization.

Other possible sources of Si include silica derived from the devitrification of volcanic glass and from the dissolution of opaline radiolaria and siliceous sponges (Blatt et al., 1980; Blatt, 1982). These sources seem unlikley for the Viking sandstone due to their clean, quartz-rich composition. Blatt et al. (1982) indicated that a likely source of Si for quartz cement in quartz-rich sandstones is from the circulation of meteoric waters since they contain the highest concentrations of dissolved Si (up to 13 ppm) when compared to sea water (<1 ppm). This would suggest that quartz cementation can occur very early in continental quartz-rich sandstones while marine quartz-rich sandstones require uplift and meteoric water flushing before extensive quartz cement can develop (Sibley and Blatt, 1976; Blatt et al., 1980; Blatt, 1982).

In the Alberta basin uplift and meteoric water invasion is commonly associated with the second phase of the Laramide

orogeny (Hitchon and Friedman, 1969; Hitchon, 1984; see also Figure 1.4). The circulation of ground waters at or near maximum burial of the Viking may have been an important step towards the development of extensive quartz overgrowths. A continued influx of meteoric water may have provided a transport mechanism for large volumes of Si derived at depth and at high temperatures through pressure solution. Si solubility increases at high temperatures (Blatt, 1982) and the presence of organic acids, associated with hydrocarbon maturation, may have further increased Si solubility (Curtis, 1983). Upon entering more shallow buried regions of the Viking, the Si solubility of the meteoric waters would have decreased and extensive quartz overgrowths may have resulted.

Albitization

Following quartz cementation changes in pore fluid chemistry resulted in the dissolution and albitization of feldspar and crystallization of carbonates (e.g., Plate 3.9D) and minor amounts of authigenic kaolin group minerals, mostly dickite (e.g., Plate 3.9F). Albitization is most evident in Viking "A" rocks since they contain high percentages of detrital feldspar that commonly show replacement by carbonates (e.g., Plate 3.9D). Microprobe analysis of the feldspar inclusions within these carbonates indicate a nearly pure albite phase (An_0)(e.g., see Table 3.7, analysis #25), whereas surrounding feldspars have

compositions ranging from An_5 to An_{35} (based on optical and X-ray diffraction techniques). In the Gulf Coast region the appearance of such textural and mineralogical relationships usually indicates that albitization has occurred and that there has been an influx of acidic fluids (Milliken et. al., 1981; Boles, 1982; Siebert et al., 1984; Dutton and Land, 1985). The generation of an acidic fluid capable of dissolving feldspar at or near maximum burial is commonly associated with the release of CO_2 and carboxylic acids during hydrocarbon maturation (Carothers and Kharaka, 1978; Momper, 1978; Al-Shaieb and Shelton, 1981; Porter and Wiemer, 1982; Surdam et al., 1984).

In the Alberta basin, the generation of hydrocarbons and acidic fluids from Cretaceous source rocks probably occurred at the end of the Paleocene/early Eocene when maximum burial depths and temperatures were reached (Taylor et al., 1964; Deroo et al., 1977). The timing of hydrocarbon generation would have also overlapped with the influx of meteoric waters associated with overthrusting during the second Laramide orogeny (Hitchon and Friedman, 1969; Hitchon, 1984). Given these circumstances, it is likely that albitization in the Viking sandstones was initiated by an influx of acidic fluids derived from a mixing of meteoric waters and acidic fluids released from shales.

Assuming an average feldspar composition of An_{20} (oligoclase) for detrital feldspar in the Viking, albitization during an influx of acidic fluids (denoted H^+)

can be expressed as the following:

$Na_{0.8}Ca_{0.2}Al_{1.20}Si_{2.85}O_8 + 0.4H_2O + 0.2H^+ = 0.8NaAlSi_3O_8 + 0.2Al_2Si_2O_5(OH)_4 + 0.2Ca^{2+} + 0.05H_4SiO_4$

Albitization, as shown in the reaction above, does not require an influx of Na and is similar to reactions written for feldspar dissolution in Gulf Coast sandstones (e.g., Siebert et al., 1984). It is likely that albitization in the Viking was a form of dissolution where only the Ca-rich domains of a feldspar grain were dissolved leaving behind the Na-rich domains; these textural features have been observed in some Gulf Coast sandstones (Siebert et al., 1984). In the Viking, albitization (or selective dissolution) of a few percentage of detrital feldspar can account for the occurrence of albite inclusions within some carbonate cements (e.g., Plate 3.9D). Complete dissolution of other feldspar grains may have provided a source of Na for local albite overgrowths (e.g., Plate 3.8B).

The minor amounts of authigenic kaolin group minerals associated with feldspar dissolution (e.g., Plate 3.9F) may have also formed during albitization. Boles (1982) indicated that dickite was a common product of albitization in the Frio Sandstone (Gulf Coast) and formed from the excess Al released during the reaction (see reaction above).

The calcium released during albitization can be used in the formation of local carbonate cements, as seen in many Gulf Coast sandstones (e.g., Siebert et al., 1984). In order to crystallize calcite in an acidic environment fluids would

have to contain high CO_2 levels and an acid buffer reaction, such as decarboxylation (Crossey et al., 1984; Surdam et al., 1984). Carbon isotopic analyses of Fe-calcite and ankerite from the Viking indicate that they probably formed from CO_2 released from decarboxylation; $\delta^{13}C$ values of -6 to -8 are common for these carbonates (Milliken et al., 1981; Figure 4.1).

Albitization alone cannot account for the total volume of carbonates present in some rocks. For example, sample M631 contains 12% Fe-calcite and 6% detrital feldspar (Table 3.2). Textural evidence indicates that some of the Fe-calcite has replaced feldspar (e.g., Plate 3.9B) but if albitization only releases 0.2 moles of calcium for every 1 mole of feldspar (see reaction written previously) then 66% feldspar must have originally been present. This is highly unlikely and suggests that the fluids entering at this time also contained Ca. The additional Ca may have been brought in with the meteoric waters because, before entering the Viking, these fluids would have had undergone fluid-rock interactions with deeper Mississippian and Devonian carbonates (Clayton et al., 1966; Hitchon and Friedman, 1969; Longstaffe, 1984; Figure 1.4).

Ankeritization

Ankerite occurs as a discrete cement (e.g., Plate 3.9C), as a replacement of feldspar (e.g., Plate 3.9D) and as a replacement of detrital dolomite (e.g., Plate 3.7B).

Microprobe data obtained for these ankerites indicates they contain a high Ca content (Figure 4.2). Discrete ankerite and ankerite replacing feldspar contain an average of 58% Ca; ankerite replacing dolomite has an average of 61% Ca. These compositions are higher than the ideal field for ankerite established by Deer et al. (1962) and are similar to those reported by Boles (1978) (Figure 4.2). The excess Ca was interpreted by Boles (1978) to represent ankeritization of a Ca-rich precursor, such as calcite. In the Viking fine-grained sandstones the excess Ca was probably derived from the ankeritization of dolomite. In the coarse-grained rocks Ca was probably derived from the ankeritization of calcite that either formed during albitization or that crystallized from Ca-rich, meteoric water. The preservation of some Fe-calcite indicates that ankeritization is incomplete.

Using the average compositions for Fe-calcite and ankerite, ankeritization of Fe-calcite can be expressed as:

$$Ca_{.89}Fe_{.01}CO_3 + 0.106Fe^{2+} + 0.17Mg^{2+} = 2Ca_{.58}Mg_{.25}Fe_{.17}(CO_3)_2$$

Using the average compositions obtained for detrital dolomite and ankerite rims, the following reaction can be written to express ankeritization of dolomite:

$$Ca_{.81}Mg_{.89}(CO_3)_2 + 0.14Fe^{2+} = 0.83Ca_{.61}Mg_{.25}Fe_{.14}(CO_3)_2 + 0.28Mg^{2+}$$

Both reactions shown require an influx of Fe and Mg. In the Gulf Coast region ankeritization of calcite is thought to be related to the late-stage release of Fe and Mg from smectite

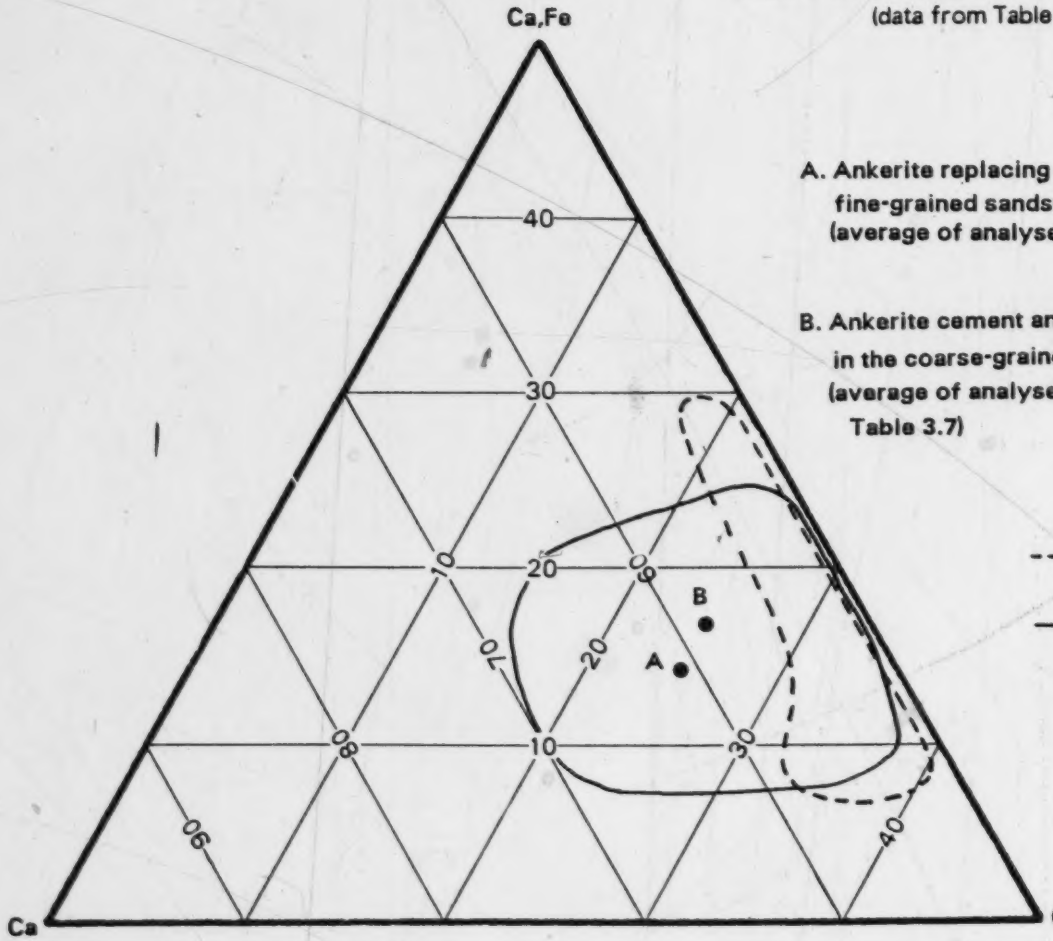

Figure 4.2. Average compositions of Viking Carbonates (data from Table 3.7) (modified after Boles, 1978).

A. Ankerite replacing dolomite in the fine-grained sandstones (average of analyses 13 & 14, Table 3.7)

B. Ankerite cement and ankerite replacing feldspar in the coarse-grained sandstones and conglomerates (average of analyses 15, 16, 17, 18, 19, 20, 23 & 24, Table 3.7)

--- Ankerite Field (Deer et al, 1962)

—— Ankerite Field (Boles, 1978)

diagenesis (Boles, 1978; Boles and Franks, 1979). Shales associated with the Viking Formation contain small percentages of illite/smectite (Table 3.1) and it is unlikely that any Fe or Mg were provided by smectite diagenesis. It is possible that Fe and Mg were derived from the breakdown of organic matter (Irwin, 1980) or from the breakdown of previously formed Fe-bearing minerals, such as siderite or chamosite.

In order to mobilize Fe and Mg for ankerite reducing conditions must have developed near maximum burial. The development of reducing conditions may be associated with late stage hydrocarbon maturation and an influx of H_2S (Hunt, 1979). Initially CO_2 levels may have been high enough to stabilized Fe and Mg with respect to ankerite. As H_2S levels rose Fe would have been reduced to pyrite, much of the late pyrite may have formed in this manner.

Late Clay Minerals

Authigenic clay minerals are very common in the Viking sandstones and appear to be among the last phases to have formed, commonly lining earlier cements, such as quartz overgrowths and ankerite (e.g., Plate 3.8B & 3.12G). These clays minerals include dickite, illite, illite/smectite and smectite.

Dickite was the first clay mineral to form and it is the most extensive, comprising up to 10% of some coarse-grained rocks (e.g., sample M55, Table 3.2). Dickite

occurs mainly as a pore-filling (e.g., Plate 3.9E) but, in some places, it appears to have formed through the solution/recrystallization of detrital kaolinite (e.g., Plate 3.10F & 3.11E). In a similar fashion, Wilson (1982) indicated that much of the original kaolinite found in quartz-rich sandstones, such as the Spirit River (Alberta) and Hosston (Louisiana), has also been converted to dickite during diagenesis.

The crystallization of dickite probably reflects continued mixing of surface waters with pre-existing formation fluids. Kaolin group minerals are usually stable in the presence of meteoric waters due to its low pH and low ionic strength (Hurst and Irwin, 1982). Flushing of sandstones by groundwaters is considered an important step in the kaolinitization of many quartz-rich sandstones (Almon and Davis, 1979; Bjørlykke et al., 1979). In the Alberta basin, fresh water flushing is related to overthrusting and uplift during the second phase of the Laramide orogeny (Hitchon, 1984). Authigenic kaolin group minerals are the most widely distributed authigenic clay mineral in many Cretaceous and Tertiary sandstones found in the foothills and plains region of Albterta (Carrigy and Mellon, 1964) and probably formed when acidic groundwaters started to flush through the basin. In the Viking, the crystallization of dickite suggests that temperatures were still high when flushing occurred; dickite is usually the most stable polytype at high temperatures (Brown and Brindley, 1980).

Most of the Si and Al for dickite was probably brought in with the meteoric waters although some Si and Al may have been provided by the solution of detrital kaolinite. Al mobility may have been enhanced by the presence of organic acids associated with hydrocarbon maturation (Curtis, 1983).

The crystallization of dickite instead of quartz indicates that there was an increase in the Al/Si ratio of the fluids entering the Viking (Blatt, 1982). As uplift continued and temperatures started to drop quartz stability would have been greatly reduced (Drever, 1982, pg., 101) and crystallization of quartz may have been confined to deeper formations. As a result, fluids entering the Viking would have been less Si-rich and more stable with respect to dickite.

Authigenic illite and illite/smectite are also common in the Viking sandstones and crystallized after dickite (e.g., Plate 3.11G & 3.11H). X-ray diffraction studies of illite/smectite indicate they contain between 70 and 80 percent illite layers (e.g., Table 3.4). The composition of illite/smectite in shales is commonly associated with illitization reactions with increasing temperature (depth) (Boles and Franks, 1979). This relationship may exist in the shales associated with the Viking (Table 3.1), but no relationship between burial depth and illite/smectite composition is apparent in the sandstones (Table 3.4). This suggests that the most important factor that controlled the crystallization of the illitic clays was fluid chemistry.

Hurst and Irwin (1982) indicated that the formation of illitic clays instead of kaolin group minerals reflects a change from an acidic fluid low in ionic strength to a less acidic fluid with high concentrations of potassium.

In the Viking, a similar change in fluid chemistry may be associated with decreasing temperatures during uplift. As temperatures decreased the crystallization of kaolin group minerals and quartz probably occurred in deeper parts of the basin. As a result, fluids moving into shallower buried formations were richer in dissolved cations, such as K^+, relative to Si and Al. These changes in fluid chemistry may have initiated the crystallization of the illitic clays.

Smectite also occurs as a late clay mineral phase in some coarse-grained rocks (e.g., Plate 3.12B). EDAX analysis indicates that these smectites contain Ca, Fe and Mg (e.g., Plate 3.12D). The crystallization of smectite appears to coincide with the formation of illite and illite/smectite but is difficult to determine because of the similar morphologies of these clays (e.g., Plate 3.12B). The crystallization of smectite probably reflects local variations in pore fluid chemistry where concentrations of Fe, Mg and Ca were higher than K.

B. Isotopic Constraints on Diagenesis

Oxygen-isotope ratios of authigenic minerals are useful in determining temperatures and fluid conditions during their crystallization, assuming these values have remained

unchanged during later diagenesis. Isotopic exchange is reported to be negligible in quartz under 300°C and negligible in kaolin group minerals under 100°C (O'Neil and Kharaka, 1976; Yeh and Savin, 1977; Longstaffe, 1983). Isotopic exchange in carbonate minerals, especially calcite, is likely to be more important during later stages of diagenesis (Clayton, 1959; Clayton et al., 1966).

The relationship between $\delta^{18}O$ - mineral, $\delta^{18}O$ - water, and temperature were shown in Figure 3.9. In order to calculate temperatures of crystallization for the authigenic minerals the following parameters must be known: (1) maximum depths and temperatures of burial; (2) evolution of $\delta^{18}O$ - water during burial and uplift; and (3) the paragenetic sequence.

Present burial depths for most of the samples selected for isotopic analysis range between 1500m (Gilby/Joffre fields) and 2500m (Caroline field). Using a surface temperature of 5°C and a geothermal gradient of 24°C/km for southwestern Alberta (Hitchon, 1984), 40 to 60°C can be calculated for present day formation temperatures. This agrees with actual field measurements (corrected bottom-hole temperatures) for some Viking fields that occur within the study area (e.g., the Viking Formation a Chigwell (≃1500m depth) is at 46°C, Hitchon and Friedman, 1969). During burial and before the second phase of the Laramide orogeny, geothermal gradients were approximately 26°C/km (Hacquebard, 1977; Hitchon, 1984) and surface temperatures were about

16°C (Piel, 1971). In order to calculate the maximum temperature of burial the amount of overburden removed must also be known.

Estimates on the amount of overburden removal in the Alberta basin have been calculated based on shale compaction and coal maturation data. Magara (1976) used shale compaction data obtained from transit times on sonic logs and calculated the amount of overburden removed in the Caroline field at 1400m. Nurkowski (1984) studied equilibrium moisture content of near surface, Cretaceous coals and calculated the amount of removed overburden in the Gilby area to be 1600 to 1700m. Maximum estimates of overburden removal for south-central Alberta were obtained using vitrinite reflectance and moisture content data from coals (Hacquebard, 1977; and Hitchon, 1984) and indicate up to 2300m removed at Gilby and 2500m at Caroline. Using these maximum estimates, a paleogeothermal gradient of 26°C, and a paleosurface-temperature of 16°C, maximum burial temperatures of approximately 115°C (Gilby/Joffre) to 150°C (Caroline) can be calculated. These estimates also agree with the temperatures needed to account for the level of illite/smectite diagenesis seen in the Viking shales (Chapter III-A).

Another important assumption concerns the $\delta^{18}O$ composition of the fluids during diagenesis. Present day formation waters in the Viking are depleted in $\delta^{18}O$; values of around -6 permill have been reported by Hitchon and

Friedman (1969). These values indicate that a significant fraction of meteoric water has mixed with the original connate water (seawater) (Clayton et al., 1966; Hitchon and Friedman, 1969).

The starting composition of the formation waters probably depends on the location of the reservoir relative to the Viking paleoshoreline (Figure 4.3). Offshore regions, such as Gilby, Joffre, Willesden Green, Ferrier and Harmattan East, probably had an original $\delta^{18}O$ fluid composition of 0 due to the presence of trapped seawater (Figure 4.3). A rooted zone has been identified in the southwestern part of the study area (Hein et al., in press; Lecke, in press) and probably represents a nearshore, deltaic or barrier island environment (Figure 4.3). Original fluids in this area were probably brackish due to the mixing of sea water ($\delta^{18}O = 0$) and fresh water ($\delta^{18}O \simeq -16$; Clayton et al., 1966; Hitchon and Friedman, 1969). Isotopic studies of the Cretaceous Basal Belly River Formation (Longstaffe, in press), lying stratigraphically above the Viking (Figure 1.4), indicate that original shoreline-delta related formation waters were probably brackish and had $\delta^{18}O$ values of -5 to -9.

It is unlikely that meteoric waters penetrated the formation during burial since the hydrodynamic regime was probably controlled by compaction, similar to most Gulf Coast areas (Galloway, 1984). It is probable that during burial fluids became enriched in $\delta^{18}O$ through fluid-rock

Figure 4.3. Location of some of the wells containing samples analyzed for isotopic compositions.

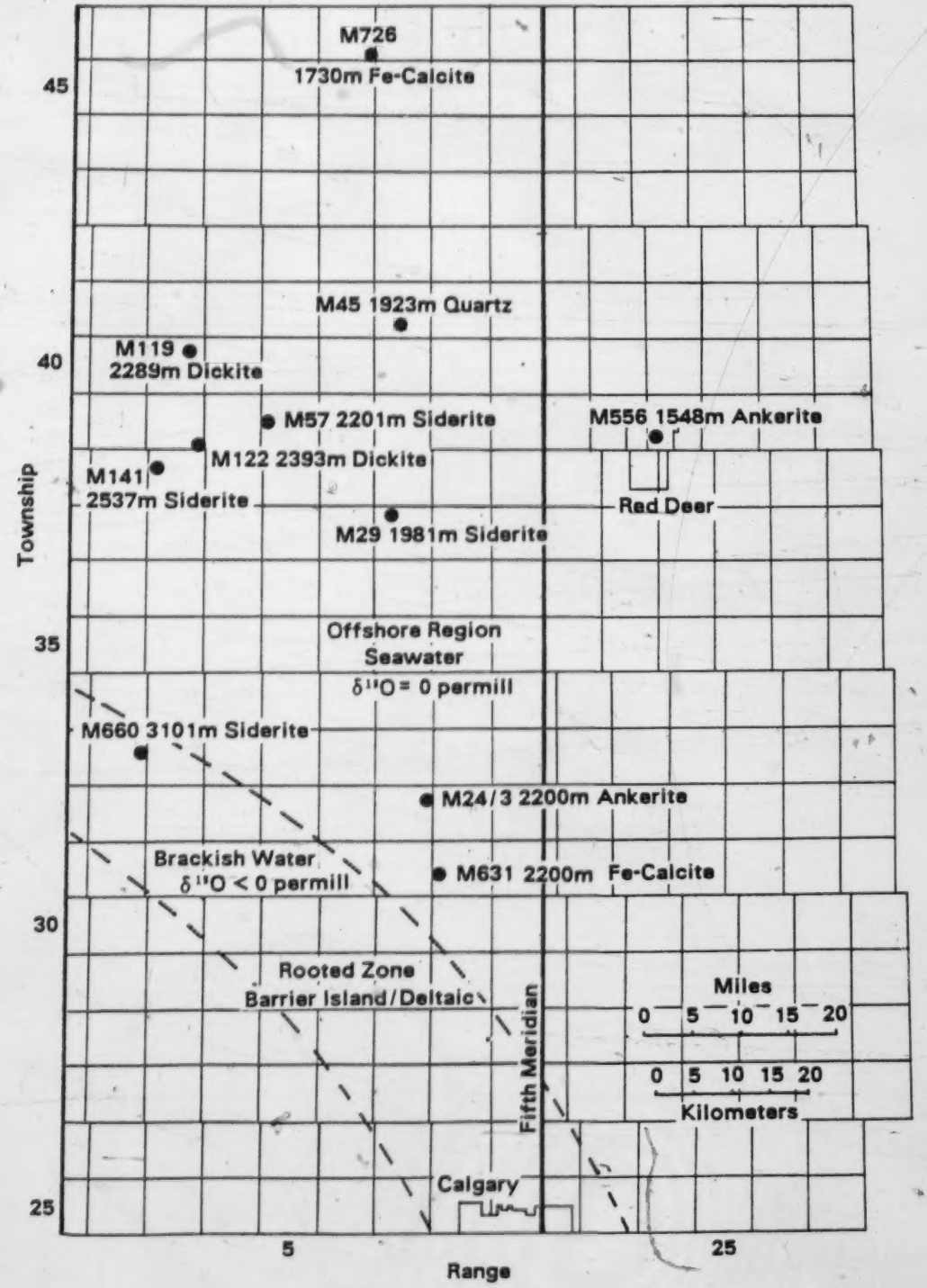

interactions with carbonates or feldspars (Clayton et al., 1966; Hitchon and Friedman, 1969; Longstaffe, 1983, in press). Enrichments of +2 to +4 permill are common in deeply buried sandstones in the Gulf Coast region (Land and Dutton, 1978; Milliken et al., 1981; Dutton and Land, 1985). Most of the $\delta^{18}O$ depletion in the Viking and other formations in the Alberta basin probably occurred because of an influx of meteoric water associated with the second phase of the Laramide orogeny (Clayton et al., 1966; Hitchon and Friedman, 1969; Longstaffe, 1984, in press).

Using the above information and the petrographic data (discussed in Chapter III) it is possible to reconstruct the evolution path of the formation fluids and its relationship to the oxygen-isotope curves of the diagenetic phases (Figure 4.4). The following parameters have been assumed: initial fluid composition of 0 permill (offshore region, Figure 4.3); present fluid composition of approximately -6 permill; an average present temperature of 50°C; an average maximum temperature of 130°C.

During burial fluids probably became enriched in $\delta^{18}O$ through fluid-rock interactions; an enrichment of +2 permill at maximum burial has been assumed (Stage I, Figure 4.4). Textural evidence indicates that siderite formed during early burial and probably crystallized during this intial enrichment trend (Figure 4.4).

Siderite shows a large variation in $\delta^{18}O$ values, ranging from +18.1 to +23.9 (Figure 4.4). Assuming that all

Figure 4.4. Fluid evolution model showing the relationship between $\delta^{18}O$ - mineral (average values), $\delta^{18}O$ - fluid, and temperature. Evolution of a fluid with a starting $\delta^{18}O$ composition of 0 permill is shown (dashed line #1). Where the dashed line crosses the $\delta^{18}O$ - mineral curves this indicates possible temperatures of crystallization (see text for further discussion).

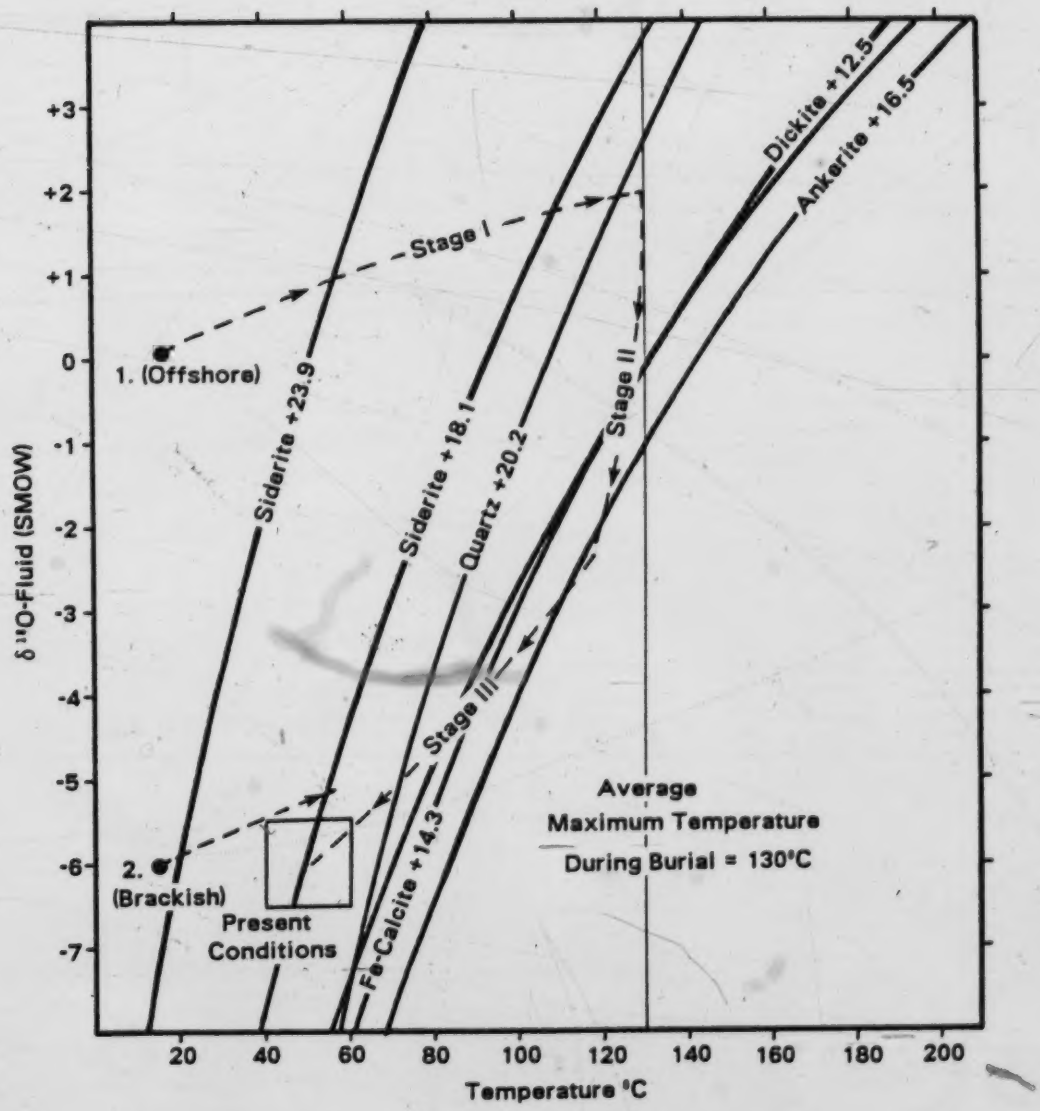

reservoirs had a starting fluid composition of 0 permill the observed temperatures of crystallization would be 55 to 110°C (Figure 4.4). These temperatures are much higher than those reported for most siderites forming in the bacterial fermentation zone (Irwin et al., 1977; Irwin, 1980; Gautier, 1982). The thermal destruction of these bacteria usually occurs around 60°C and after this thermal catalytic reactions in shales produce fluids that dissolve carbonates (Surdam et al., 1984; Figure 4.1).

Due to the location of siderites analyzed it is more likely that original fluid compositions varied. Sample M660 ($\delta^{18}O$ = +18.1) occurs in the extreme southwestern part of the study area within the rooted zone (Figure 4.3). Using an original fluid composition of -6 permill (brackish water) a crystallization temperature of 55°C can be calculated for siderite in sample M660 (dashed line #2, Figure 4.4). The other siderites analyzed are located further offshore (Figure 4.3) and initial fluid compositions were probably closer to 0 permill. A crystallization temperature of approximately 55°C can also be calculated for samples M29 and M57 ($\delta^{18}O$ = +23.3 and +23.9) using a fluid of 0 permill (dashed line #1, Figure 4.4). Assuming a $\delta^{18}O$ - water of 0 permill, siderite in sample M141 ($\delta^{18}O$ = +22.0) either crystallized at a slightly higher temperature than the other siderites or the original pore fluid was slightly less than 0 permill. A lower starting $\delta^{18}O$ - water is probable because of the close proximity of sample M141 to the paleoshoreline

(Figure 4.3). Thus, the observed variation in $\delta^{18}O$ values for siderite (Figure 3.9 & 4.4) probably reflects crystallization from fluids with different starting $\delta^{18}O$ compositions rather than crystallization at different temperatures.

At or near maximum burial there was an influx of meteoric waters associated with the second Laramide orogenic pulse (Stage II, Figure 4.4). Petrographic data indicates that extensive silica cementation occurred after siderite (e.g., Plate 3.9A) and probably reflects an influx of Si-rich, meteoric water. An $\delta^{18}O$ value of +20.2 was obtained for one sample containing mostly pore-lining authigenic quartz (Figure 4.4). According to the model (Figure 4.4) crystallization of this authigenic quartz appears to have occurred towards the end of Stage I. However, by changing some of the assumptions used to construct the model, such as using an enrichment of +3 instead of +2 permill during initial burial or by using a maximum temperature of burial of 120°C instead of 130°, this quartz could have crystallized at the beginning of Stage II. Placing the formation of quartz cement at the beginning of Stage II would still be consistent with the petrographic data and would correlate better with the influx of Si-rich meteoric water.

The crystallization of Fe-calcite and ankerite occurred following quartz, and, in the model (Figure 4.4), is accompanied by a rapid decrease in $\delta^{18}O$ - water. Isotopic

studies of the Basal Belly River Sandstone (Longstaffe, in press; Ayalon and Longstaffe, 1985), lying stratigraphically above the Viking, indicated a similar feature which has been interpreted to represent meteoric water influx during overthrusting (beginning of second Laramide orogeny) and before significant erosion. This caused a rapid depletion in $\delta^{18}O$ - water values and a slight decrease in temperature.

The exact timing of Fe-calcite and ankerite crystallization cannot be deduced from textural evidence since they rarely coexist; however isotopic evidence suggests that Fe-calcite predated ankerite (Figure 4.4). $\delta^{18}O$ values for Fe-calcite average +14.3 and for ankerite +16.5 and during the rapid decrease in $\delta^{18}O$ - water (Stage II, Figure 4.4) it appears Fe-calcite crystallized first followed by ankerite. The observed separation in the oxygen-isotope curves of the carbonate phases may be related to varying rates of isotopic exchange (Clayton et al., 1966); however microprobe data supports crystallization at different times. The average $\delta^{18}O$ - ankerite (+16.5, Figure 4.4) was obtained from samples M556 and M24/3 (Table 3.5); these samples were also analyzed by electron microprobe (Table 3.7). Both these ankerites contain excess Ca in their structures (Figure 4.2) and may have formed as a replacement of calcite. This would suggest that calcite crystallized first and was later ankeritized.

The uplift stage (Stage III, Figure 4.4) is characterized by decreasing temperatures and further

decreases in $\delta^{18}O$ - water. Many of the authigenic clay minerals probably formed during this cooling period since they appear to be the last phases to have crystallized (e.g., Plate 3.8B & 3.12G). Dickite was the first clay mineral to form (e.g., Plate 3.11H) and has an average $\delta^{18}O$ value of +12.5 indicating crystallization from $\delta^{18}O$ - poor fluids (Figure 4.4).

Isotopically, dickite could have formed at the same time as Fe-calcite (Stage II, Figure 4.4) or later, during cooling (Stage III, Figure 4.4). It is unlikely that extensive dickite cement formed during Stage II since kaolin group minerals are unstable in solutions that crystallize carbonates (Surdam et al., 1984). The decrease in temperature associated with stage III (Figure 4.4) may better account for the crystallization of large quantities of dickite since Al and Si solubilities decrease rapidly with decreasing temperatures (Drever, 1982, pg. 96).

C. Diagenetic Model - Summary

The crystallization of diagenetic minerals occurred during burial and uplift (Figure 4.5). The burial sequence reflects changes that occurred as a result of increasing temperature and compaction. In the early Eocene the second Laramide orogenic pulse allowed an influx of meteoric waters which contributed to a decrease in temperature (Figure 4.5). Further reduction of porosity and permeability occurred because of the crystallization of authigenic phases,

Figure 4.5. Diagenetic model showing the relationship between the timing of cementation in the Viking, tectonics and fluid evolution. An average maximum burial temperature of 130°C has been used in this model.

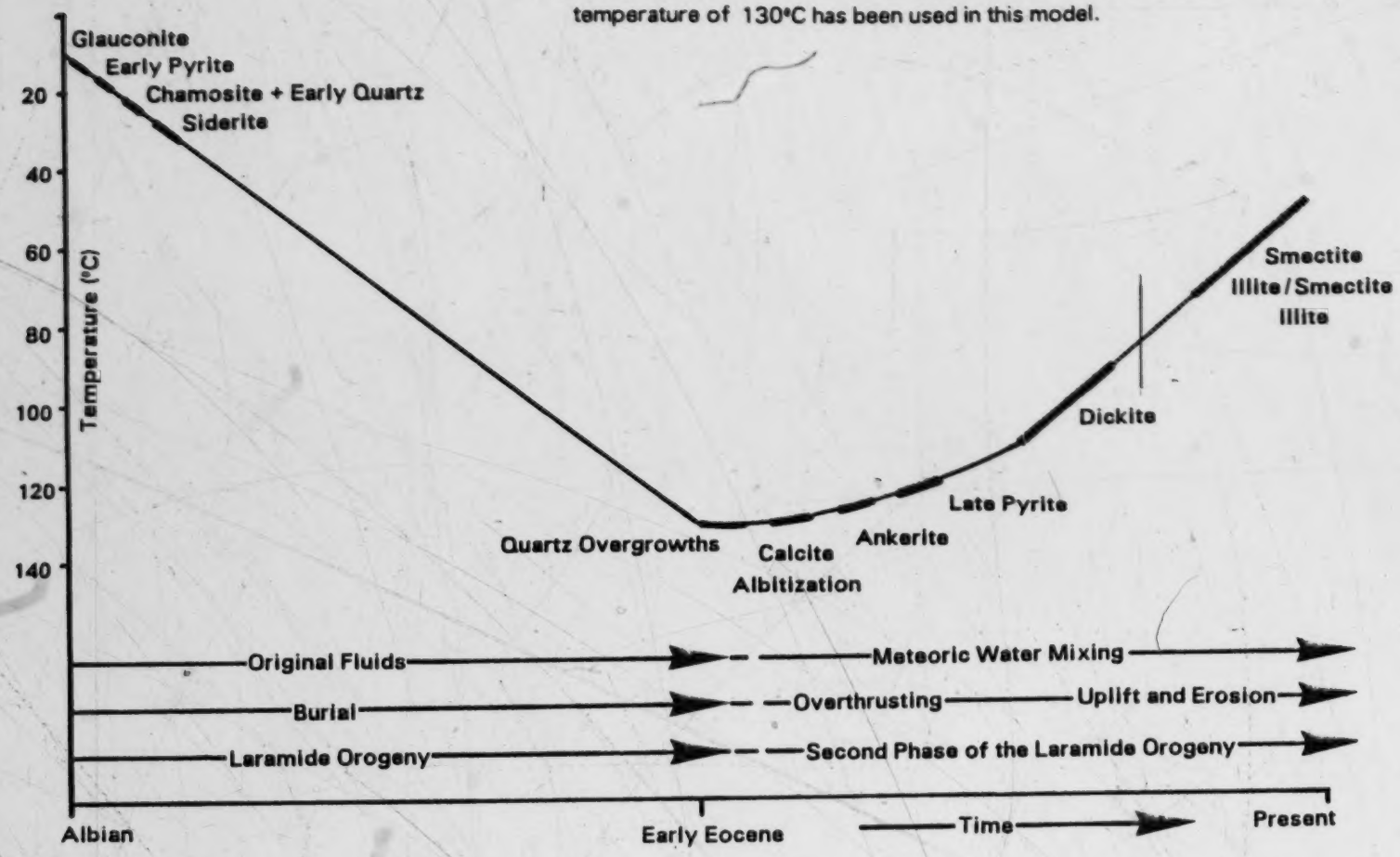

especially quartz overgrowths and dickite.

The crystallization of early glauconite, pyrite, chamosite and siderite indicates that reducing conditions existed during shallow burial (Figure 4.5). Under these conditions oxidized Fe-bearing phases dissolved, mobilizing iron. The iron was combined intially with amorphous Si and Al gels or biogenically altered detrital clays to form glauconite. With greater burial, sulfate reducing bacteria produced HS^-, which combined with the iron to form early pyrite. After a few meters of burial, marine sulfate levels declined and solutions became saturated with iron. This probably enhanced the replacement of some detrital kaolinite by chamosite, through an intermediate phase, such as berthierine. The excess Si released from this transformation produced early authigenic quartz. The introduction of dissolved CO_2, probably from bacterial fermentation, eventually stabilized iron with respect to siderite. Siderite is the most extensive of the early cements and, in some sandstones, competely destroyed the original porosity. The abundance of these early cements was probably controlled by the availability of detrital Fe-bearing minerals, organic matter and clays.

It is possible that during burial of the Viking other diagenetic phases crystallized but no record of these phases is preserved (Figure 4.5). In the Gulf Coast region many stages of carbonate cementation are recognized during the burial of sandstones (e.g., Franks and Forester, 1984). It

is likely additional phases of carbonate cement formed during burial of the Viking. However carbonates, especially calcite, are very susceptible to recrystallization (Franks and Forester, 1984) and isotopic exchange (Clayton et al., 1966). For these reasons it is unlikely that early stages of calcite cementation would be preserved.

The beginning of the second Laramide orogenic pulse occurred near maximum burial of many Cretaceous clastic rocks and resulted in overthrusting and an influx of meteoric water (Figure 4.5). The influx of ground waters probably altered the pore-fluid chemistry and resulted in the crystallization of most of the authigenic phases seen in the Viking sandstones.

One of the first phases to have crystallized during meteoric water invasion was probably quartz (Figure 4.5). The circulation of groundwater through the Viking probably resulted in the transport of large volumes of Si, derived from pressure solution at greater depths, into shallow buried regions were extensive quartz overgrowths formed.

Following quartz overgrowths, albitization of detrital feldspar and crystallization of albite and calcite occurred (Figure 4.5). The crystallization of carbonates indicates that high PCO_2 levels were present and may reflect the release of CO_2 - rich fluids associated with hydrocarbon maturation (Surdam et al., 1984). The calcium ions were probably derived from the albitization of detrital feldspar (Boles, 1982) and additional calcium may have been

transported into the sandstones along with the meteoric waters (Hitchon and Friedman, 1969).

Isotopic and microprobe evidence indicates that ankerite formed after calcite and probably replaced some of the calcite and detrital dolomite. The ankeritization of calcite places some unusual constraints on the nature of the fluids entering at this time since it is unlikely that the meteoric waters suddenly became rich in Fe and Mg. The formation of ankerite may be associated with late stage hydrocarbon generation since the reducing conditions, needed to mobilize Fe and Mg, could have been created by an influx of H_2S-bearing fluids (Figure 4.5). The Fe and Mg may have been derived from the dissolution of earlier formed minerals, such as chamosite and siderite, or brought in with the fluids released from the maturation of organic matter (Irwin, 1980). In areas that contained high PCO_2 levels ankerite would have been stable and ankeritization of calcite and detrital dolomite may have occurred. As H_2S levels rose, Fe would have been reduced to pyrtie (late pyrite, Figure 4.5).

Further meteoric water mixing resulted in the crystallization of dickite, sometime after the carbonate phases (Figure 4.5). Meteoric waters entering the Viking sandstones probably contained high levels of dissolved silica and intially this resulted in the crystallization of quartz. The crystallization of dickite instead of quartz reflects an increase in the activity of aluminum relative to

silica (Drever, 1982, pg 96). An increase in the activity of Al may be associated with the maturation of organic matter; Curtis (1983) indicated that the solubility of Al is greatly enhanced by the presence of organic complexes. The decrease in temperatures associated with uplift (Figure 4.5) would have lowered silica saturation and may have resulted in the crystallization of dickite. Some of the dickite may have also formed through the solution-recrystallization of detrital kaolinite (e.g., Plate 3.1E).

Following dickite, illite, illite/smectite and minor smectite crystallized (Figure 4.5) and reflects an increase in pH and ionic strength of the pore fluids. The crystallization of illitic clays instead of dickite indicates that the pore-fluids became rich in potassium (Blatt, 1982). An increase in the K content relative to Si and Al may have been a function of uplift and decreasing temperatures. The solubility of Si and Al are greatly lowered as temperatures decrease and quartz and kaolin group minerals may have crystallized in deeper formations. As meteoric fluids reached the Viking potassium levels may have increased enough relative to Si and Al to stabilize illite and illite/smectite. Variations in the concentrations of dissolved K, Ca, Fe and Mg may have resulted in the crystallization of smectite instead of illitic clays.

CONCLUSIONS

Sedimentological, mineralogical and geochemical studies were conducted on the Viking Formation in south-central Alberta in order to determine the diagenetic history. The results of the study show that:

1. The Viking Formation consists of two main depositional units, the lower Viking "B" deposits and the upper Viking "A" deposits. The Viking "B" consists of two coarsening upward sequences capped by conglomerate. The lower coarsening upward sequence consists of 15-20m of silt and shale and is capped by a thin (<0.5m) conglomerate. This conglomerate is well developed in the north east (Gilby field) and becomes poorly defined towards the southwest (Caroline field) and probably had a westerly source. The upper coarsening upward sequence consists of 20-25m of shale and fine-grained sandstone at Caroline and pinches out towards Gilby (northeast). The upper conglomerate varies from <1 to 8 m in thickness and is the dominant reservoir in most fields. Thick accumulations of this upper conglomerate occur in stratigraphic lows and may reflect channel deposition.

   Viking "A" consist of sheet-like deposits of coarse-grained sandstone and conglomerate usually 0.5 to 2m thick. At Caroline 2 or more pulses of Viking "A" are present while in the northwestern part of Gilby and Willesden Green 1 to 2 pulses are present.

2. Shales interbedded with the Viking Formation contain

mostly illite (60-85%) and lesser amounts of illite/smectite (5-25%), kaolin group minerals (t-20%), chlorite (t-10%) and smectite (nd-5%). The illite/smectite shows a decrease in percent smectite layers and an increase in ordering with depth. These changes probably reflect various stages of smectite diagenesis associated with increasing depth and temperature during burial. A comparison of the illite/smectite compositions of Viking shales to illite/smectite compositions of Gulf Coast shales indicates that burial temperatures in the Viking probably exceeded 100°C in the past.

Sandstones and conglomerates in the Viking are composed mainly of quartz (5-60%), chert (5-80%), feldspar (nd-30%) and shale rock fragments (nd-24%). Viking "B" rocks contain low percentages of detrital feldspar (nd-5%) and are usually quartzarenites, sublitharenites or litharenites depending on detrital clay content. Viking "A" rocks contain high percentages of detrital feldspar (nd-30%) and consist of arkoses, subarkoses and lithic arkoses. The change in feldspar content reflects a change in source for the Viking "A" deposits.

3. Diagenetic minerals in the sandstones and conglomerates consist of glauconite, pyrite, chamosite, siderite, quartz, albite, Fe-calcite, ankerite, dickite, illite, illite/smectite and smectite. Glauconite is a minor

component in the offshore areas (e.g., Gilby field) and is usually absent in the nearshore areas (e.g., Caroline). Siderite cementation is most extensive in the fine-grained sandstones (t-63%) and may reflect their lower energy, more reducing environment of deposition and their higher initial organic matter content. Quartz cementation is more extensive in the fine and coarse-grained sandstones (3-25%) than in the conglomerates (2-24%). Albitization and the formation of albite and carbonate cements is more extensive in Viking "A" rocks because of their higher detrital feldspar content. Dickite is the most common clay mineral, especially in the coarse-grained rocks (nd-10%). All other authigenic phases occur in minor or trace amounts.

The illite/smectite present in the sandstones and conglomerates (authigenic illite/smectite) does not show any relationship between burial depth and composition. This would indicate that fluid chemistry instead of temperature was the dominant factor that controlled its formation.

4. The combination of petrographic and isotopic data indicates that siderite ($\delta^{18}O$ = +18.1 to +23.9, $\delta^{13}C$ = -1.5 to -6.33) formed during shallow burial from ^{13}C - rich CO_2, probably derived from bacterial fermentation and from ^{18}O - rich connate water. Quartz ($\delta^{18}O$ = +20.2), Fe-calcite ($\delta^{18}O$ = +13.9 to +14.6, $\delta^{13}C$ = -7.2 to -8.4), ankerite ($\delta^{18}O$ = +16.5 to +16.6, $\delta^{13}C$ = -6.3

to -12.4) and dickite ($\delta^{18}O$ = +12.4 to +12.6) crystallized from ^{13}C - poor CO_2, probably derived from the thermal destruction of organic matter and ^{18}O - poor water, probably associated with an influx of meteoric water.

5. Diagenesis of the Viking Formation reflects a large meteoric water influence associated with overthrusting, uplift and erosion initiated by the second phase of the Laramide orogeny. Glauconite, early pyrite, chamosite + minor quartz, and siderite are the only cements that record changing fluid chemistry during burial. These cements formed during shallow burial and are probably associated with the bacterial breakdown of organic matter. It is possible that other cements formed during burial (e.g., calcite) and were not preserved. The formation of extensive quartz overgrowths probably marks the beginning of the second Laramide orogenic pulse when ground waters began transporting large volumes of Si through the Viking. The thermal maturation of organic matter in shales probably occurred during maximum burial and the acidic fluids released (containing CO_2 and organic acids) also entered the Viking. This may have resulted in albitization of some detrital feldspar, and formation of calcite and minor amounts of authigenic kaolin group minerals (dickite). Additional calcium for calcite may have been brought in with the meteoric waters since they probably passed through thick

carbonate sequences before entering the Viking.

The ankeritization of calcite and detrital dolomite occurred after albitization and reflects the mobility of Fe and Mg. The reducing conditions needed to mobilize these ions may have been generated during the late stage release of H_2S from organic matter maturation. Initially CO_2 levels may have been high enough to stabilize ankerite and as H_2S levels increased Fe was probably reduced to pyrite. The Fe and Mg may have been brought in with the fluids released from organic matter maturation or derived from the dissolution of Fe-bearing phases, such as chamosite or siderite.

Extensive pore-fillings of dickite formed as uplift continued. Decreasing temperatures probably decreased the solubility of Si relative to Al and stabilized incoming meteoric waters with respect to kaolin group minerals. Al mobility may have been enhanced by the presence of organic acids.

During further uplift, pore-linings of illite, illite/smectite and smectite formed and reflects an increase in the K^+/H^+ ratio of the fluids. The increase in the ionic strength of the fluids (i.e., K-content) may have been a function of decreasing temperatures during uplift. During uplift, the Viking Formation would have moved out of the temperature zone in which quartz and dickite were stable and these phases would have started to crystallize in deeper, hotter formations. As

a result, fluids entering the Viking would have become depleted in Si and Al relative to K^+, and other cations, and saturated with respect to illite, illite/smectite and smectite.

BIBLIOGRAPHY

Almon, W.R., and Davies, D.K., 1979, Regional diagenetic trends in the lower Cretaceous Muddy Sandstone, Powder River Basin, In, Scholle, P.A., and Schluger, P.R., (eds.), Aspects of Diagenesis, Society of Economic Paleontologists and Mineralogists Special Publication 26, p. 379-400.

Al-Shaieb, Z., and Shelton, J.W., 1981, Migration of hydrocarbons and secondary porosity in sandstones, Bulletin of the American Association of Petroleum Geologists, v. 65, p. 2433-2436.

Amajor, L.C., 1978, Some Viking bentonites, south-central Alberta, Unpublished M.Sc. Thesis, University of Alberta, 104 pp.

------1980, Chronostratigraphy, depositional patterns and environmental analysis of sub-surface Lower Cretaceous (Albian) Viking reservoir sandstones in central Alberta and part of southwestern Saskatchewan, Ph.D. Thesis, University of Alberta, 596 pp.

------1984, Lower Cretaceous Viking barrier island, southwestern Alberta, Canada, (Abstract) Bulletin of

the American Association of Petroleum Geologists, v. 68, p. 448.

Bailey, S.W., 1980, Chapter 1, Structure of layer silicates, In, Brindley, G.W., and Brown, G. (eds.), Crystal structures of clay minerals and their X-ray identification, Mineralogical Society, Monograph 5, London.

Ayalon, A., and Longstaffe, F.J., 1985, Mineralogic, petrographic and isotopic studies of diagenesis in the Basal Belly River Sandstone, Alberta, (Abstract) 36th Annual Technical Meeting of the Petroleum Society of the Canadian Institute of Mineralogy, June, 1985, Edmonton.

Bayliss, P., and Syvitski, J.P.M., 1982, Clay diagenesis in recent marine fecal pellets, Geo-Marine Letters, v. 2, p. 83-88.

Beaumount, C., 1981, Foreland basins, Royal Astronomical Society Geophysical Journal, v. 65, p. 291-329.

Beaumount, E.A., 1984, Retrogradational shelf sedimentation: Lower Cretaceous Viking Formation, central Alberta, In Tillman, R.W., and Siemers, C.T. (eds.), Siliciclastic Shelf Sediments, Tulsa, Oklahoma,

Society of Economic Paleontologists and Mineralogists, Special Publication 34, p. 163-177.

Berg, R.R., and Davies, D.K., 1968, Origin of Lower Cretaceous Muddy Sandstone at Bell Creek field, Montana, Bulletin of the American Association of Petroleum Geologists, v. 52, p. 1888-1898.

Berner, R.A., 1981a, A new geochemical classification of sedimentary environments, Journal of Sedimentary Petrology, v. 51, p.359-365.

------1981b, Authigenic mineral formation resulting from organic matter decomposition in modern sediments, Fortschritte der Mineralogie, v. 59, p. 117-135.

Bhattacharyya, D.P., 1983, Origin of berthierine in ironstones, Clays and Clay Minerals, v. 31, p. 173-182.

Birch, G.F., Willis, J.P., and Rickard, R.S., 1976, An electron microprobe study of glauconites from the continental margin off the west coast of South Africa, Marine Geology, v. 22, p. 271-283.

Bjørlykke, K., Elverhoi, A., and Malm, D., 1979, Diagenesis in Mesozoic sandstones from Spitzbergen and the

North Sea - a comparison. Geologie Rundschau, v. 68, p. 1152-1171.

Bjørlykke, K., 1984, Formation of secondary porosity: how important is it?, In McDonald, D.A. and Surdam, R.C. (eds.), Clastic Diagenesis, American Association of Petroleum Geologists, Memoir 37, p. 277-286.

Blatt, H., Middleton, G., and Murray, R., 1980, Origin of Sedimentary Rocks, Chapter 9, Cementation and deep diagenesis of sandstones, Prentice-Hall Inc., p. 332-368.

Blatt, H., 1982, Sedimentary Petrology, Chapter 6, Conglomerates and sandstones: diagenesis, W.H. Freeman and Company, p. 197-240.

Boer, R.B. De, Nagtegaal, P.J.C., and Duyvis, E.M., 1977, Pressure-solution experiments on quartz sand, Geochimica et Cosmochimica Acta, v. 41, p. 257-264.

Boles, J.R., 1978, Active ankerite cementation in the subsurface Eocene of Southwest Texas, Contributions to Mineralogy and Petrology, v. 68, p. 13-22.

------and Franks, S.G., 1979, Clay diagenesis in Wilcox sandstones of Southwest Texas: implications of

smectite diagenesis on sandstone cementation, Journal of Sedimentary Petrology, v. 49, p. 55-70.

------1981, Sandstone cementation, In, Longstaffe, F.J. (ed.), Clays and the resource geologist, Mineralogical Association of Canada Short Course 7, p. 148-168.

------1982, Active albitization of plagioclase, Gulf Coast Tertiary, American Journal of Science, v. 282, p. 165-180.

------1984, Secondary porosity reactions in the Stevens Sandstone, San Joaquin Valley, California, In McDonald, D.A. and Surdam, R.C. (eds), Clastic Diagenesis, American Association of Petroleum Geologists, Memoir 37, p. 217-224.

Brindley, G.W., 1951, The crystal structure of some chamosite minerals, Mineral Magisine, v. 30, p. 57-70.

------and Youell, R.F., 1953, Ferrous chamosite and ferric chamosite, Mineral Magisine, v. 30, p. 57-70.

Brown, G., and Brindley, G.W., 1980, Chapter 5, X-ray diffraction procedures for clay mineral

identification, In Brindley, G.W., and Brown (eds), Crystal structures of clay minerals and their X-ray identification, Mineralogical Society, Monograph 5, London.

Bullock, D.B., 1950, A micro faunal study of the Basal Lloydminster Shale, Unpublished M.Sc. Thesis, University of Alberta, 43 pp.

Burst, J.F., 1958, 'Glauconite' pellets: their mineral matrix and applications to stratigraphic interpretations, Bulletin of the American Association of Petroleum Geologists, v. 42, p. 310-327.

--------- 1969, Diagenesis of Gulf Coast clayey sediments and its possible relation to petroleum migration, Bulletin of the American Association of Petroleum Geologists, v. 53, p. 73-93.

Carothers, W.W., and Kharaka, Y.K., 1980, Stable carbon isotopes of HCO_3 in oil field waters - implications for the origin of CO_2, Geochimica et Cosmochimica Acta, v. 44, p. 323-332.

Carrigy, M.A., and Mellon, G.B., 1964, Authigenic clay mineral cements in Cretaceous and Tertiary

sandstones of Alberta, Journal of Sedimentary Petrology, v. 34, p. 461-472.

Clayton, R.N., 1959, Oxygen isotope fractionation in the system calcium carbonate-water, Journal of Chemical Physics, v. 30, p. 1246-1250.

------ and Mayeda, T.K., 1963, The use of bromine pentafluoride in the extraction of oxygen from oxides and silicates for isotopic analysis, Geochimica et Cosmochimica Acta, v. 27, p. 43-52.

Clayton, R.N., Friedman, I., Graf, D.L., Mayeda, K., Meents, W.F., and Shimp, N.F., 1966, The origin of saline formation waters, 1, Isotopic composition, Journal of Geophysical Research, v. 71, p. 3869-3882.

Cloud, Jr. P.E., 1955, Physical limits of glauconite formation, Bulletin of the American Association of Petroleum Geologists, v. 39, p. 484-492.

Craig, H., 1957, Isotopic standards for carbon and oxygen and correction factors for mass-spectrometric analysis of carbon dioxide, Geochimica et Cosmochimica Acta, v. 12, p. 133-149.

------ 1961, Standards for reporting concentrations of

deuterium and oxygen-18 in natural waters, Sience, v. 133, p. 1833-1834.

Crossey, L.J., Frost, B.R., and Surdam, R.C., 1984, Secondary porosity in laumontite-bearing sandstones, In McDonald, D.A., and Surdam, R.C. (eds.), Clastic Diagenesis, American Association of Petroleum Geologists, Memoir 37, p. 225-237.

Curtis, C.D., 1983, Link between aluminum mobility and destruction of secondary porosity, Bulletin of the American Assciation of Petroleum Geologists, v. 67, p. 380-393.

Deer, W.A., Howie, R.A., and Zussman, J., 1962, Rock-forming minerals, v. 5, p. 371 - non-silicates, New York, John Wiley and Sons, Inc.

Deroo, G., Powell, T.G., Tissot, B., and McCrossman, R.G., 1977, The origin and migration of petroleum in the western Canadian sedimentary basin, Alberta - a geochemical and thermal maturation study, Bulletin of the Geological Survey of Canada, v. 262, 136 pp.

DeWiel, J.E.F., 1956, Viking and Cardium not turbidity current deposits, Bulletin of the Alberta Society of Petroleum Geologists, v. 4, p. 173-174.

Dickinson, W.R., and Snyder, W.S., 1978, Plate tectonics of the Laramide orogeny, In Mathews, V. III, (ed.), Laramide folding associated with basement block faulting in the western United States, Geological Society of America, Memoir 151, p. 355-366.

Drever, I.J., 1982, The Geochemistry of Natural Waters, Prentic-Hall Inc., 388 pp.

Dutton, S.P., and Land, L.S., 1985, Meteoric burial diagenesis of Pennsylvanian arkosic sandstones, southwestern Anandarko Basin, Texas, Bulletin of the American Association of Petroleum Geologists, v. 69, p. 22-38.

Epstein, S., Graf, D.L., and Degens, E.T., 1964, Oxygen isotope studies on the origin of dolomite, In Craig, H., et al (eds.), Isotopic and cosmic chemistry, Amsterdam, North Holland Publishing Company, p. 169-180.

Eslinger, E.V., 1971, Mineralogy and oxygen isotope ratios of hydrothermal and low grade metamorphic argillaceous rocks, Ph.D. Dissertation, Case Western Reserve University, 205 pp.

Franks, S.G., and Forester, R.W., 1984, Relationship amoung

secondary porosity, pore-fluid chemistry and carbon dioxide, Texas Gulf Coast, In McDonald, D.A., and Surdam, R.C. (eds.), Clastic Diagenesis, American Association of Petroleum Geologists, Memoir 37, p. 63-79.

Friedman, I., and O'Neil, J.R., 1977, Compilation of stable isotope fractionation factors of geochemical interest, In Fleischer, M. (ed.), Data of geochemistry, 6th. ed., United States Geological Survey Professional Paper 440-KK, 12 pp.

Folk, R.L., 1968, Petrology of sedimentary rocks, Austin, Texas, Hemphill's book store.

Foscolos, A.E., Reinson, G.E., and Powell, T.G., 1982, Controls on clay-mineral authigenesis in the Viking sandstone, central Alberta, 1. shallow depths, Canadian Mineralogist, v. 20, p. 141-150.

Galloway, W.E., 1984, Hydrogeologic regimes of sandstone diagenesis, In McDonald, D.A. and Surdam, R.C. (eds.), Clastic Diagenesis, American Association of Petroleum Geologists, Memoir 37, p. 3-13.

Gammell, H.G., 1955, The Viking Member in central Alberta, Bulletin of the Alberta Society of Petroleum

Geolgists, v. 3, p. 63-69.

Garrels, R.M., and Christ, C.L., 1965, Solution, minerals and equilibria, Freeman, Cooper and Company, San Francisco, 450 pp.

Gautier, D.L., 1982, Siderite concretions: indicators of early diagenesis in the Gammon Shale (Cretaceous), Journal of Sedimentary Petrology, v. 52, p. 859-871.

------ 1983, Diagenesis, In Rice, D.D. and Gautier, D.L. (authors), Patterns of sedimentation, diagenesis and hydrocarbon accumulation in Cretaceous rocks of the Rocky Mountains, Society of Economic Paleontologists and Mineralogists, Special Publication 11, p. 4.1-4.14.

Glaister, R.R., 1958, Petrology of the Blairmore sandstone, Bulletin of the Alberta Society of Petroleum Geologists, v. 6, p. 43-49.

Grant, S.K., 1985, Geologic studies of the Garrington oil field, south-central Alberta, M.Sc. thesis, University of Alberta.

Hacquebard, P.A., 1977, Rank of coal as an index of organic metamorphism for oil and gas in Alberta, In, The

origin and migration of petroleum in the Western Canadian sedimentary basin, Alberta, Bulletin of the Geological Survey of Canada, v. 262, p. 11-22.

Harder, H., 1980, Synthesis of glauconite at surface temperatures, Clays and Clay Minerals, v. 28, p. 217-222.

Hayes, J.B., 1979, Sandstone diagenesis - the whole truth, Society of Economic Paleontologists and Mineralogists, Special Publication 26, p. 127-139.

Hein, F.J., Dean, M.E., DeIure, A.M., Grant, S.K., Robb, G.A., and Longstaffe, F.J., (in press), Regional sedimentology of the Viking Formation, Caroline, Garrington and Harmattan East fields, western south-central Alberta: Storm and current-influenced shelf settings, Bulletin of the Canadian Society of Petroleum Geologists.

Hitchon, B., 1984, Geothermal gradients, hydrodynamics, and hydrocarbon occurences, Alberta, Canada, Bulletin of the American Association of Petroleum Geologists, v. 68, p. 713-743.

Hitchon, B., and Friedman, I., 1969, Geochemistry and origin of formation waters in the western Canada

sedimentary basin, 1, Stable isotopes of hydrogen and oxygen, Geochimica et Cosmochimica Acta, v. 33, p. 1321-1349.

Hower, J., 1961, Some factors concerning the nature and origin of glauconite, American Mineralogist, v. 46, p. 313-334.

------ Eslinger, E.V., Hower, M.E., and Perry, E.A., 1976, Mechanisms of burial metamorphism of argillaceous sediments 1, mineralogical and chemical evidence, Bulletin of the Geological Association of America, v. 87, p. 725-737.

------ 1981, Shale diagenesis, In, Longstaffe, F.J., (ed.), Clays and the resource geologist, Mineralogical Association of Canada Short Course 7, p. 60-80.

Hume, G.S., 1933, Oil and gas in western Canada, Geological Survey of Canada, Economic Geology Series, n. 5, 359 pp.

Hunt, W.C., 1954, The Joseph Lake-Armena-Camrose producing trend, Alberta, In Clark, L.M. (ed.), Western Canada Sedimentary Basin, p. 452-463.

Hurst, A., and Irwin, H., 1982, Geological modelling of clay

diagenesis in sandstones, Clay Minerals, v. 17, p. 5-22.

Ignasiak, T.M., Kotlyar, L., Longstaffe, F.J., Strausz, O.P., and Montgomery, D.S., 1983, Separation and characterization of clay form Athabasca asphaltene, Fuel, v. 62, p. 353-362.

Iijima, A., and Matsumoto, R., 1982, Berthierine and chamosite in coal measures of Japan, Clays and Clay Minerals, v. 30, p. 264-274.

Irwin, H., 1980, Early diagenetic carbonate precipitation and pore fluid migration in the Kimmeridge Clay of Dorset, England, Sedimentology, v. 27, p. 577-591.

Irwin, H., Curtis, C., 1977, and Coleman, M., 1977, Isotopic evidence for source of diagenetic carbonates formed during burial of organic-rich sediments, Nature, v. 269, p. 209-213.

Jackson, R.C., Myhr, D.W., Groeneweg, B., Palmer, H.R., Mclean, G.G., Loney, C.D., and Dolphen, D.R., 1975, Geological highway map of Ablerta, de Wit, R. (ed.), Canandian Society of Petroleum Geologists, Calgary.

Jordan T.E., 1981, Thrust loads and foreland basin

evolution, Cretaceous, western United States, Bulletin of the American Association of Petroleum Geologists, v. 65, p. 2506-2520.

Kharaka, Y.K., Berry, A.F., and Friedman, I., 1973, Isotopic compositions of oil-field brines from Kettleman North Dome, California and their geological implications, Geochimica et Cosmochimica Acta, v. 37, p. 1899-1908.

Land, D.R., and Prezbendowski, 1981, The origin and evolution of saline formation waters: Lower Cretaceous carbonates, south cetral Texas, USA, Journal of hydrology, v. 54, p. 51-74.

Land, L.S., 1984, Frio sandstone diagenesis, Texas, Gulf Coast: a regional isotopic study, In McDonald, D.A. and Surdam, R.C. (eds.), Clastic Diagenesis, American Association of Petroleum Geologists, Memoir 37, p. 47-62.

Land, L.S., and Dutton, S.P., 1978, Cementation of a Pennsylvanian deltaic sandstone: isotopic data, Journal of Sedimentary Petrology, v. 48, p. 1167-1176.

------ and Milliken, K.L., 1981, Feldspar diagenesis in the

Frio Formation, Brazoria County, Texas Gulf Coast, Geology, v. 9, p. 314-318.

Leckie, D., (in press), Viking Formation, Caroline area, a transgressive tide dominated shelf-ridge complex, Bulletin of the Canadian Society of Petroleum Geologists.

Lerbekmo, J.F., 1963, Petrology of the Belly River Formation, southern Alberta foothills, Sedimentology, v. 2, p. 54-86.

Longstaffe, F.J., 1983, Stable isotopic studies of diagenesis in clastic rocks, Geoscience Canada, v. 10, p. 43-58.

------ 1984, The role of meteoric water in diagenesis of shallow sandstones: stable isotope studies of the Milk River aquifer and gas pool, southeastern Alberta, In McDonald, D.A., and Surdam, R.C. (eds.), Clastic Diagenesis, American Association of Petroleum Geologists, Memoir 37, p. 81-98.

------ (in press), Oxygen-isotope studies of diagenesis in the Basal Belly River Sandstone, Pembina I-Pool, Alberta, Journal of Sedimentary Petrology.

Magara, K., 1973, Compaction and fluid migration in Cretaceous shales of western Canada, Canadian Geological Survey Paper 72, 65 pp.

------ 1976, Thickness of removed sedimentary rocks, paleopore pressure, and paleotemperature, southwestern part of Western Canada Basin, Bulletin of the American Association of Petroleum Geologists, v. 60, p. 554-565.

Magdich, F.S., 1955, The Viking Formation in Saskatchewan, Unpublished M.Sc. Thesis, University of Saskatchewan, Saskatoon.

Manheim, F.J., 1967, Evidence for submarine discharge of water on the Atlantic continental slope of southern United States and suggestions for further research, Transactions of the New York Academy of Sciences, v. 11, p. 839-853.

------ and Paull, C.K., 1981, Patterns of groundwater salinity changes in a deep continental oceanic transect off the southeastern Altantic Coast of the U.S.A., Journal of Hydrology, v. 54, p. 95-105.

McConchie, D.M., Ward, J.B., McCann, V.H., and Lewis, D.W., 1979, A mossbauer investigation of glauconite and

its geological significance, Clays and Clay Minerals, v. 27, p. 339-348.

McCrea, J.M., 1950, On the isotopic chemistry of carbonates and a paleotemperature scale, Journal of Chemical Physics, v. 18, p. 849-857.

McRae, S.G., 1972, Glauconite, Earth Science Reviews, v. 8, p. 397-440.

Milliken, K.L., Land, L.S., and Loucks, R.G., 1981, History of burial diagenesis determined from isotopic geochemistry, Frio Formation, Brazoria County, Texas, Bulletin of the American Association of Petroleum Geologists, v. 65, p. 1397-1413.

Momper, J.A., 1978, Oil migration limitations suggested by geological and geochemical considerations, In Physical and chemical constraints on petroleum migration, American Association of Petroleum Geologists, Short Course 8, p. B.1-B.60.

Nauss, A.W., 1945, Cretaceous stratigraphy of Vermillion area, Alberta, Canada, Bulletin of the American Association of Petroleum Geologists, v. 29, p. 1615-1618.

Nurkowski, J.R., 1984, Coal quality, coal rank variation and its relation to reconstructed overburden, Upper Cretaceous and Tertiary plains coals, Alberta, Canada, Bulletin of the American Association of Petroleum Geologists, v. 68, p. 285-295.

O'Neil, J.R., and Kharaka, Y.F., 1976, Hydrogen and oxygen isotope exchange reactions between clay minerals and water, Geochimica et Cosmochimica Acta, v. 40, p. 241-246.

Perry, E., and Hower, J., 1970, Burial diagenesis of Gulf Coast pelitic sediments, Clays and Clay Minerals, v. 18, p. 165-177.

Piel, K.M., 1971, Palynology of Oligocene sediments of central British Columbia, Canadain Journal of Botany, v. 49, p. 1885-1920.

Pittman, E.D., 1972, Diagenesis of quartz in sandstones as revealed by scanning electron microscopy, Journal of Sedimentary Petrology, v. 42, p. 507-519.

Porrenga, D.H., 1967, Glauconite and chamosite as depth indicators in marine environments, Marine Geology, v. 5, p. 495-501.

Porter, K.W., and Weimer, R.J., 1982, Diagenetic sequence related to structural history and petroleum accumulation: Spindle field, Colorado, Bulletin of the American Association of Petroleum Geologists, v. 66, p. 2543-2560.

Price, R.A., 1973, Large scale gravitational flow of supracrustal rocks, southern Canadian Rockies, In DeJong, K.A., and Scholten, R. (eds.), Gravity and Tectonics, New York, John Wiley and Sons, p. 491-502.

Pryor, W.A., 1975, Biogenic sedimentation and alteration of argillaceous sediments in shallow marine environments, Bulletin of the Geological Society of America, v. 86, p. 1244-1254.

Reynolds, Jr. R.C., and Hower, J., 1970, The nature of interlayering in mixed-layer illite-montmorillonites, Clay and Clay Minerals, v.18, p. 25-36.

Rice, D.D., 1980, Coastal and deltaic sedimentation of Upper Cretaceous Eage Sandstone: relation of shallow gas accumulations, north-central Montana, Bulletin of the American Association of Petroleum Geologists, v. 64, p. 316-338.

Robb, G.A., 1985, Geological studies of the Garrington oil field, south-central Alberta, M.Sc. thesis, University of Alberta.

Roessingh, H.K., 1959, Viking deposition in the southern Alberta Plains, Alberta Society of Petroleum Geologists, 9th. Annual Field Conference, p. 130-137.

Rosenfield, W.D., and Silverman, S.R., 1959, Carbon isotopic fractionation in bacterial production of methane, Science, v. 130, p. 1658.

Rudkin, R.A., 1964, Chapter II: Lower Cretaceous, In McCrossan, R.G., and Glaister, R.R. (eds.), Goelogical history of western Canada, Canadian Society of Petroleum Geologists, Calgary, Alberta, p. 156-168.

Savin, S.M., and Epstein, S., 1970a, The oxygen and hydrogen isotope geochemistry of clay minerals, Geochimica et Cosmochimica Acta, v. 34, p. 25-42.

Savin, S.M., and Epstein, S., 1970b, The oxygen and hydrogen isotope geochemistry of ocean sediments and shales, Geochimica et Cosmochimica Acta, v. 34, p. 43-63.

Savin, S.M., and Yeh, H., 1981, Stable isotopes in ocean sediments, In Emiliani, C. (ed.), The Sea, Volume 7, The Oceanic Lithosphere, John Wiley and Sons, New York, p. 1521-1554.

Schwartz, F.W., Muehlenbachs, K., and Chorley, D.W., 1981, Flow system controls of the chemical evolution of groundwater, Journal of Hydrology, v. 54, p. 225-243.

Sibley, D.F., and Blatt, H., 1976, Intergranular pressure solution and cementation of the Tuscarora orthoquartzite, Journal of Sedimentary Petrology, v. 46, p. 881-896.

Siebert, R.M., Moncure, G.K., and Lahann, R.W., 1984, A theory of framework grain dissolution in sandstones, In McDonald, D.A., and Surdam, R.C. (eds.), Clastic Diagenesis, American Association of Petroleum Geologists, Memoir 37, p. 163-175.

Siever, R., 1959, Petrology and geochemistry of silica cementation in some Pennsylvanian sandstones, In, Ireland, H.A. (ed.), Silica in sediments, Society of Economic Paleontologists and Mineralogists, Special Paper 7, 175 pp.

Slipper, S.E., 1918, Viking gas field, structure of area, Geological Survey Summary Department 1917, Part C, p. 8c.

Sorokin, V.I., and Vlasov, V.V., 1979, Effect of the medium on development of glauconite composition, Lithology and Mineral Resources, USSR, v. 14, p. 690-693.

Srodon, J., 1984, X-ray powder diffraction identification of illitic materials, Clays and Clay Minerals, v. 32, p. 337-349.

Stelck, C.R., 1958, Stratigraphic position of the Viking sand, Bulletin of the Alberta Society of Petroleum Geologists, v. 6, p. 2-7.

------ 1975, The Upper Albian *Miliammina manitobensis* zone in northeastern British Columbia, In Caldwell, W.G.E. (ed.), The Cretaceous system in the Western Interior of North America, Geological Association of Canada, Special Paper 13, p. 253-275.

Surdam, R.C., Bosse, S.W., and Crossey, L.J., 1984, The chemistry of secondary porosity, In McDonald, D.A., and Surdam, R.C. (eds.), Clastic Diagenesis, American Association of Petroleum Geologists, Memoir 37, p. 127-149.

Syers, J.K., Chapman, L.S., Jackson, M.L., Rex, R.W., and Clayton, R.N., 1968, Quartz isolation from rocks, sediments and soils for determination of oxygen isotopic compositions, Geochimica et Cosmochimica Acta, v. 32, p. 1022-1025.

Taylor, R.S., Mathews, W.H., and Kupsch, W.O., 1964, Tertiary, In, McCrossan, R.G., and Glaister, R.P. (eds.), Geological history of western Canada, Canadian Society of Petroleum Geologists, Calgary, Canada, p. 190-194.

Thomas, J.B., 1978, Diagenetic sequences in low-permeability argillaceous sandstones, Geological Society of London, v. 135, p. 93-99.

Thomas, M.B., and Oliver, T.A., 1979, Depth-porosity relationships in the Viking and Cardium Formations of central Alberta, Bulletin of Canadian Petroleum Geology, v. 27, p. 209-228.

Thompson, G.R., and Hower, J., 1975, The mineralogy of glauconite, Clays and Clay Minerals, v. 23, p. 289-300.

Tizzard, P.g., 1974, Viking deposition in the Suffield area, Alberta, Unpublished M.Sc. Thesis, University of

Alberta, 126 pp.

Tooth, J.W., Kavanagh, P.T., and Peter, S.E., 1984, Reservoir quality of the Viking Formation, Dodsland area, Saskatchewan, Oil and Gas in Saskatchewan, p. 245-253.

Toth, J., 1980, Cross-formational flow of groundwater: a mechanism for transport and accumulation of petroleum (The generalized hydraulic theory of petroleum migration), In, Roberts, W.H. III, and Cordell, R.J., (eds.) Problems in Petroleum Migration, American Association of Petroleum Geologists Studies in Geology 10, p. 121-167.

Walthers, Jr., L.J., Claypool, G.E., and Choquette, P.W., 1972, Reaction rates and O^{18} variation for the carbonate-phosphoric acid preparation method, Geochimica et Cosmochimica Acta, v. 36, p. 129-140.

Wheeler, J.O., Charlesworth, H.A.K., Monger, J.W.H., Muller, J.E., Price, R.A., Reesor, J.E., Roddick, J.A., and Simoney, P.S., 1974, Western Canada, In Spencer, A.M. (ed.), Mesozoic-Cenozoic orogenic belts, Geological Society, Speical Publication 4, p. 591-624.

Williams, G.D., and Stelck, C.R., 1975, Speculations on the Cretaceous paleogeography of North America, In Caldwell, W.G.E. (ed.), The Cretaceous system in the Western Interior of North America, Geological Association of Canada, Special Paper 13, p. 1-7.

Wilson, M.D., 1982, Origins of clays controlling permeability in tight gas sands, Journal of Petroleum Technology, v. 7, p. 2871-2876.

Wilson, M.D., and Pittman, E.D., 1977, Authigenic clays in sandstones: recognition and influence on reservoir properties and paleoenvironmental analysis, Journal of Sedimentary Petrology, v. 47, p. 3-31.

Yeh, H., and Savin, S.M., 1977, Mechanisms of burial metamorphism of argillaceous sediments: O-isotope evidence, Bulletin of the Geological Society of America, v. 85, p. 1321-1330.

APPENDIX I

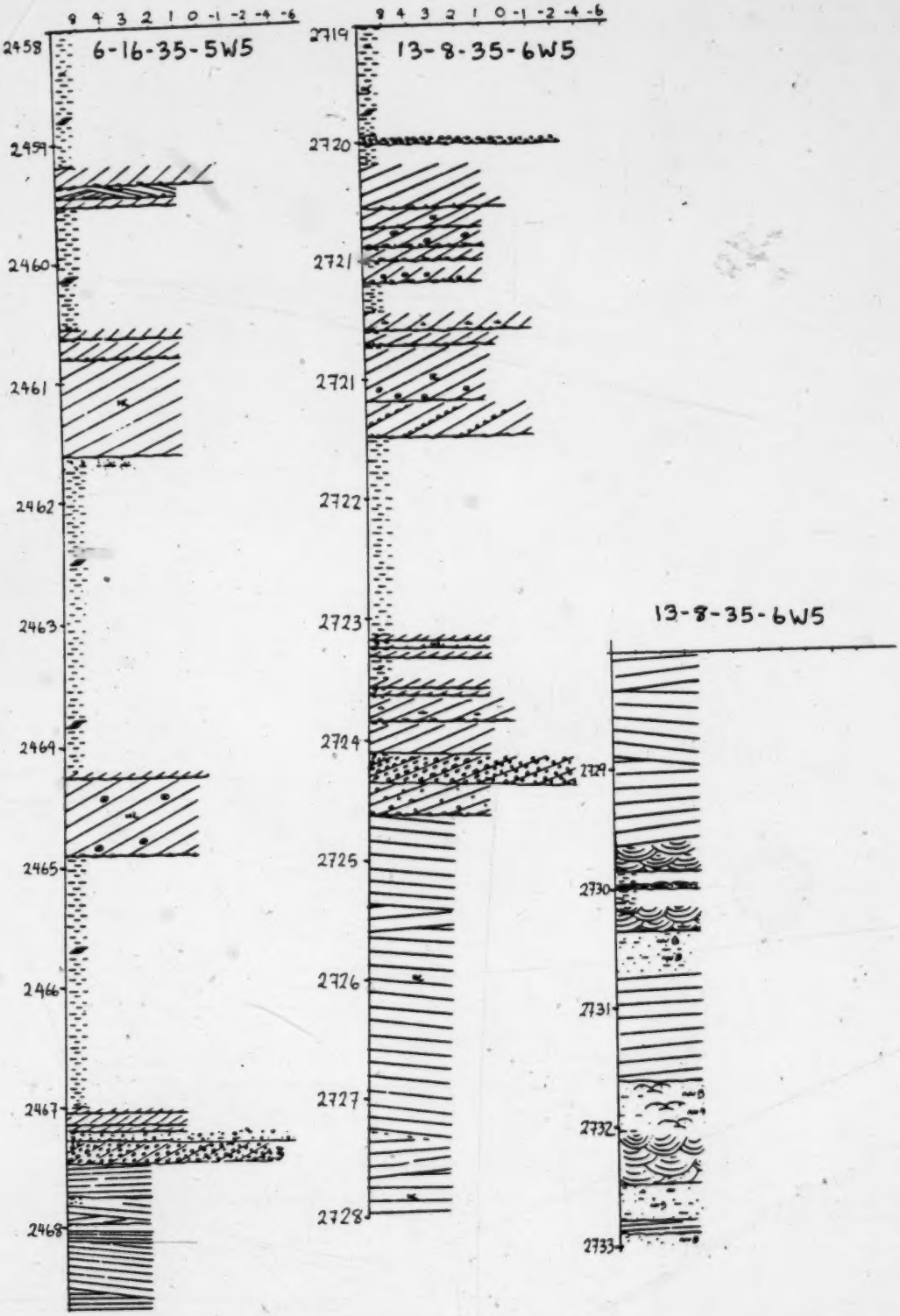
9 4 3 2 1 0 -1 -2 -4 -6
6-16-35-5W5
2458
2459
2460
2461
2462
2463
2464
2465
2466
2467
2468
9 4 3 2 1 0 -1 -2 -4 -6
13-8-35-6W5
2719
2720
2721
2721
2722
2723
2724
2725
2726
2727
2728
13-8-35-6W5
2729
2730
2731
2732
2733

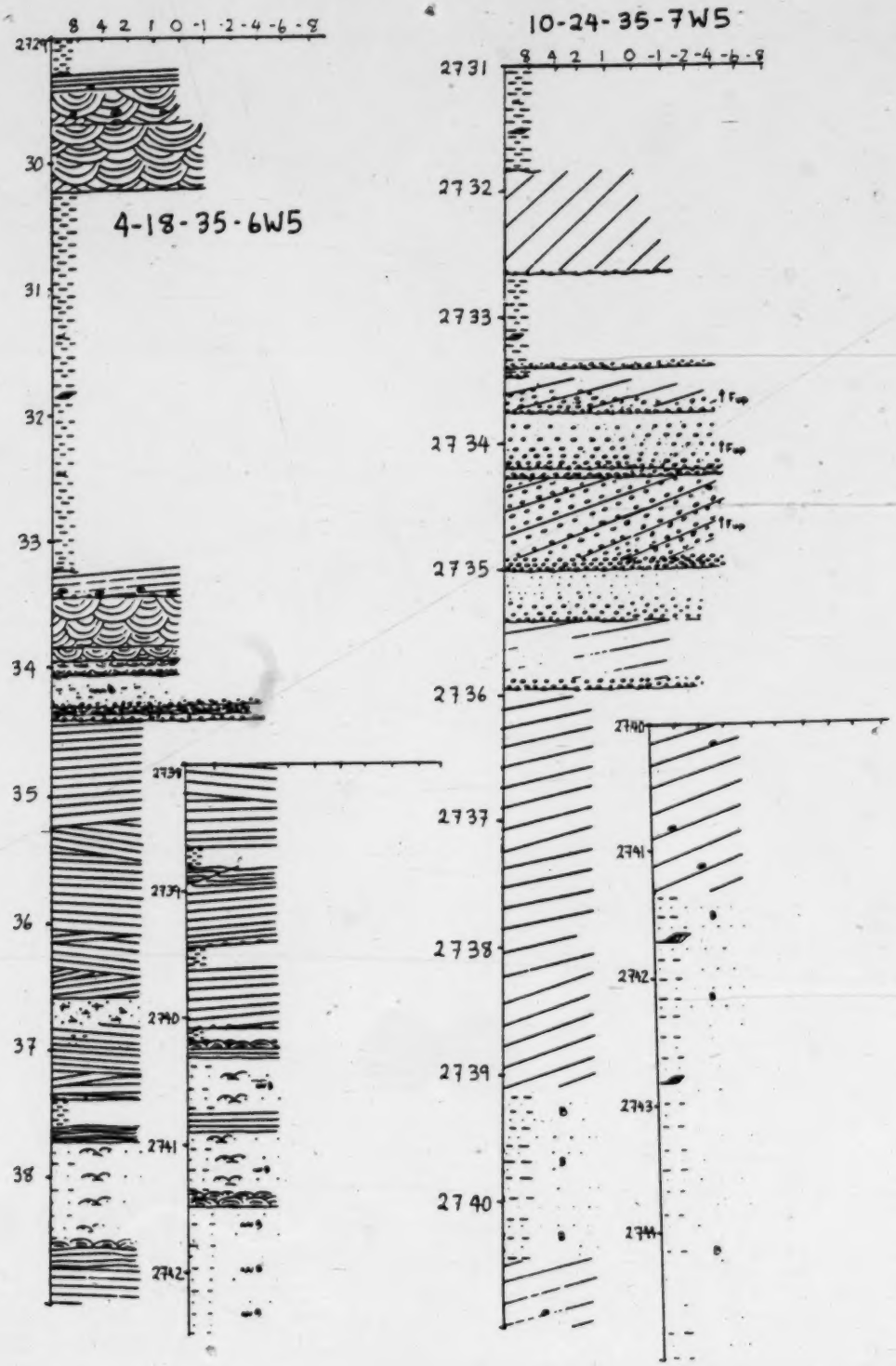
8 4 2 1 0 -1 -2 -4 -6 -8
4-18-35-6W5
10-24-35-7W5
8 4 2 1 0 -1 -2 -4 -6 -8
2729
30
31
32
33
34
35
36
37
38
2731
2732
2733
2734
2735
2736
2737
2738
2739
2740
2739
2740
2741
2742
2740
2741
2742
2743
2744

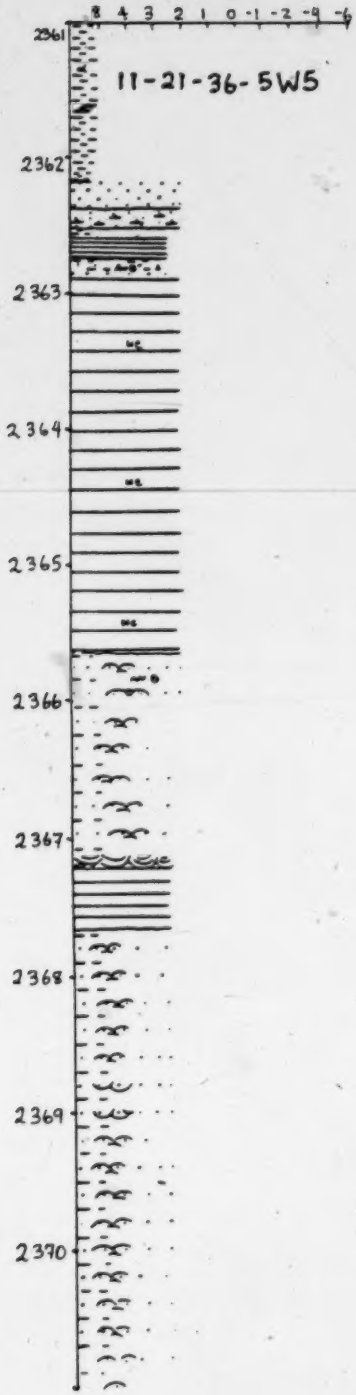
8 4 3 2 1 0 -1 -2 -3 -4
2361
11-21-36-5W5
2362
2363
2364
2365
2366
2367
2368
2369
2370

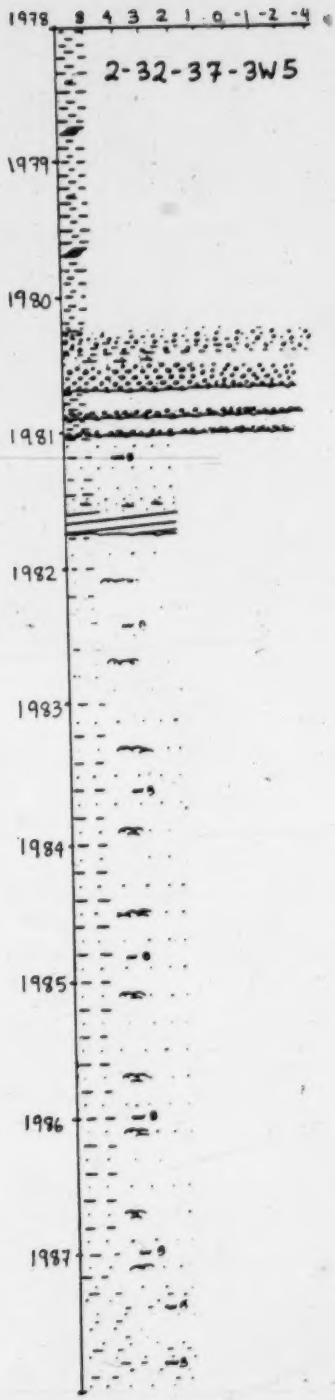
1978
8 4 3 2 1 0 -1 -2 -4
2-32-37-3W5
1979
1980
1981
1982
1983
1984
1985
1986
1987

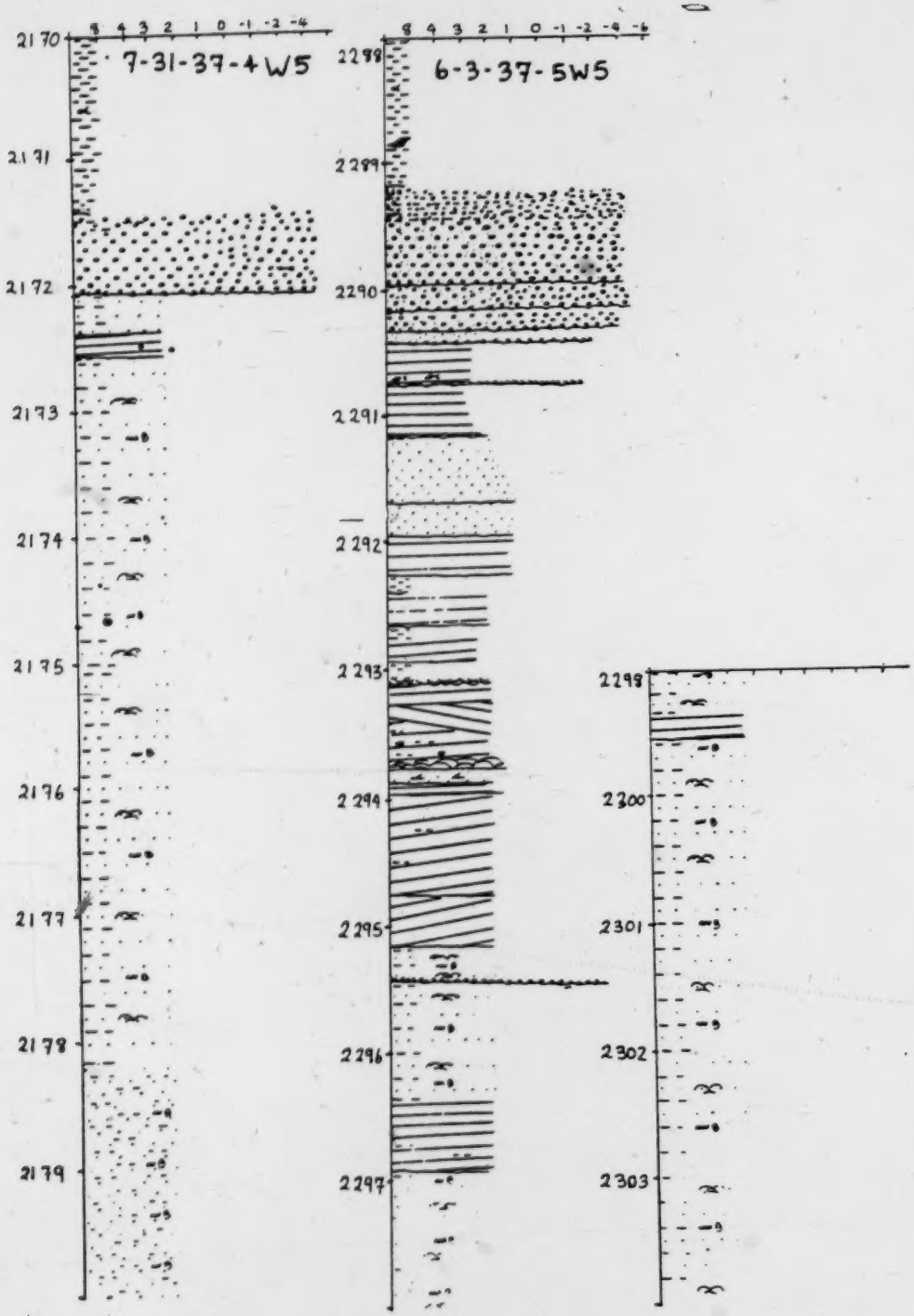
7-31-37-4W5
6-3-37-5W5
2170
2171
2172
2173
2174
2175
2176
2177
2178
2179
2289
2290
2291
2292
2293
2294
2295
2296
2297
2298
2300
2301
2302
2303

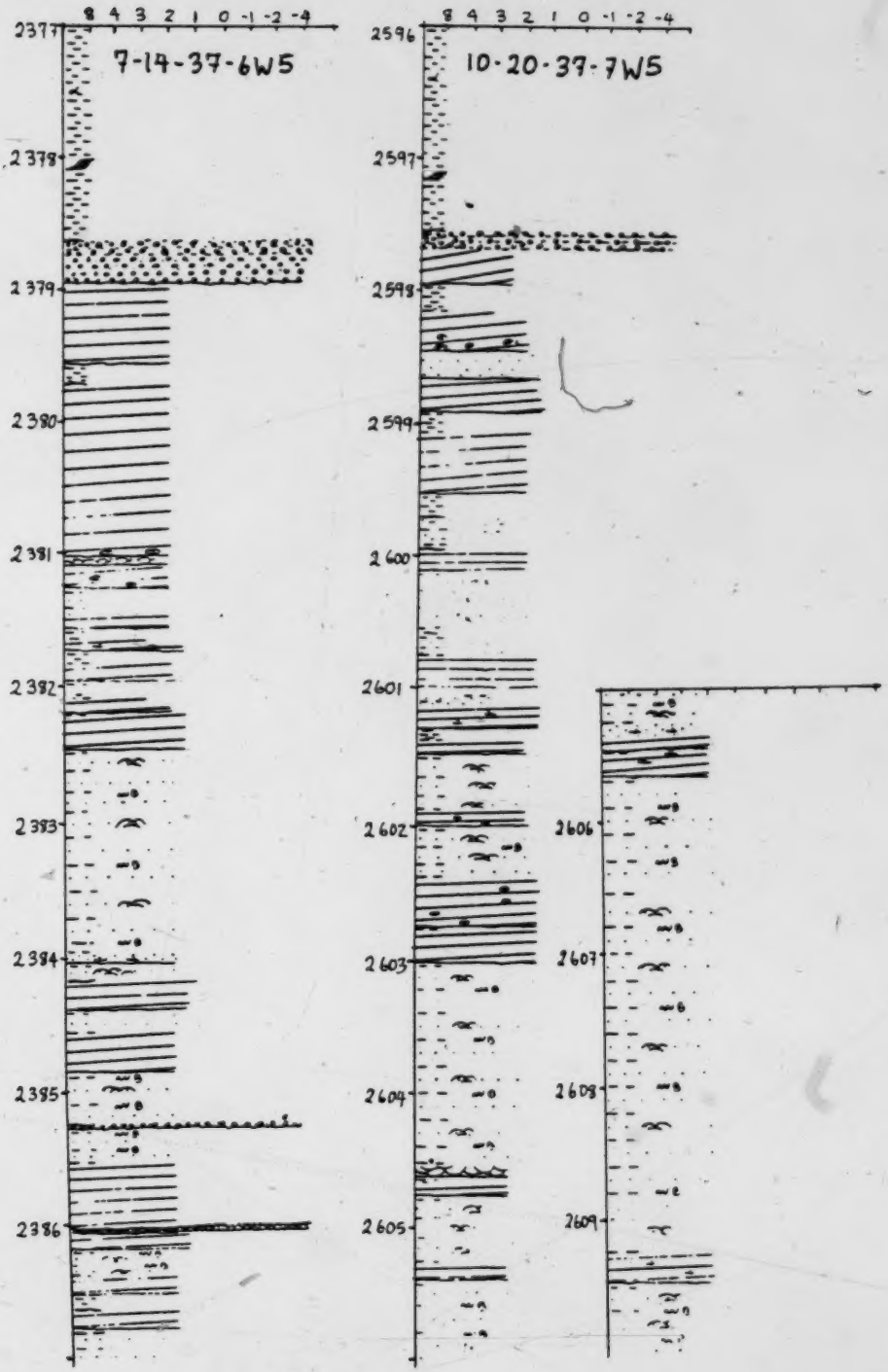
8 4 3 2 1 0 -1 -2 -4
7-14-37-6W5
2377
2378
2379
2380
2381
2382
2383
2384
2385
2386
8 4 3 2 1 0 -1 -2 -4
10-20-37-7W5
2596
2597
2598
2599
2600
2601
2602
2603
2604
2605
2606
2607
2608
2609

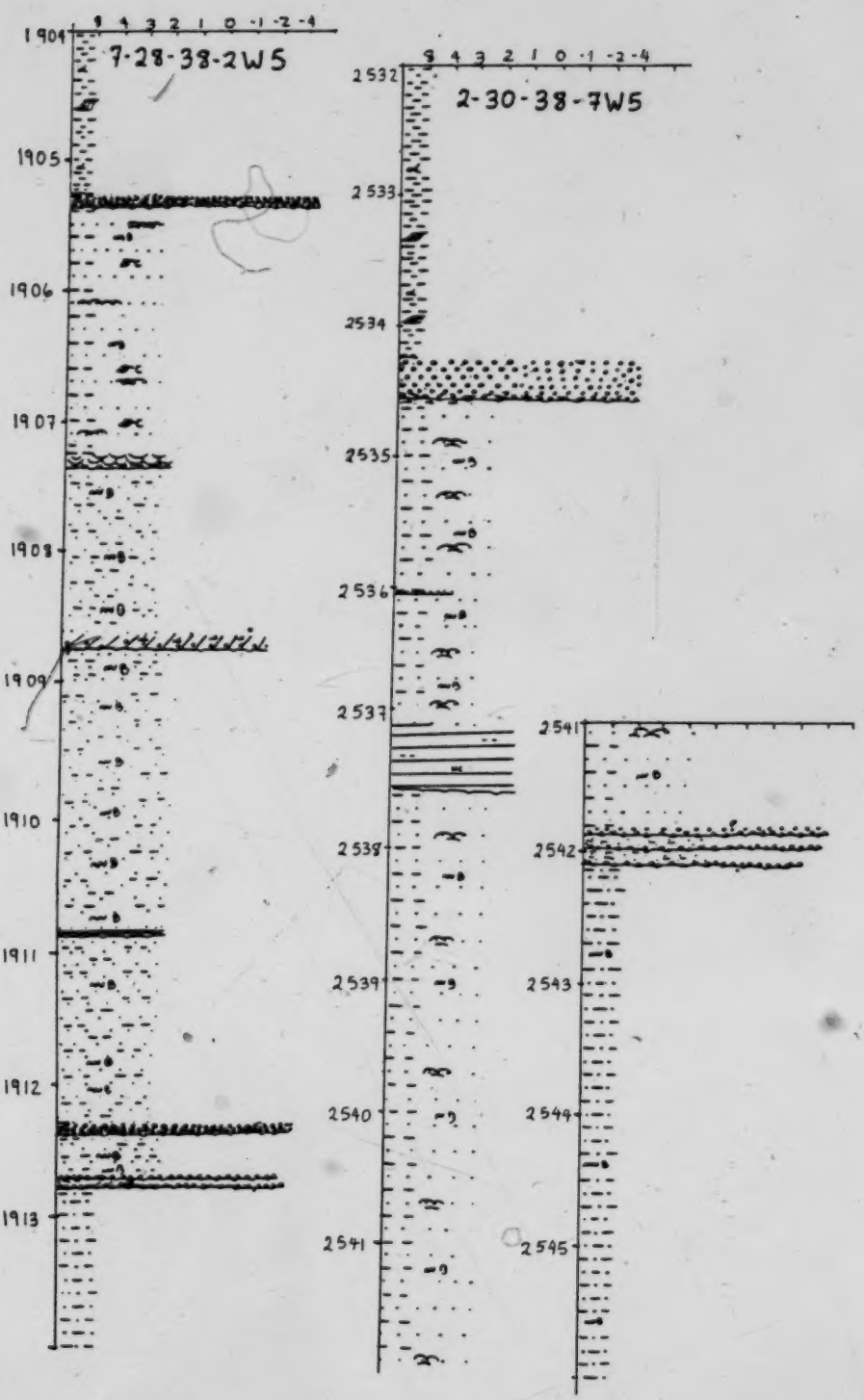
7-28-38-2W5
2-30-38-7W5
1904
1905
1906
1907
1908
1909
1910
1911
1912
1913
2532
2533
2534
2535
2536
2537
2538
2539
2540
2541
2541
2542
2543
2544
2545

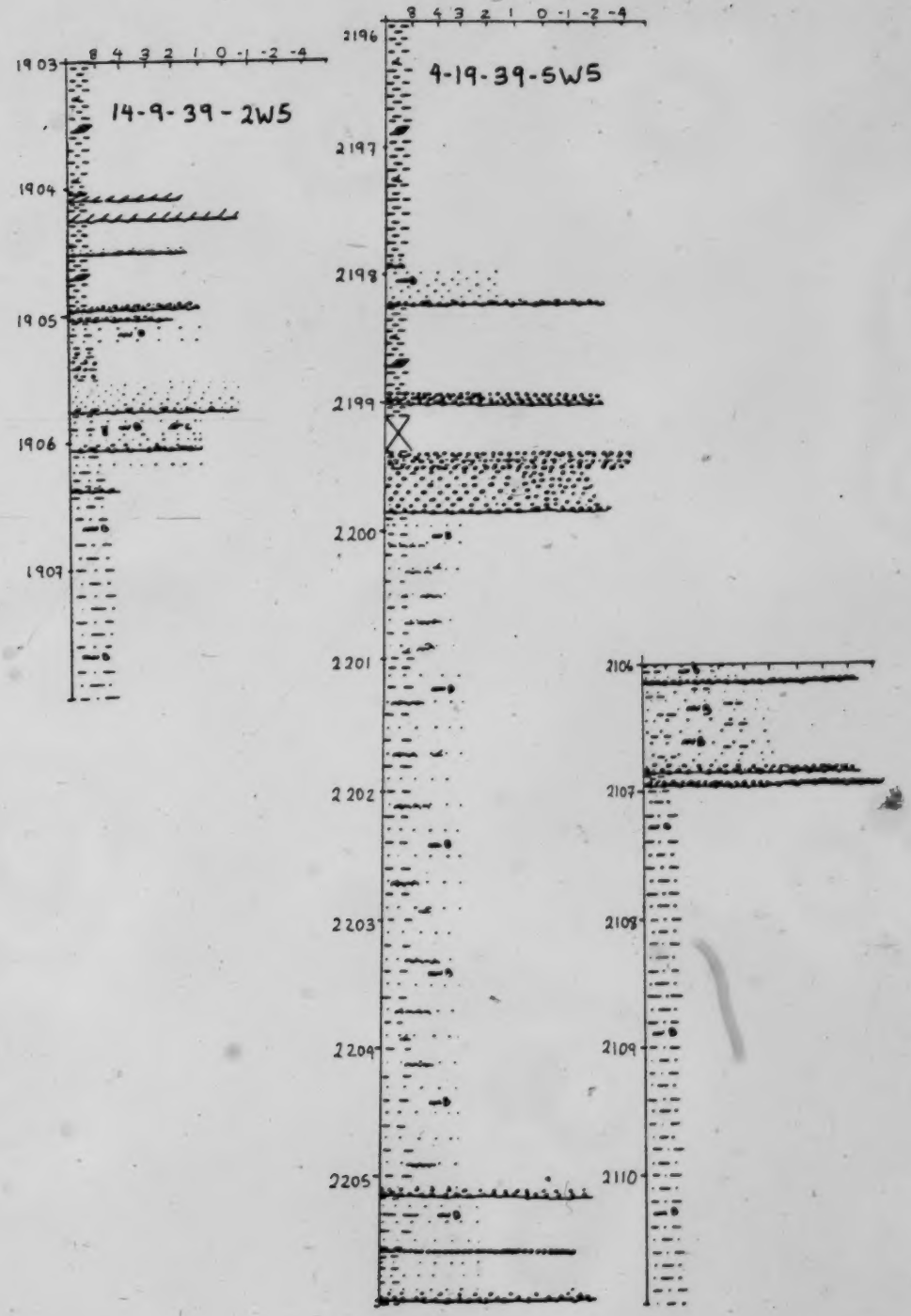
8 4 3 2 1 0 -1 -2 -4
1903
14-9-39-2W5
1904
1905
1906
1907
8 4 3 2 1 0 -1 -2 -4
2196
4-19-39-5W5
2197
2198
2199
2200
2201
2202
2203
2204
2205
2104
2107
2108
2109
2110

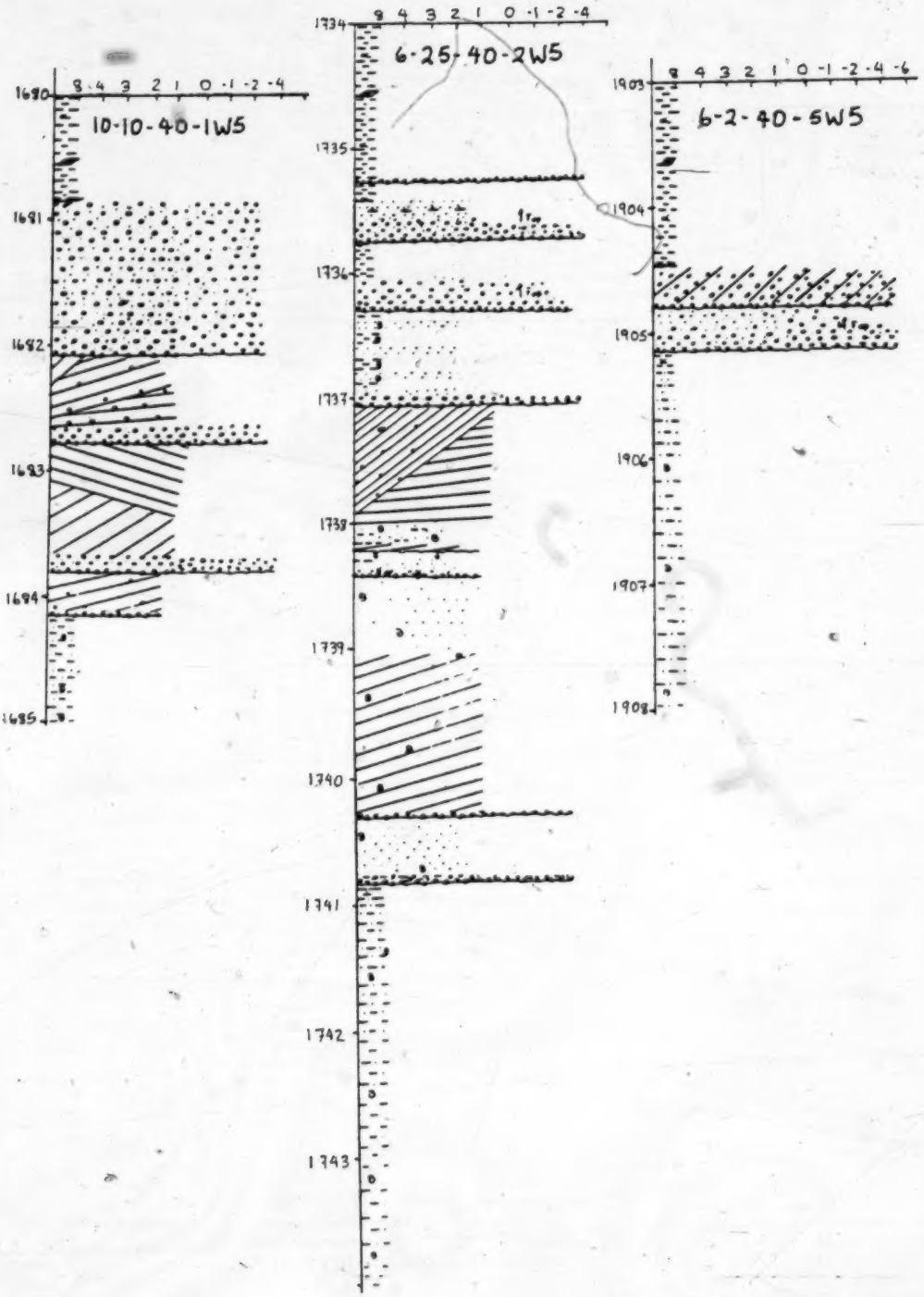
10-10-40-1W5
6-25-40-2W5
6-2-40-5W5

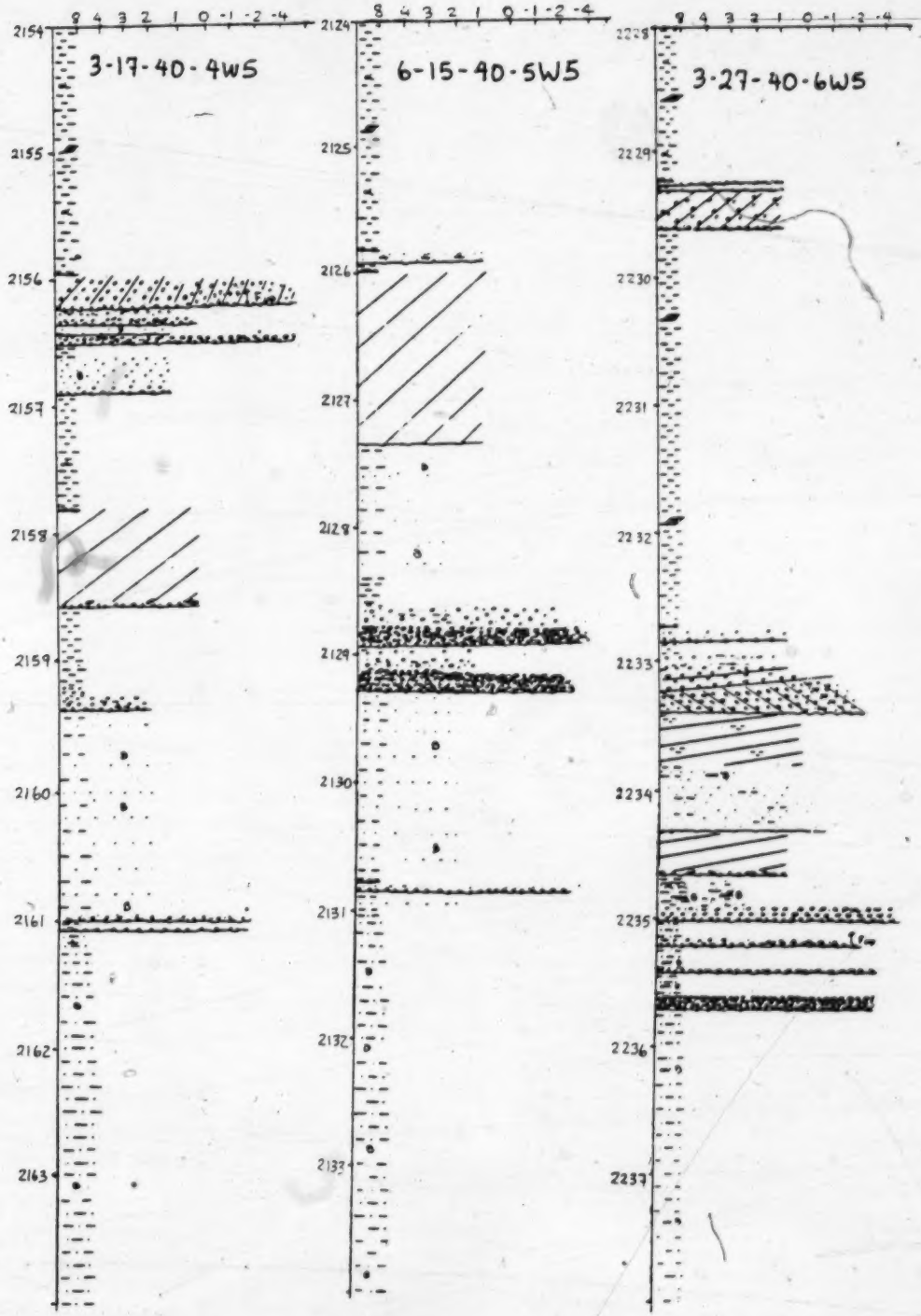
8 4 3 2 1 0 -1 -2 -4
2154
2155
2156
2157
2158
2159
2160
2161
2162
2163
3-17-40-4W5
8 4 3 2 1 0 -1 -2 -4
2124
2125
2126
2127
2128
2129
2130
2131
2132
2133
6-15-40-5W5
8 4 3 2 1 0 -1 -2 -4
2228
2229
2230
2231
2232
2233
2234
2235
2236
2237
3-27-40-6W5

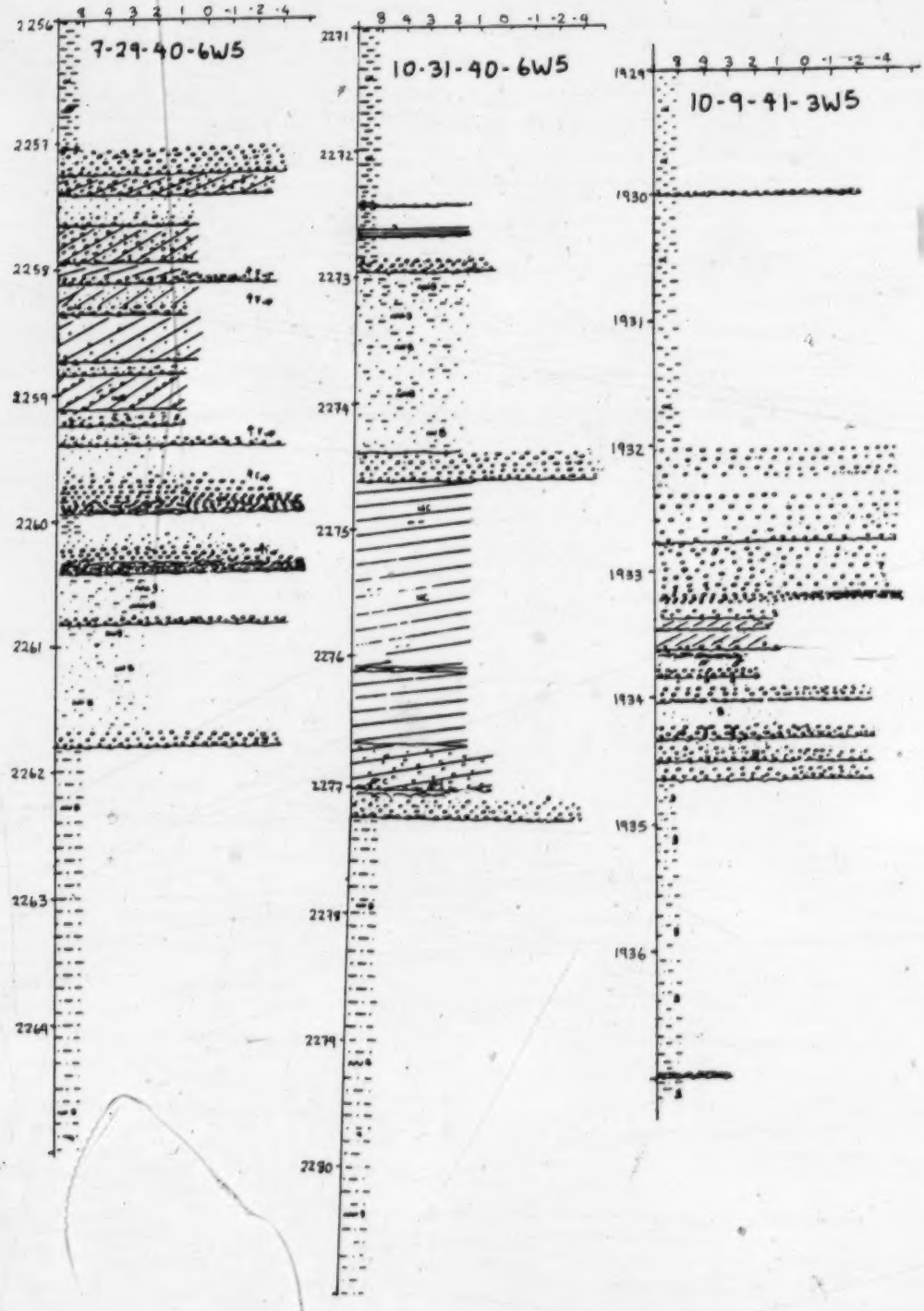
7-29-40-6W5
10-31-40-6W5
10-9-41-3W5

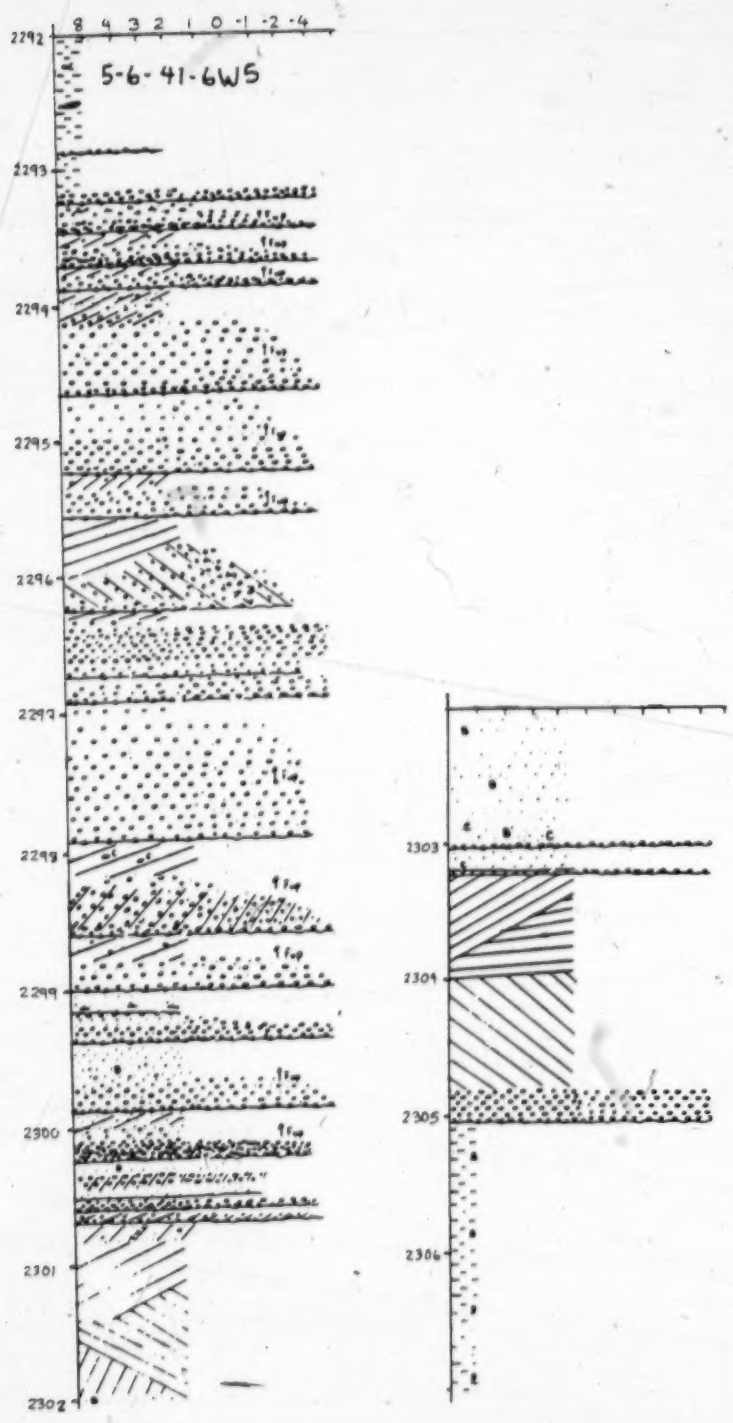
8 4 3 2 1 0 -1 -2 -4
5-6-41-6W5
2292
2293
2294
2295
2296
2297
2298
2299
2300
2301
2302
2303
2304
2305
2306

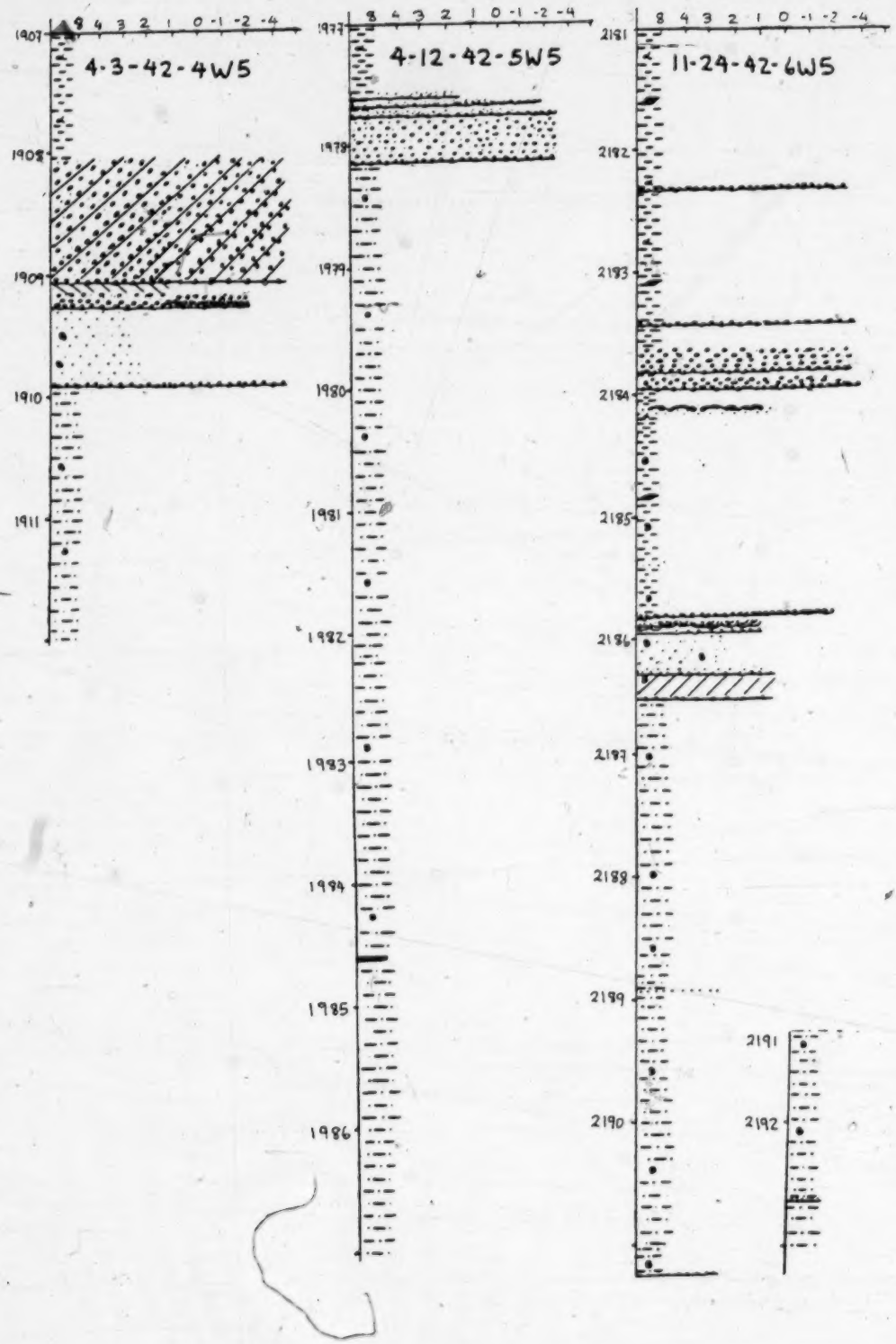
4-3-42-4W5
8 4 3 2 1 0 -1 -2 -4
1907
1908
1909
1910
1911
4-12-42-5W5
8 4 3 2 1 0 -1 -2 -4
1977
1978
1979
1980
1981
1982
1983
1984
1985
1986
11-24-42-6W5
8 4 3 2 1 0 -1 -2 -4
2181
2182
2183
2184
2185
2186
2187
2188
2189
2190
2191
2192